POLITECNICO
MILANO 1863

SCUOLA DI INGEGNERIA INDUSTRIALE
E DELL'INFORMAZIONE

State of the art and decarbonization options for glass industry: the case of Bormioli Pharma

School of industrial and information engineering

Master of Science in Energy Engineering – power generation

Candidate: **Marco Cappelli**

Student ID:	953306
Supervisor:	Prof. Matteo Vincenzo Rocco
Company supervisor:	Eng. Davide Faverzani, Eng. Federico De Martino
Academic Year:	2020-2021

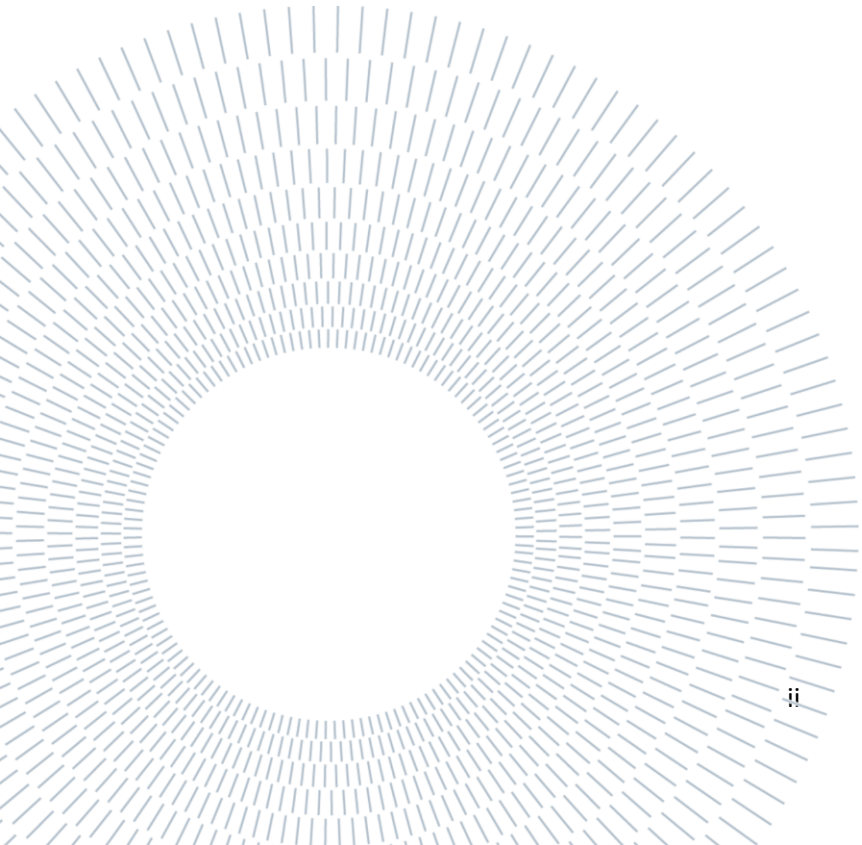

Abstract

The Thesis work has been conducted in collaboration with Bormioli Pharma, an industrial group with headquarter in Parma and active in the pharmaceutical packaging supply sector, specifically in the production of glass, plastic and rubber. The group counts on more than 1200 employees and nine plants between Italy, Germany and France.
The Thesis has the intention to address the topic of decarbonisation of the glass industry from the viewpoint of a company that directly operates in the field. In this light, the **first chapter** wants to present the types of glasses for the specific sector as well as the different furnaces with their characteristics. The **second chapter** pursues an in-depth analysis of the state-of-art from the energetic point of view, by tuning the energy balances with the data made available by the Company itself. This is of key importance because allows to understand where the Company is right now, in terms of energy demand and carbon intensity. In the **third chapter** the outcomes of chapter two are exploited in order to compare the different furnaces, which allows to understand the impact of each system on the energy demand as well as CO_2 emissions.
The decarbonization options are discussed in the **fourth chapter** in terms of *waste heat recovery*, *fuel switch* and *process optimization in combustion*: for each technology considered, a critical analysis of pros and cons is carried out based on literature review, as well as with their impact and readiness level in the market. In the **fifth chapter** is reported the case study of waste heat recovery approach aimed at the production of mechanical/electrical power applied to a glass furnace with similar characteristics as those of Bormioli Pharma, executed by researchers of the University of Padova. The focus is on the potential employment of not-traditional thermodynamic cycles against the well-established and market-ready Organic Rankine Cycle, such as closed-loop Joule-Brayton cycles employing supercritical CO_2 as working fluid.
The **sixth chapter** contains the core of the work, which consists in the thermodynamic and economic assessment of a peculiar waste heat recovery approach: steam methane reforming exploiting the residual thermal power of flue gases. This, applied to an end-port furnace, represents a novel approach for heat recovery in the glass field. The analysis comprises the modelling of the furnace as well as of the components required, together with their sizing, and is built on the basis of mass and energy balances together with chemical equilibrium approach for the reforming reactions. The project is closed with a quotation of the main relevant pieces of equipment and with the economic assessment of the overall system by means of the Net present Value approach.
Eventually, in the **conclusions** the outcomes of the Thesis are reported and summarized.

Key words: pharmaceutical glass, decarbonization glass sector, heat recovery glass furnaces, ORC glass furnaces, steam methane reforming glass furnaces

Sommario

Il progetto di Tesi è stato condotto in collaborazione con l'azienda Bormioli Pharma, gruppo industriale con sede a Parma e attivo nella produzione di packaging farmaceutico in vetro, plastica e gomma. L'azienda conta oltre 1200 dipendenti e nove plants produttivi tra Italia, Germania e Francia.
La Tesi ha l'obiettivo di discutere il tema della decarbonizzazione dell'industria vetraria dal punto di vista di una azienda realmente operante nel settore. In questa luce, il **primo capitolo** vuole presentare i diversi tipi di vetro sul mercato e le diverse fornaci, con le rispettive caratteristiche. Il **secondo capitolo** si concentra sull'analizzare nel dettaglio lo stato dell'arte dal punto di vista energetico, andando a settare i bilanci di energia con i dati messi a disposizione dall'Azienda stessa. Questo è di importanza assoluta poiché permette di capire dove l'Azienda si trovi in questo momento, in termini di consumo energetico e di intensità emissiva.
Nel **terzo capitolo** i risultati del capitolo due vengono utilizzati per confrontare i diversi forni, cosa che permette di notare l'impatto di ciascun sistema sulla richiesta energetica e sulle emissioni di CO_2.
Le opzioni per la decarbonizzazione sono discusse nel **quarto capitolo** in termini di *recupero termico*, *combustibili alternativi* e *ottimizzazione del processo di combustione*: per ciascuna tecnologia considerata è proposta una analisi critica dei pro e dei contro, basata su ricerche in letteratura, insieme al loro impatto e al loro livello di prontezza nel mercato. Nel **quinto capitolo** è riportato il caso dell'approccio al *recupero termico* volto alla produzione di potenza meccanica/elettrica applicato a un forno vetrario con caratteristiche simili a quelli di Bormioli Pharma, eseguito da ricercatori dell'Università di Padova. Il focus è sul potenziale utilizzo di cicli termodinamici non tradizionali rispetto al ben consolidato e già disponibile sul mercato Organic Rankine Cycle, come cicli Joule-Brayton chiusi con fluido di lavoro CO_2 supercritica.
Il **sesto capitolo** contiene il cuore del lavoro, che consiste nella valutazione termodinamica ed economica di un particolare approccio al recupero termico: lo steam reforming del metano, utilizzando la potenza termica residua dei gas di scarico. Questo, applicato a un forno di tipo end-port, rappresenta un approccio innovativo per il recupero termico applicato al mondo vetrario. L'analisi comprende la modellizzazione della fornace e dei componenti richiesti, insieme al loro dimensionamento, ed è costruito sulla base dei bilanci di massa ed energia insieme all'equilibrio chimico per le reazioni di reforming. Il progetto è chiuso con la quotazione dei componenti principali e con la valutazione economica del sistema complessivo attraverso l'approccio del Net Present Value.
Infine, nelle **conclusioni** vengono riportati e riassunti i risultati ottenuti nel progetto di Tesi.

Parole chiave: vetro farmaceutico, decarbonizzazione settore vetro, recupero termico forni vetro, ORC forni vetro, steam methane reforming forni vetro

Contents

Introduction 4

1. Pharmaceutical glass industry – state of art 6

1.1: Pharmaceutical glass 6

1.2: Energy demand for glass production 6

1.3: Types of furnaces 8

1.3.1: Energy source 8

1.3.2: Energy recovery 10

1.3.3: Oxidant 11

1.4: Borosilicate glass furnaces 12

1.4.1: Cyclope 12

1.4.2: Electric 13

1.4.3: Oxy-fuel 14

1.5: Soda-Lime glass furnaces 14

1.5.1: End-port 14

1.5.2: Unit melter 15

2. Furnace data analysis for different types of glass 16

2.1: Approach and method 16

2.1.1: Energy efficiency index EEI 16

2.1.2: Heat balance 17

2.1.3: CO_2 emission along campaign 19

2.1.4: CO_2 emission vs electric input vs cullet 20

2.2: Comparison among Borosilicate furnaces 21

2.2.1: Full electric furnace 21

2.2.2: Cyclope furnace 24

2.3: Comparison among soda - lime furnaces 29

2.3.1: End port furnace 29

2.3.2: Unit melter furnace 34

3. Furnaces comparison for different types of glass 39

3.1: Approach and method 39

3.1.1: Energy efficiency index EEI for different furnaces 39

3.1.2: CO_2 emissions for different furnaces 40

3.1.3: Heat input Qtot for same glass production for different furnaces at fixed pull by varying cullet and Qee 41

3.1.4: Electric vs hybrid furnace: economic competitiveness and overall carbon emissions 43

4. Decarbonization options 47
4.1: Waste heat recovery 47
4.1.1: Heat - to - power 47
4.1.2: Thermochemical heat recovery 48
4.2: Fuel substitution 49
4.2.1: Biogas 49
4.2.2: Hydrogen 49
4.3: Process optimization in combustion 51
5. Waste heat recovery: heat to power 52
5.1: HRS 52
5.1.1: Open loop, air JB cycle 52
5.1.2: Closed loop, $sCO2$ JB cycle 53
5.1.3: Closed loop, $sCO2$ JB cycle with combustion air preheating 54
5.1.4: Organic Rankine cycle 56
5.2: Working conditions 57
5.3: Methods 57
5.4: Results 59
5.4.1: Thermodynamic performances 59
5.4.2: Economic performances 59
5.5: Summary 64
6. Waste heat recovery: steam methane reforming 65
6.1: Approach and method 65
6.2: Furnace modelling without SMR 66
6.2.1: Input and variables 66
6.2.2: Heat balance on the furnace 68
6.2.3: Heat balance on the regenerator 71
6.2.4: Model validation 71
6.3: Furnace modelling with SMR 72
6.3.1: Input and variables 73
6.3.2: Chemical equilibrium at SMR reactor 76
6.3.3: Heat balance on the furnace 80
6.3.4: Heat balance on the regenerator 80
6.3.5: Heat balance SMR unit 81
6.3.6: Heat balance on HRSG and methane preheater 84
6.3.7: Schematized procedure 86
6.4: Methane preheater and HRSG sizing 88

6.4.1: Methane preheater 88
6.4.2: HRSG 89
6.5: Results and sensitivity 90
6.5.1: Potential $CH4$ and $CO2$ savings 90
6.5.2: Heat exchangers size 96
6.5.3: Equipment quotation 98
6.6: Economic analysis 103
Conclusions 107
List of figures 110
List of tables 112
Bibliography 113
Nomenclature 115
Symbols 115

Introduction

Bormioli Pharma is an Italian company, with headquarter in Parma, operating in the pharmaceutical packaging sector supply, specifically in the production of glass, plastic and rubber. The group counts on nine plants in three countries (Italy, Germany and France), with overall more than 1200 employees.
In the industrial panorama, glass industry doubtlessly belongs to the so-called *energy intensive sector*, due to its high share of energy consumption per tonne of product. By definition energy intensive industries are those whose annual energetic consumption exceeds 1 GWh [1]. Examples of such sectors are the industries of aluminium (90–100 GJ/ton) and steel (20 – 30 $\mathrm{GJ/ton}$), that lead the list, followed by cement (3–6 GJ/ton) and glass production (4 – 17 GJ/ton) [2], [3].
Pharmaceutical glass industry does not make exception. Actually, it is possibly even more energetically demanding: high quality standards must be satisfied, imposed by the international pharmacopeia, which are meant to grant safety and efficacy of the drugs that would be stored inside the glass bottles, such as chemical stability and inertia. These levels of the products are achieved either by maintaining a furnace temperature (T > 1500 °C) above the average of the lower quality glass and by performing a more accurate and severe inspection and rejection of the final good. Moreover, a lower share of cullet[1] is employed in the melting batch to avoid potential impurities in the final product. As a result, all these aspects combined bring to a greater energy consumption per tonne of product.

For what concerns the European Union in 2007 the sector of container glass accounted for the 58% of the overall European production (21,4 Mton), of which only the 5% is attributed directly to the pharmaceutical sector (comprising cosmetic and perfume as well), and a total carbon dioxide emission of 12,64 MtonCO2 that accounted for the 47% of the overall European glass industry [3].
Also, it was estimated a specific energy consumption of 6,4 GJ/ton for the container glass sector and, regarding specific emissions, 0,38 tonCO2/ton and 0,1 tonCO2/ton respectively due to combustion and process [3], the latter being those carbon emissions due to the melting of raw materials containing carbonates[2].

It appears clear that glass manufacturing contributes massively to carbon emission into atmosphere, and prompt actions should be taken in order to drive the sector towards a more sustainable production.

In this regard, since 2003 the European Union has put in place its plan to decarbonise the industrial sectors by means of the Emission Trading System ETS. The action plan, which is currently in its fourth and last phase, is structured such that by 2030 the overall carbon emissions in the continent will be cut by 43% with respect to the levels registered in 2005 [4]. Even more ambitious goals have been endorsed by the European Union: carbon neutrality by 2050 is at the heart of the *European Green Deal* [5], in line with the Paris Agreement pledge to keep the atmosphere temperature rise well below the 2°C (possibly 1,5°C) with respect to the pre-industrial levels [6], in order to reduce severe and irreversible risks coming from climate changes. Moreover, the European commission on 14 July 2021 set out a series of legislative proposals that strive to reach 55% of net reduction in greenhouse gas emission[3] by 2030 [7], thus replacing the initial target of 43%.

[1] Cullet represents the amount of recycled glass either from internal or external source, in term of mass, used within the batch. Bottles manufacturers achieve share of cullet up to 80-90%, whereas pharmaceutical levels are limited to the range 20-50%
[2] These emissions are unavoidable and can only be mitigated by increasing the cullet share
[3] With respect to 1990 levels

More specifically, the ETS currently covers more than 10000 installations in the power sector and manufacturing industry, as well as airlines operators, reaching up to the 40% of the overall European greenhouse gas emissions.
ETS is basically a "cap and trade" mechanism, where the cap is the overall allowed emissions which is progressively being reduced thus leading to a fall in total emissions in the years. Emitters must acquire, in a dedicated market, the so-called *emissions allowances* which represent the right to pollute: at the end of the period (year), each player has to surrender enough allowances to fully cover its emissions, otherwise heavy fines are imposed by the authority. In case of reduction in the emissions, the industry can either keep the remaining for the following period or trade[4] them on the market [8].
Such a philosophy is supposed to discourage inefficient technologies and, at the same time, promote investments towards low-carbon ones.
ETS covers not only CO_2 but also N_2O and perfluorocarbons (PFCs), and the participation is mandatory for companies belonging to the power sector (electric/thermal) as well as for energy intensive industries.
Moreover, in order to tackle the risk of delocalization of these highly consuming companies[5], which are potentially attracted to regions where greenhouse gas policies are not as strong as in Europe, and to maintain their competitiveness in their market, the free allocation of a given number of allowances is confirmed also in the ETS fourth phase, according with specific regulations based on the production volumes of the company and comparing it with the benchmark[6] for such a good.

From the industry side, in order to get aligned with the European and national regulations, an important commitment and a huge effort has to be put in the research on advanced heat recovery and combustion systems, as well as on alternative fuels exploitation such as hydrogen and/or biofuels. Possibly, alternative methods for glass melting to the traditional fossil fuels fired furnaces should be implemented. Full electric melting is actually a well-established and widely employed technology, however it is not really well suited for large furnaces because of the electricity price, which is still way higher than natural gas, and besides, the carbon emission would anyway come up in the equation as an indirect production for power generation.

However, in order to boost the employment of these technologies, industries need first to handle the know-how as it is still not clear how, for instance, a fuel switch would possibly affect the glass quality. Such a consideration is particularly relevant for energy-intensive industries that are capital intensive, highly cost-competitive and so sensible to product quality.
Therefore, it is suggested that investments and incentives should be granted by authorities and countries to support research, pilot projects and tests in order to speed up the energetic transition of the glass sector.

[4] This is why ETS is "cap and trade" mechanism

[5] Phenomenon known as "carbon leakage"

[6] Based on the performance of the most efficient plants. As a reference value, the benchmark for the "Bottles and jars of colourless glass" between 2021-2025 is 0,290 $\frac{\text{ton}_{CO_2}}{\text{ton}_{\text{glass}}}$ [30]

1. Pharmaceutical glass industry – state of art

1.1: Pharmaceutical glass

There exist different types of pharmaceutical glass. In the first place, it can be distinguished between white and amber colour: the latter is best suited for photosensitive prescription, as it provides an intense UV protection. Moreover, it is possible to classify depending on the degree of chemical resistance offered [9]:

- **Type I – Borosilicate**: composed of silica, boric oxide, aluminium oxide and alkali and/or alkaline earth oxides. It is chemically inert and possesses high hydrolytic resistance due to the presence of boric oxide, as well as thermal shock resistance.
  It is mainly used for parenteral solutions but can also contain strong acids.

- **Type II – Soda-Lime**: composed of silica, sodium oxide, calcium oxide and small amounts of aluminium oxide. It is produced from Type III, after "sulphur treatment" that removes the superficial sodium thus making the glass more chemically stable than Type III.
  Mainly employed with most acidic and neutral aqueous preparations.

- **Type III – Soda-Lime**: It is untreated and provides lower chemical resistance. Suited to store all types of solid dosage and syrup.

1.2: Energy demand for glass production

Once the "glass recipe" has been defined, it is possible to mix up all the raw materials: the result is the so called "batch", which is fed into the furnace at high temperature through the doghouse. The process of glass melting starts here.
The energy demand in the **batch-to-melt conversion** implies:

1. the heat needed to bring the raw materials up to the reaction temperatures

2. the net heat required for the reactions (determined by both endothermic reactions and exothermic reactions), such as decarbonation, dehydration (moisture content always present to reduce dust and powders) and solid-state dissolution

3. the heat required for the further heating of the melt phases and the volatile reaction products such as CO_2, SO_2, HBO_2 and water vapour up to the temperature at the furnace exit (throat, canal, exhaust ports)

Glass melting is in general a seriously energy intensive process, as huge temperatures are attained in order to produce the desired glass quality. Rough values of the melt:

- borosilicate: temperature at the throat section around 1420 °C

- soda-lime: temperature at the throat section around 1350 °C

However, the temperature in the chamber can easily exceed values of 1500 °C.
To partially reduce the energy demand, **cullet** is employed in variable percentage such that the net heat for the reactions turns to be lower. It has been estimated that an increase of 10 % by weight corresponds to a reduction in energy consumption of 2-3 % and therefore a CO_2 emission reduction.

To better understand how the overall process evolves, **Figure 1** shows a generic furnace section, with flow profile, that represents the **melting and fining** processes:

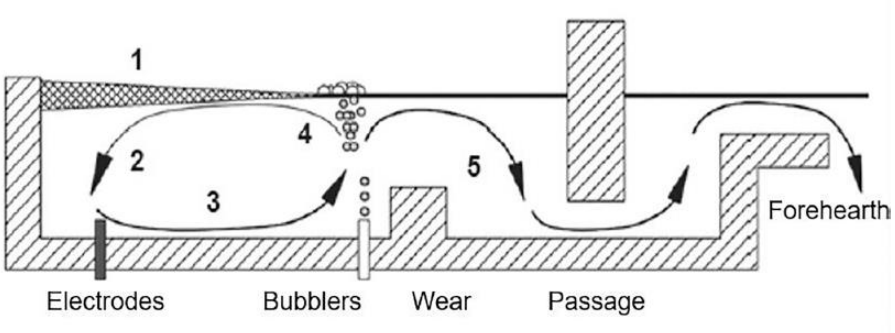

***Figure 1** - furnace section and flow profile*

The main purpose is to supply the forming step, which is downstream the furnace, with a melt that is as much homogeneous as possible, either from a thermal and chemical perspective.
The flow profile results from a superposition of natural and forced convection: the first is induced by density gradients due to temperature stratification in the molten glass, the second results from the possible action of the so-called bubblers, devices that inject compressed air from the bottom so to promote the recirculation on the melt.
It is possible to individuate five main phases: in the first (1), the solid material is continuously fed through the doghouse, and it is heated up by irradiation of flames and side walls/crown refractories, plus conduction of the molten material below. Being colder, this material tends to sink (2) and, as its temperature increases, reactions do occur as well as evaporation of volatile species, thus setting bubbles free. Such convective motions contribute to the mixing process (3), that is enhanced by bubblers and electrodes which provide heat locally. Eventually, the melt rises again (4) at the so-called hot spot and the first fining occurs: the vertical motion induces the removal of gases such as CO_2 and SO_2, which is completed in the fining section (5) with the aid of a fining agent such as $NaSO_4$.
Eventually, the molten glass is forced to pass through the **throat** which represents the outlet section of the furnace. It is important to ensure the correct temperature of the glass at this point: the product quality depends on the efficiency of bubbles removal and homogeneity, which are enhanced at high temperatures.

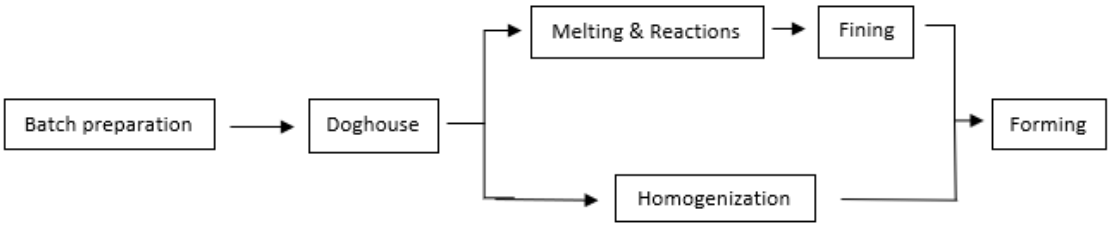

Figure 2 *- Steps in glass melting*

1.3: Types of furnaces

The design of the furnace strongly depends on the type of glass that it is going to be produced. This consideration is particularly relevant for the pharmaceutical glass industry when it comes to deal with aggressive compositions, such as borosilicate glass. Indeed, it is definitely the most challenging among the others because of highest required temperatures, as well as strongest corrosive tendency on refractories materials by both molten mixture and generated vapours. Therefore, we should expect **lower lifetime** of the furnace itself, in jargon *"campaign"*, and **higher energy demand**.

This fundamental distinction based on glass nature drives all the downstream design choices: energy source, combustion approach, energy recover approach, oxidant, refractories materials, etc.
In the following there will be presented the state-of-art furnaces for pharmaceutical glass production, specifically for soda-lime and borosilicate.
A quick overview is here provided for each:

Borosilicate		
Electric	Oxy – fuel	Cyclope

Soda - Lime	
End port	Unit melter

To classify each of them, it is useful to define three main peculiar aspects: *energy source, energy recovery* and *oxidant*.

1.3.1: Energy source

The most widely employed energy source is by far the **combustion of a fossil fuel**, typically natural gas. Burners are installed above the melt and heat transfer by radiation occurs. Typical conditions inside the combustion chambers are of temperatures well above 1300 °C.
It is worth to mention that the disposition of burners plays an important role in the heat exchange process:

- **Longitudinal**: burners placed at the back wall such that flames and melt proceed in the same direction. Flames extension is almost over the entire length of the furnace, which increases the residence time in the combustion chamber thus achieving a better combustion. Then, exhaust gases turn and leave the chamber from the same back wall. Such a configuration is called ***end port***.

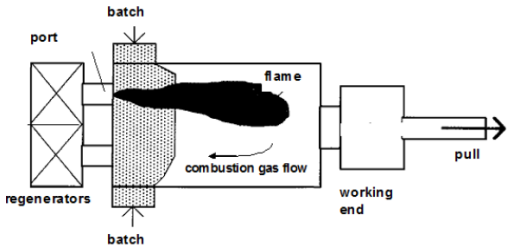

***Figure 3** - end port*

- **Lateral**: burners placed along the longitudinal direction, at the side wall of the furnace. Such a configuration is compatible with chambers with longer extent since end port would not guarantee a satisfactory temperature profile. Therefore, it is best suited for big size furnaces.
  Such a configuration is called ***side port***.

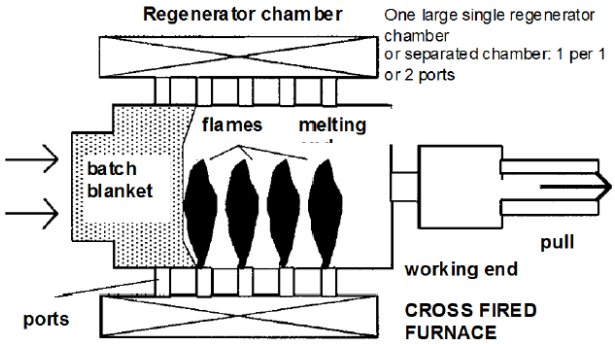

***Figure 4** - side port*

Combustion of fossil fuels is not the only possible option though. As an alternative, **electric furnaces** can be employed and they are, indeed, a well-established technology widely accepted by industries. They require couples of electrodes directly immersed into the molten glass, and the principle is to exploit its electric conductivity as well as the Joule effect, thus converting electric power into thermal. An important difference with combustion-based chambers is that heat is supplied locally, so to achieve a good temperature distribution it is necessary to install several electrodes. Moreover, the upper side of the melt is at relatively low temperature (~ 100 °C), which is why they can be addressed as "cold blanket", and that means that thermal structural issues are less severe.

Many are the advantages of electric furnaces over combustion-based, such as: higher thermal efficiency, smaller chamber volumes, no need for regenerators nor high-T expensive crown refractories, more effective heating of bottom layers, no combustion-based CO_2/ SO_2 emissions and therefore no carbon allowances. However, they face two relevant issues:

1. <u>*Low pull flexibility*</u>: to keep the viscosity within the acceptable range for a successful glass manufacture, also the temperature needs to be within given values. When the pull rate is, for instance, increased then the risk of lowering too much the T exists at fixed heat input, and the opposite happens if the production decreases. Hence, it is important to not exceed pre-established pull ranges, because electric furnaces show higher difficulty in adapting quickly the temperature

profile which means that it is not feasible to flexibly adjust the heat supply as much as it would be needed to ensure those temperature limitations.

2. *electricity price*: despite avoiding the cost for emitting CO_2, the difference between natural gas and electricity price has not reached a level that makes electric economically convenient up now. Moreover, the thermal power released by the combustion of one standard cubic meter of natural gas is roughly five times the one made available by one kWh of electric power, considering reference values for thermal efficiencies of 0,5 and 1 respectively[7]. As a consequence, neglecting at first the cost of carbon emissions, to make electric economically convenient the cost of natural gas should be five times the cost of electricity[8].

To smooth the drawbacks of either natural gas and electric, and to exploit their positive aspects the possibility is to employ a **hybrid melting** consisting of combustion and electric combined together. The electric boosters play a double role as they supply a given share of the overall thermal energy required and, at the same time, heat up efficiently the lower layers of the bath. Besides, by doing so the convective motions are enhanced.
Hybrid systems are particularly relevant when producing borosilicate glass due to the need for higher temperatures, but also with amber glass because radiative thermal power tends to be absorbed in the upper layers: electric boosters supply the bottom ones.

1.3.2: Energy recovery

Exhaust gases from glass melting furnaces have a huge thermal energy available. The commonly adopted way of exploiting it is to preheat the incoming combustion air, and two choices can be adopted: **recuperative** or **regenerative** heat recovery.
In the first case, hot flue gases exchange power **continuously** with air inside metallic (chrome-nickel steel) heat exchangers. Because of the limited temperature that these can endure, combustion air reaches at most 700÷800 °C.

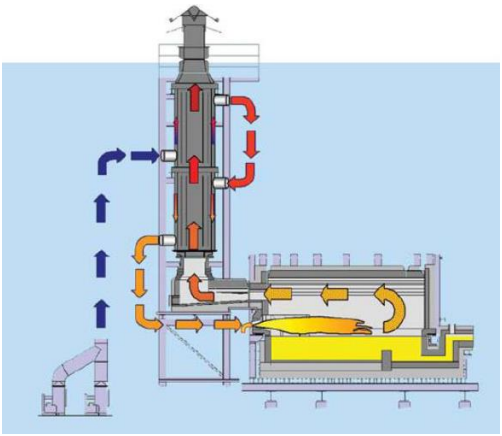

Figure 5 *- recuperative tower*

[7] Electric power fully converted into thermal power to the glass, whereas roughly half of the heat released by combustion goes to the melting
[8] Costs of electricity and natural gas are referred respectively for kWh_e and sm^3

In the second instead, heat exchange happens inside regenerators which are towers tall up to 10-12 meters of refractory bricks. Typically, these are used in couples because the process is **discontinuous**: while flue gases flow downward through one tower losing energy, in the other combustion air flows upward and warms up. In such an alternating process, whose period is twenty minutes, the exhaust gases lose around 1000 °C (from 1500 to 500 °C) whereas air reaches up to 1300 °C.
It is interesting to point out that heat is, in the first period, exchanged from flue gases to bricks, and then from bricks to air in the second: there is no direct exchange between exhaust gas and air.

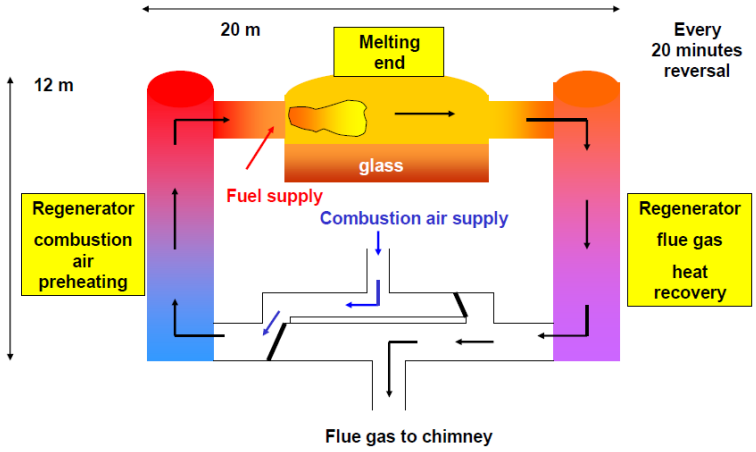

***Figure 6** - regenerative towers*

Regenerative heat recovery is more efficient, since a large ΔT is exploited, and the fact that combustion air is fed into the furnace at higher temperature allows to expect that combustion, which occurs due to self-ignition of the fuel when injected in the hot atmosphere of the chamber, proceed more efficiently, with a lower consumption of fuel.
On the other hand, regenerators are more expensive and represent an important part of the investment costs of the furnace.

1.3.3: Oxidant

Air as oxidant agent is not the unique choice. It is definitely the cheapest and easily supplied to the combustion chamber, through the heat recovery system, via dedicated fans.
The drawback of air as oxidant is the presence of N_2 which inevitably is converted into NO_2, since combustion is operated with a given O_2 excess to make sure the reaction is complete – and also achieve reduction in CO production-. This is also enhanced by the huge temperatures in the chamber ("*thermal* NO_x"), as well as the small amounts of N_2 that the fuel might contain ("*fuel* NO_x"). Besides, the presence of N_2 is also undesirable because it reduces the energy efficiency of the furnace as, for each cubic meter of O_2, five of N_2 are receiving heat. Therefore, large volumetric flow rate is to be forecasted when combustion is operated with air.

As an alternative, it is possible to employ pure O_2 as oxidizing agent. This would solve the problems related to N_2 and therefore we would expect higher energy efficiency and lower volumetric flow rate, so also a lower fuel utilisation, as well as a higher flame temperature. Therefore, from a combustion perspective this type of configuration is truly beneficial. However, it must be considered that such a furnace is not really compatible

with heat recovery systems and, in addition, O_2 cost may overcome the saving in fuel consumption. Moreover, because of higher flame temperatures it becomes absolutely fundamental to employ high-T crown refractories which are more expansive.
Plants employing O_2 do exist: the so called ***oxy-fuel***.

As a matter of fact, oxy-fuel furnaces are not so widespread because of the complex technical management and expansive supply of O_2, which makes them attractive and competitive in particular for high-quality glasses such as borosilicate.

1.4: Borosilicate glass furnaces

As already mentioned, borosilicate glass is complicated to dealt with. Regardless the specific furnace configuration, the common characteristics are the *energy source* and the *refractories materials*.
Regarding the first one, combustion approach alone is rarely the choice because of the high operating temperatures that must be guaranteed. Therefore, at least hybrid furnaces are required such that a good heating is also conferred at the lower layers. However, it is also possible to employ full electric chambers as long as the correct temperature profile is achieved, thus installing the correct number of boosters.
About the refractories materials the main issue is related to the presence of boron components either in the melt, which enhances the erosion of the side walls, and in the flue gases.
Combining these two effects, the campaign of the borosilicate furnaces turns out to be around three years.

In the following it is presented a brief description of each configuration.

1.4.1: Cyclope

Cyclope furnace is employed by the company and specifically intended for borosilicate glass production. Its main advantage is the capability of producing high quality glass combined with a flexible pull adjustment, which is made possible thanks to peculiar furnace design and operativity choices which comprise steadily-operated bubblers, able to ensure together with electric boosters a good refining effectiveness.
Regarding the furnace structure, it resembles an end port with flames propagating from the back side wall. However, the substantial difference lays in the regenerative chambers which are operated continuously, without switching period, and coupled with two metallic heat exchangers in series. Moreover, these regenerative chambers are structured such that they can mitigate the corrosive tendency of the boron components in the waste gasses. Such a heat recovery system is able to preheat combustion air up to 900 - 1100 °C, whereas exhaust gases are cooled down from 1500°C to about 350 °C.

Figure 7 - *Cyclope regenerative chambers*

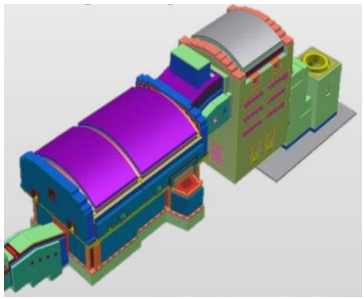

Figure 8 - *Cyclope furnace*

1.4.2: Electric

As it was previously discussed, electric furnaces are an established technology for this type of glass because they can deliver the required **heat locally**, thus minimizing thermal losses, with a good precision for the temperature profile that it is requested for delivering the correct glass quality.
Despite the positive aspects already mentioned such as zero (direct) emissions and lower volumes, the main limitations in their expansion on the market are related to the limited pull flexibility and the cost of electricity.

Figure 9 - *full electric furnace*

1.4.3: Oxy-fuel

Oxy-fuel furnaces operate combustion with pure O_2 thus avoiding the presence of inert nitrogen into the chamber. Oxygen is supplied from the side wall where burners are also placed, resembling a unit melter configuration. However, heat recovery is not typically performed and exit ports are placed on the opposite side of the flame. The choice of renouncing on heat recovery is mainly due to the presence of boron in flue gases, which would complicate the design of the recovery system in terms of structural degradation. An additional limiting factor is the amount of flow rate in exhaust gases, which is way lower with respect to air combustion due to nitrogen absence.
As anticipated, this type of combustion allows the fuel saving and to strongly reduce NO_2 emissions. Unfortunately, the cost of oxygen united with the higher flame temperature, that requires the use of high-T refractories for the crown, limits the potential expansion of the technology in the field.

***Figure 10** - oxy-fuel furnace*

1.5: Soda-Lime glass furnaces

Despite being less critical than borosilicate, soda-lime glass is still produced at more than 1300 °C. The positive aspect if compared to borosilicate is that the molten material and the exhaust gases are not as corrosive, so it is possible to employ either metallic recuperator or silica regenerator without chemical stability issues. Therefore, the average lifetime is way longer than those of borosilicate reaching up to eight-ten years. The campaign is mainly affected by carry-over phenomena, that is dust filling the heat recovery system's channels, and the erosion of walls at the interface molten-refractories. These two are also present with borosilicate glass, but corrosion by boron components in waste gases is way faster and more critical.

1.5.1: End-port

End-port is a consolidated configuration that employs tall regenerative chambers operated discontinuously where high thermal recovery efficiency is achieved: flue gases see a cooling ΔT up to 1000 °C and combustion air achieves temperatures up to 1300 °C. By considering that flames are injected from back side wall, it should be expected that chambers length is kept limited and therefore also the production capacity: typical design values are about 200-250 ton/day.
With a period of 20 minutes, regenerators are switched: in the first period combustion air flows bottom-up, being heated, whereas in the other tower flue gasses flow up-bottom, being cooled. After 20 minutes, the flows are switched.

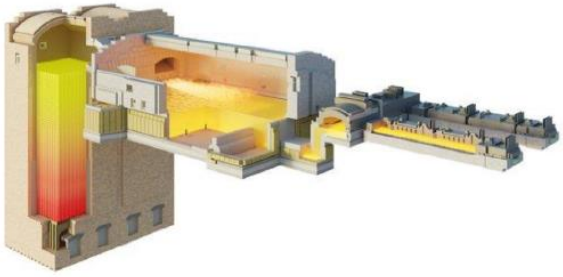

Figure 11 *- end-port furnace*

1.5.2: Unit melter

Unit melter furnaces employ recuperative chambers and, differently from the previously discussed solutions, employ a pre-mixed mixture for combustion, which is operated from side-wall burners.
The positive consequences are lower investment costs and continuous operation of the recovery units, whereas the limitations are in the heat recovery efficiency due to metallic exchangers: combustion air achieves temperatures limited to a temperature range between 500 and 800 °C, way lower than regenerative furnaces.

Figure 12 *- unit melter furnace*

2. Furnace data analysis for different types of glass

2.1: Approach and method

Within the current chapter there will be investigated and processed the data of each type of furnace employed at Bormioli Pharma. The purpose is to discuss their energetic behaviour based on the type of glass produced, starting from the knowledge of the furnace operating conditions made available directly by Bormioli Pharma in terms of cullet and pull, as well as its energetic consumption as electric and natural gas demand along the considered campaign.
Also the colour of the glass is relevant for the energetic demand of the furnace, however its role is not of primary importance in the discussion of the behaviour along the campaign since the production plan can require several colour switches thus making it not really possible to track its impact on the furnace performance.
The following points have been analysed:

- Energy efficiency index EEI
- Heat balance
- CO_2 emission along campaign
- CO_2 emission vs electric input vs cullet

In the following sections, a brief description of each is provided.

2.1.1: Energy efficiency index EEI

It is an index that tells how much the ageing process affects the energetic performance of the furnace. It is defined as the ratio between the actual specific energy demand and the specific energy demand when the furnace is new (EEI = 100 %).

$$\mathrm{EEI} = \frac{\frac{\mathrm{kWh_{actual}}}{\mathrm{ton_{glass}}}}{\frac{\mathrm{kWh_{new}}}{\mathrm{ton_{glass}}}} \qquad [2.\ 1]$$

The index will be plotted twice. The first represents the expected trend, which is a result of historical data on past campaigns, thus playing the role of reference [9]. The second, instead, is the actual curve computed once the energetic consumption is known[10]. It can be forecasted that these two are close within the first months of campaign, however it is typical to spot the onset of a gap or oscillatory trend since the actual curve depends on how the furnace is being operated: pull, type of glass, quality issues or ageing are the most likely sources of discrepancy, as well as undesirable faults or damages.

[9] Not only: it is also important when defining the energetic budget for the following year. It is an esteem of the energetic demand
[10] Precise electricity and fuel consumption read, monthly, on the corresponding bills

Therefore, it is important to take into account the EEI as it provides a picture of the health state of the system.

2.1.2: Heat balance

By means of the heat balance, it has been possible to establish the overall heat demand of the furnace as well as each heat streams. Moreover, it was possible to determine the role of three independent and important variables in the system operating conduction: pull, electric input and cullet.
The final goal is to provide a forecast of the natural gas consumption for different furnaces and glass productions when these three figures change.
As for the control volume, the overall system has been considered, comprehensive of basin and heat recovery system:

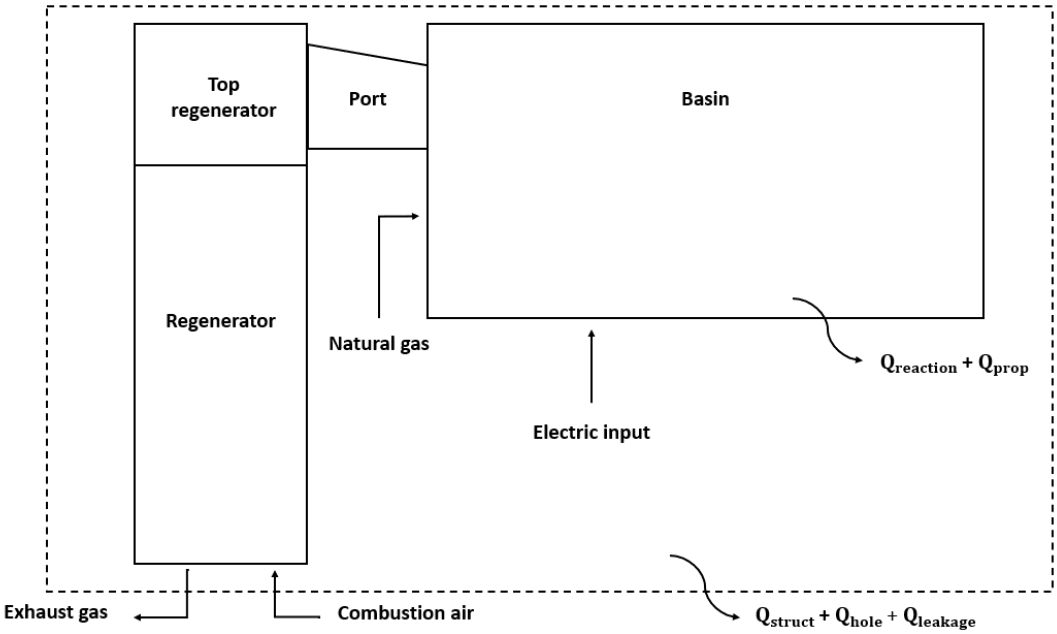

Figure 13 *- Control volume heat balance*

The term "$Q_{reaction} + Q_{prop}$ " represents the sum of the net heat required by chemical reactions within the bath and the heat flux of the molten glass that leaves the chamber, whereas "$Q_{struct} + Q_{hole} + Q_{leakage}$ " accounts for the overall heat losses through the system.
By assuming that both combustion air and natural gas get into the control volume at the reference conditions, it follows that their enthalpy flux will be zero. As a consequence, the heat balance turns out to be:

$$Q_{ee}{}^{11} + Q_{ng} = Q_{s,l,h} + Q_{r,p} + Q_{ex}$$

[2. 2]

[11] Heat input due to boosters

where Q_{ng} is the heat made available by combustion of natural gas due to its lower heating value, which is taken equal to 9,605 $\left[\frac{kWh}{sm3}\right]$, that is typical for a mixture of CH_4 and other hydrocarbons.

The following set of equations have been exploited to compute each component:

- $$Q_{s,l,h}\left[\frac{kWh}{kg_{glass}}\right]^{12} = \frac{\left\{\frac{F\cdot\left[1400+\left(\frac{Pull\,[\frac{ton}{d}]}{Surface\,[m^2]}-2{,}5\right)\cdot 50\right]}{1400}\cdot\frac{24}{1000\cdot Pull\,[\frac{ton}{d}]}\right\}\left[\frac{kcal}{kg_{glass}}\right]}{860\left[\frac{kcal}{kWh}\right]}$$

[2. 3]

- $$Q_{r,p}\left[\frac{kWh}{kg_{glass}}\right]^{13} = \frac{\left[q_{rea}\left(1-\frac{Cullet\,[\%]}{100}\right)+Q_{prop}\right]\left[\frac{kcal}{kg_{glass}}\right]}{860\left[\frac{kcal}{kWh}\right]}$$

[2. 4]

- $$Q_{ex}\left[\frac{kWh}{kg_{glass}}\right] = \left(Q_{s,l,h} + Q_{r,p} - Q_{ee}\right)\cdot(R-1)$$

[2. 5]

- $$R^{14} = \frac{Q_{in}-Q_{ee}}{Q_{in}-Q_{ee}-Q_{ex}} = \frac{Q_{ng}}{Q_{ng}-Q_{ex}} > 1$$

[2. 6]

It is important to highlight that such a heat balance is only valid for the furnace "as built", because both $Q_{s,l,h}$ and R are obviously a function of time or, more precisely, of how much the system is worn-out: the first term will likely increase because of a lower thermal resistance of the structure, whereas the second will decrease due to carry-over and corrosion.

Eventually, from the energy balance equation it was possible to determine the heat input related to the natural gas:

$$Q_{ng}\left[\frac{kWh}{kg_{glass}}\right] = \frac{R}{R-1}\cdot Q_{ex}$$

[2. 7]

Therefore, the volumetric demand on daily basis:

$$\dot{V}\left[\frac{sm^3}{d}\right] = \frac{Q_{ng}\left[\frac{kWh}{kg_{glass}}\right]\cdot Pull\left[\frac{kg_{glass}}{d}\right]}{LHV\left[\frac{kWh}{sm^3}\right]}$$

[2. 8]

[12] The correlation for the heat losses is empirical and based on past heat balances executed with real data of furnace conduction

[13] Both reaction and proportional heats are provided by the chemical department, and depend on the type of glass considered

[14] R represents the heat recovery coefficient. Similarly to $Q_{s,l,h}$, it is estimated by means of past heat balances

The results obtained are those which allow to close the heat balance.

2.1.3: CO_2 emission along campaign

Direct carbon emissions by glass furnaces are evaluated by considering both the combustion of a fossil fuel and the carbon content of raw materials.

For the first, an emission factor of 0,001984 $\left[\frac{\text{ton } CO_2}{\text{sm}^3}\right]$ [10] has been applied. For the second instead, the approach consists in making use of a loss factor [15] that represents the tonne of CO_2 emitted per tonne of glass produced, being its precise value dependent on the type of glass, since the carbon content of the batch depends on the raw materials employed.

Therefore:

$$\begin{cases} CO_{2,\,ng}\left[\frac{\text{ton } CO_2}{\text{month}}\right] = \text{Emission factor}\left[\frac{\text{ton } CO_2}{\text{sm}^3}\right] \cdot \dot{V}\left[\frac{\text{sm}^3}{\text{month}}\right] \\ CO_{2,\,rea}\left[\frac{\text{ton } CO_2}{\text{month}}\right] = \text{Loss factor}\left[\frac{\text{ton } CO_2}{\text{ton}_{glass}}\right] \cdot \text{Pull}\left[\frac{\text{ton}_{glass}}{\text{month}}\right] \cdot \left(1 - \frac{\%\text{ cullet}}{100}\right) \end{cases}$$

[2. 9]

Hence:

$$CO_2\left[\frac{\text{ton}}{\text{ton}_{glass}}\right] = \frac{CO_{2,\,ng}\left[\frac{\text{ton } CO_2}{\text{month}}\right] + CO_{2,\,rea}\left[\frac{\text{ton } CO_2}{\text{month}}\right]}{\text{pull}\left[\frac{\text{ton}_{glass}}{\text{month}}\right]}$$

[2. 10]

Table 1 reports the values of the loss factor employed for each type of glass:

	Borosilicate	Soda-Lime white	Soda-Lime amber
Loss factor	$\left[\frac{\text{ton } CO_2}{\text{ton pull}}\right]$	$\left[\frac{\text{ton } CO_2}{\text{ton pull}}\right]$	$\left[\frac{\text{ton } CO_2}{\text{ton pull}}\right]$
	0,01600	0,18133	0,18008

***Table 1** - Loss factor for borosilicate and soda-lime glass*

[15] Provided by the chemical department

Despite not being always possible to differentiate between the colours while computing the carbon emission along the furnace campaign, for the case of soda-lime the loss factors of both white and amber are reported just to show that white production is associated with a larger CO_2 emission.
Moreover, borosilicate glass has a loss factor that is one order of magnitude lower than those of soda-lime.
Even though the current analysis is not focused on the description of the effects of the colour, given that switches are possible along the furnace campaign, it is nevertheless something that must be taken into account by the energy manager of the company when evaluating the CO_2 emission, in order to align with the ETS. This is done on yearly basis once the production plan for the furnaces has been defined.
As a general observation, it can be stated that in borosilicate glass furnaces the role played by the raw materials is marginal if compared to the combustion of natural gas. Instead, in the case of soda-lime glass, process emissions are not negligible.

2.1.4: CO_2 emission vs electric input vs cullet

At this point, by exploiting the data gathered with the energy balance about natural gas demand, it became possible to forecast the overall daily direct CO_2 emissions at a chosen pull [16] while letting electric input and cullet percentage vary. This allows to predict the consequences of a variation in the furnace conduction on the environment. Being $CO_2\left[\frac{ton_{CO_2}}{ton_{glass}}\right]$ computed at step 2.1.3, it follows:

$$CO_2\left[\frac{ton_{CO_2}}{d}\right] = CO_2\left[\frac{ton_{CO_2}}{ton_{glass}}\right] \cdot pull\left[\frac{ton_{glass}}{d}\right] \qquad [2.\ 11]$$

With this last step a quantitative discussion over the furnace energetic behaviour is achieved, which is not only enriched but actually made possible thanks to the data availability of existing and operating furnaces.

Within the subsequent paragraphs there will be presented the obtained results, together with comments and arguments aimed at justifying their physical behaviour and trends.
The discussion is structured such that different furnaces are evaluated against the type of glass for which they are most often employed, either for traditional reasons or for design choices.

[16] Design or average pull for the furnace

2.2: Comparison among Borosilicate furnaces

For the specific case of Bormioli Pharma, two types of furnaces are currently dedicated to borosilicate glass manufacturing: full electric and Cyclope. Let's investigate them, separately.

2.2.1: Full electric furnace

The very first comment is on the energy efficiency index:

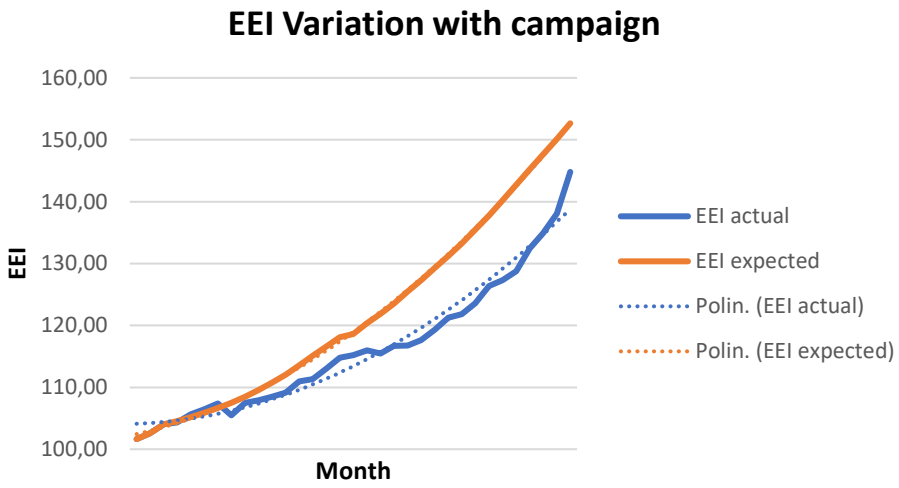

Figure 14 *- EEI full electric furnace*

For electric furnaces the expected behaviour is linear for the first seven to ten months, then it gets exponential. Such a behaviour is even worsened by the aggressive tendency of borosilicate glass.
The actual trend, despite an evident gap, lays below which means that neither issues nor unexpected events took place along the campaign.

For what concerns the heat balance instead, electric furnaces lack of both Q_{ng} and Q_{ex}. Hence, it is simply:

$$Q_{ee} = Q_{s,l,h} + Q_{r,p} \qquad [2.\ 12]$$

By evaluating $Q_{s,l,h} + Q_{r,p}$ with the equations introduced in paragraph 2.1.2, it is possible to tell how the overall heat input depends on both pull and cullet. The considered range for cullet and pull are:

$$\begin{cases} 25 < \text{Cullet } \% < 65 \\ 20 < \text{Pull } \left[\frac{\text{ton}}{\text{d}}\right] < 60 \end{cases}$$

Results are tabulated and plotted hereinafter:

$Q_{s,b,l} + Q_r + Q_p \left[\frac{kWh}{kg_{glass}}\right]$									
Pull	**Cullet [%]**								
[ton/d]	**25**	**30**	**35**	**40**	**45**	**50**	**55**	**60**	**65**
20	1,20	1,20	1,19	1,19	1,18	1,18	1,17	1,17	1,16
25	1,10	1,09	1,09	1,08	1,08	1,07	1,07	1,06	1,06
30	1,03	1,02	1,02	1,01	1,01	1,00	1,00	1,00	0,99
35	0,98	0,97	0,97	0,96	0,96	0,96	0,95	0,95	0,94
40	0,94	0,94	0,93	0,93	0,92	0,92	0,91	0,91	0,90
45	0,91	0,91	0,90	0,90	0,89	0,89	0,88	0,88	0,87
50	0,89	0,89	0,88	0,88	0,87	0,87	0,86	0,86	0,85
55	0,87	0,87	0,86	0,86	0,85	0,85	0,84	0,84	0,83
60	0,86	0,85	0,85	0,84	0,84	0,83	0,83	0,82	0,82

***Table 2** - total heat input as a function of pull and cullet*

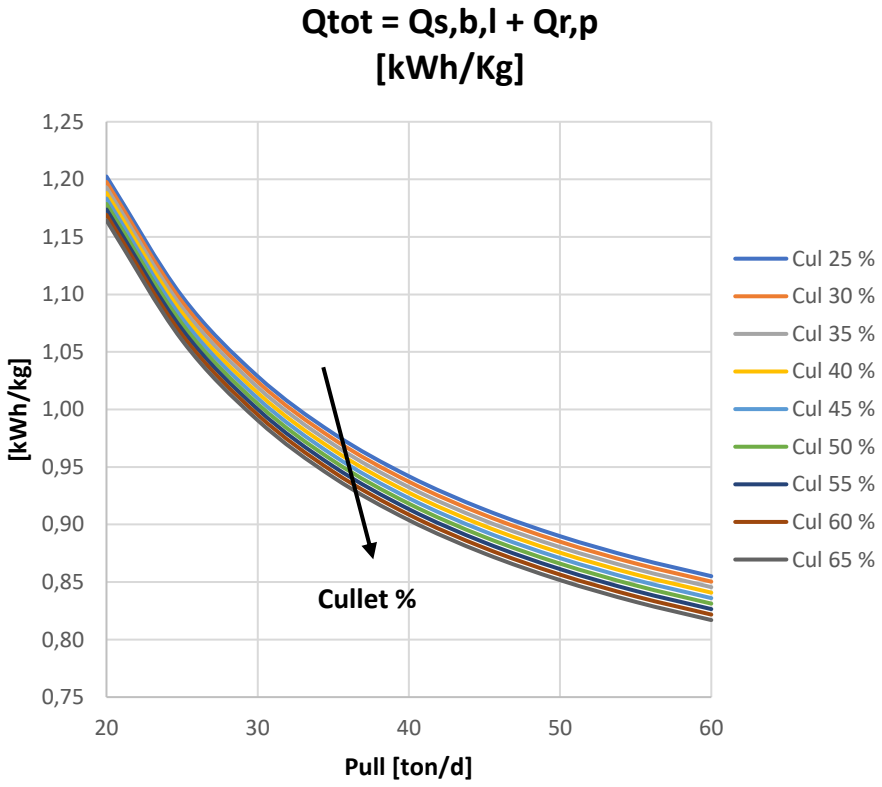

***Figure 15** - total heat input for electric furnace as a function of cullet and pull*

As one would expect, the energy input required decreases as the cullet share in the batch is increased because of a lower demand for the reactions within the melting glass. Besides, the specific energy input lowers significantly when the furnace is operated at high tonnage, which is on the one hand obvious since the denominator is higher. However, this could also be explained by considering that such a furnace conduction keeps the temperature of the chamber at high and stable levels thanks to a significant thermal inertia, whereas at low tonnages the temperature tends to decrease faster thus leading to higher specific energetic demand.

Regarding carbon emissions, being fully electric, only those due to the process are expected:

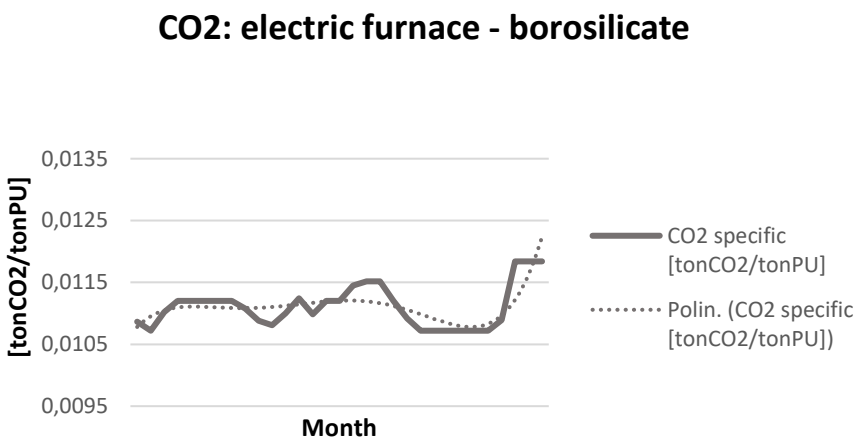

Figure 16 - *specific CO_2 emissions for electric furnace*

The trend is quite stable for the specific emissions as they are mainly a function of cullet and pull which are typically kept within given values.

Last but not least, CO_2 emissions are evaluated while letting cullet and pullet vary:

$\mathbf{CO_2}\left[\frac{\mathbf{ton_{CO_2}}}{\mathbf{d}}\right]$									
PULL	**CULLET [%]**								
[ton/d]	**25**	**30**	**35**	**40**	**45**	**50**	**55**	**60**	**65**
20	0,24	0,22	0,21	0,19	0,18	0,16	0,14	0,13	0,11
25	0,30	0,28	0,26	0,24	0,22	0,20	0,18	0,16	0,14
30	0,36	0,34	0,31	0,29	0,26	0,24	0,22	0,19	0,17
35	0,42	0,39	0,36	0,34	0,31	0,28	0,25	0,22	0,20
40	0,48	0,45	0,42	0,38	0,35	0,32	0,29	0,26	0,22
45	0,54	0,50	0,47	0,43	0,40	0,36	0,32	0,29	0,25
50	0,60	0,56	0,52	0,48	0,44	0,40	0,36	0,32	0,28
55	0,66	0,62	0,57	0,53	0,48	0,44	0,40	0,35	0,31
60	0,72	0,67	0,62	0,58	0,53	0,48	0,43	0,38	0,34

Table 3 – *total CO_2 for electric furnace as a function of cullet and pull*

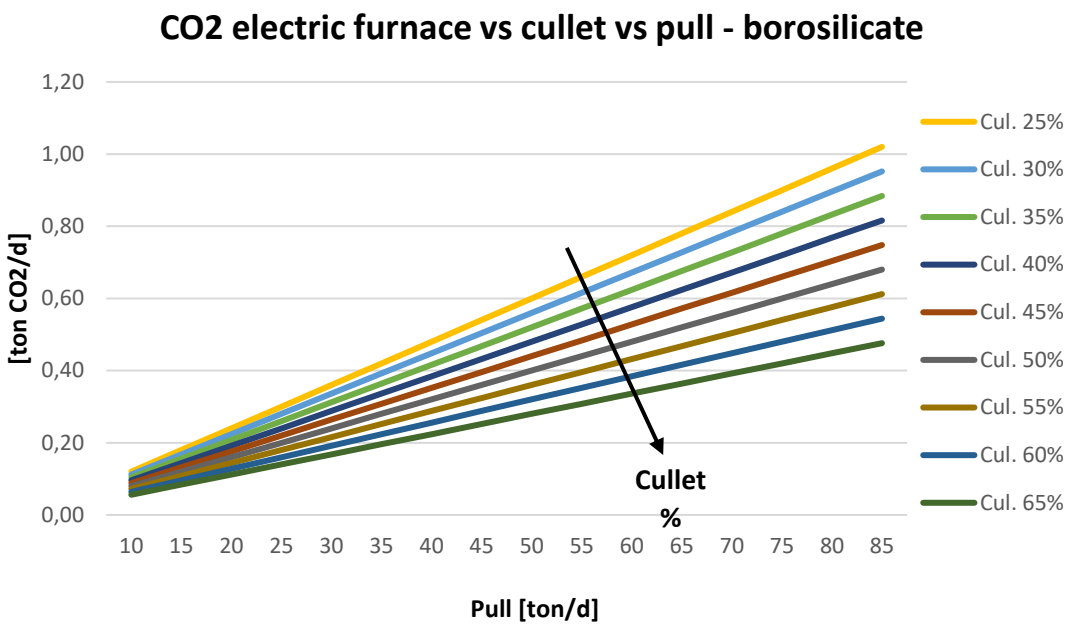

Figure 17 – *total CO_2 for electric furnace as a function of cullet and pull*

As one would expect when the cullet share is raised then the carbon emission decreases, at fixed cullet, being the carbon content in the batch reduced. Analogously, once set the cullet, emissions intensify if the pull increases.
It is interesting to note that trends are linear but with different slopes due to different cullet.

2.2.2: Cyclope furnace

Regarding the energy efficiency index:

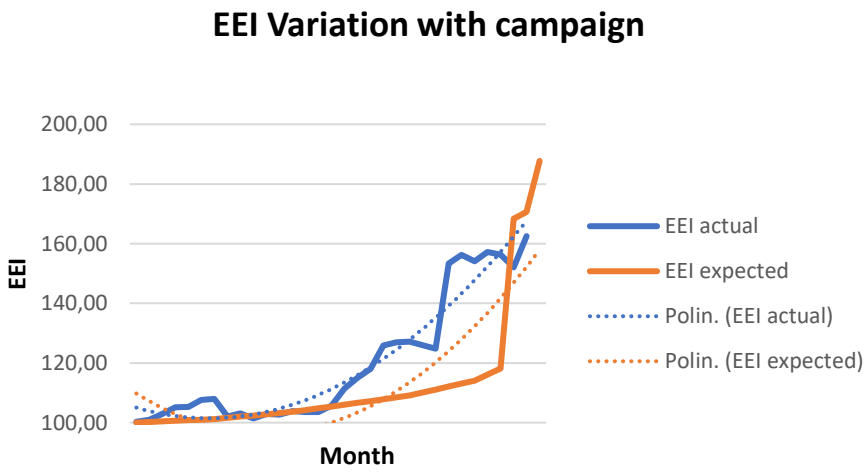

Figure 18 *- EEI Cyclope furnace*

As it can be observed, the expected behaviour would be quite linear for a long extent of the campaign, however towards the very last months of operation the index skyrockets. Such a phenomena is actually to be forecasted because of the highly corrosive tendency of the borosilicate components in the flue gases. However, such a condition of heavy corrosion might be reached in advance than the forecasts tell.

Let's now come to the heat balance:

$$Q_{ee} + Q_{ng} = Q_{s,l,h} + Q_{r,p} + Q_{ex}$$

[2. 13]

Again, by evaluating $Q_{s,l,h} + Q_{r,p}$ it is possible to tell how pull and cullet influence such a heat flow. The range for cullet and pull is:

$$\begin{cases} 20 < \text{Cullet } \% < 60 \\ 10 < \text{Pull } \left[\dfrac{\text{ton}}{\text{d}}\right] < 50 \end{cases}$$

Results are tabulated and plotted hereinafter:

$Q_{s,l,h} + Q_{r,p}\ \left[\frac{kWh}{kg_{glass}}\right]$									
PULL	**CULLET [%]**								
[ton/d]	**20**	**25**	**30**	**35**	**40**	**45**	**50**	**55**	**60**
10	3,04	3,04	3,03	3,03	3,02	3,02	3,01	3,01	3,00
15	2,28	2,27	2,27	2,26	2,26	2,25	2,25	2,24	2,24
20	1,90	1,89	1,89	1,88	1,88	1,87	1,87	1,86	1,86
25	1,67	1,66	1,66	1,65	1,65	1,64	1,64	1,63	1,63
30	1,52	1,51	1,51	1,50	1,50	1,49	1,49	1,48	1,48
35	1,41	1,40	1,40	1,39	1,39	1,38	1,38	1,37	1,37
40	1,33	1,32	1,32	1,31	1,31	1,30	1,30	1,29	1,29
45	1,26	1,26	1,25	1,25	1,24	1,24	1,23	1,23	1,22
50	1,21	1,21	1,20	1,20	1,19	1,19	1,18	1,18	1,17

***Table 4** - $Q_{s,l,h} + Q_{r,p}$ for cyclope furnace as a function of pull and cullet*

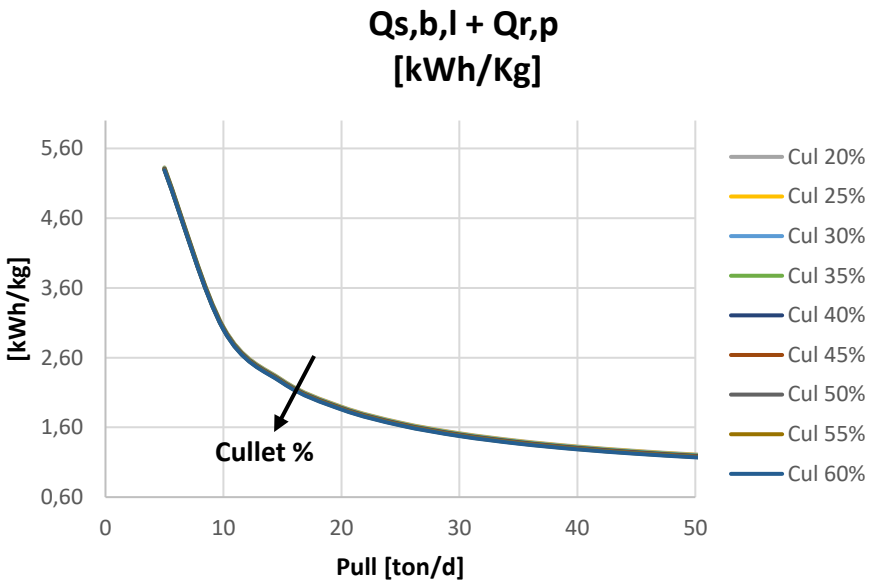

***Figure 19** - $Q_{s,l,h}$ + $Q_{r,p}$ for Cyclope furnace as a function of pull and cullet*

This time, at fixed pull, cullet is not playing a major role. Anyway, the higher it is the lower the heat flow. It is definitely more relevant the role played by the pull, and again it is confirmed that operating at high tonnage is energetically more convenient.

The next step is to apply the equations explained in paragraph 2.1.2 to first compute the heat available in the exhaust gas and, secondly, the natural gas demand. Although such a result has been achieved for any pull, cullet and electric input, here below are tabulated and plotted the outcomes when the furnace is operated around its design pull. Therefore, here is the resulting fuel demand as a function of cullet and electric input:

NG [sm3/d]									
Q EE	**CULLET [%]**								
[kWh/kg]	**20**	**25**	**30**	**35**	**40**	**45**	**50**	**55**	**60**
0,000	6401,0	6383,0	6366,0	6349,0	6332,0	6315,0	6298,0	6281,0	6264,0
0,058	6204,0	6187,0	6170,0	6153,0	6136,0	6119,0	6102,0	6085,0	6068,0
0,116	6009,0	5991,0	5974,0	5957,0	5940,0	5923,0	5906,0	5889,0	5872,0
0,174	5812,0	5795,0	5778,0	5761,0	5744,0	5727,0	5710,0	5693,0	5676,0
0,233	5616,0	5599,0	5582,0	5565,0	5548,0	5531,0	5514,0	5497,0	5480,0
0,291	5420,0	5403,0	5386,0	5369,0	5352,0	5335,0	5318,0	5300,0	5283,0
0,349	5224,0	5207,0	5190,0	5173,0	5156,0	5138,0	5121,0	5104,0	5087,0
0,407	5028,0	5011,0	4994,0	4976,0	4959,0	4942,0	4925,0	4908,0	4891,0
0,465	4832,0	4814,0	4797,0	4780,0	4763,0	4746,0	4729,0	4712,0	4695,0
0,523	4635,0	4618,0	4601,0	4584,0	4567,0	4550,0	4533,0	4516,0	4499,0
0,581	4439,0	4422,0	4405,0	4388,0	4371,0	4354,0	4337,0	4320,0	4303,0
0,640	4243,0	4226,0	4209,0	4192,0	4175,0	4158,0	4141,0	4124,0	4107,0
0,698	4047,0	4030,0	4013,0	3996,0	3979,0	3962,0	3945,0	3928,0	3911,0
0,756	3851,0	3834,0	3817,0	3800,0	3783,0	3766,0	3749,0	3731,0	3714,0
0,814	3655,0	3638,0	3621,0	3604,0	3587,0	3569,0	3552,0	3535,0	3518,0

***Table 5** - Natural gas demand for a Cyclope furnace as a function of cullet and electric input at design pull*

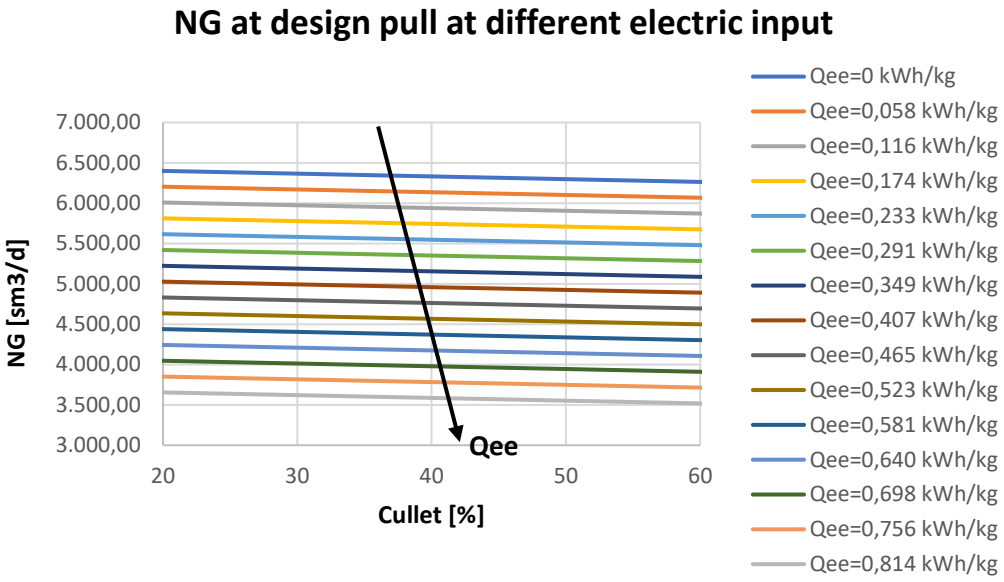

***Figure 20** - Natural gas demand for a Cyclope furnace as a function of cullet and electric input at design pull*

As one would expect, the trend of natural gas consumption is decreasing with both electric input and cullet increasing. Moreover, a large difference exists between employing boosters or not, which means that electric input plays an important role in the overall heat demand of the furnace. Therefore, it is reasonable to expect that direct carbon emissions could be strongly reduced by switching to a more intense utilisation of electric boosters.

Let's now discuss about CO_2. Being hybrid, Cyclope furnaces emit due to combustion and the process itself. Along the campaign, the specific emissions behaved as plotted:

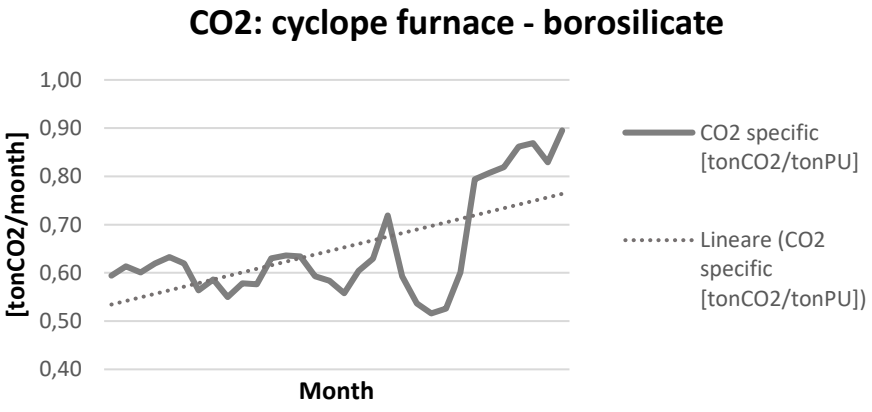

***Figure 21** - specific CO_2 emissions for a cyclope furnace*

Despite the fluctuations, due to how the furnace has been conducted, it is possible to state that the tendency (dotted lines) is linear. Moreover, regardless the pull changes, which are obviously possible along the campaign, it is expected an increase in the specific emissions because of an increase in fuel demand to cope with the furnace ageing.

Eventually, CO_2 emissions are evaluated around the design pull while letting cullet and electric input vary:

$CO_2 \left[\frac{ton_{CO_2}}{d}\right]$									
Q EE	**CULLET [%]**								
[kWh/kg]	**20**	**25**	**30**	**35**	**40**	**45**	**50**	**55**	**60**
0,000	12,96	12,91	12,86	12,81	12,76	12,71	12,66	12,61	12,56
0,058	12,57	12,52	12,47	12,42	12,37	12,32	12,27	12,22	12,17
0,116	12,18	12,13	12,08	12,03	11,98	11,93	11,88	11,83	11,78
0,174	11,79	11,74	11,69	11,64	11,59	11,54	11,49	11,44	11,39
0,233	11,40	11,35	11,30	11,25	11,20	11,15	11,10	11,05	11,00
0,291	11,01	10,96	10,91	10,86	10,81	10,76	10,71	10,66	10,61
0,349	10,62	10,57	10,52	10,47	10,42	10,37	10,32	10,27	10,22
0,407	10,23	10,18	10,13	10,08	10,03	9,98	9,93	9,88	9,83
0,465	9,84	9,79	9,74	9,69	9,64	9,59	9,54	9,49	9,44
0,523	9,45	9,40	9,35	9,30	9,25	9,20	9,15	9,10	9,05
0,581	9,06	9,01	8,96	8,91	8,86	8,81	8,76	8,72	8,67
0,640	8,67	8,63	8,58	8,53	8,48	8,43	8,38	8,33	8,28
0,698	8,29	8,24	8,19	8,14	8,09	8,04	7,99	7,94	7,89
0,756	7,90	7,85	7,80	7,75	7,70	7,65	7,60	7,55	7,50
0,814	7,51	7,46	7,41	7,36	7,31	7,26	7,21	7,16	7,11

***Table 6** - CO_2 emissions for a Cyclope furnace as a function of cullet and electric input at design pull*

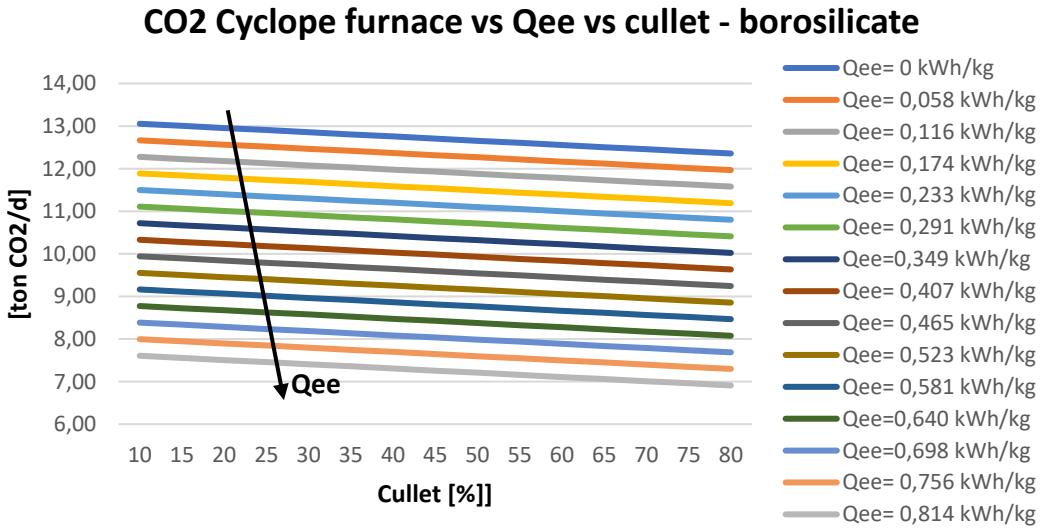

***Figure 22** - CO_2 emissions for a Cyclope furnace as a function of cullet and electric input at design pull*

The results are aligned with those of the heat balance, showing the same trend that was achieved regarding the consumption on natural gas. Indeed, the model shows that strong direct carbon emission could be avoided if the furnace was operated at higher electric input.

2.3: Comparison among soda - lime furnaces

The case of soda-lime is investigated on the base of data coming from two different types of furnaces: end port and unit melter.
Not surprisingly, the length of the considered campaigns is way longer than that registered by borosilicate glass furnaces. It is worth it to pay attention on that, because it allows to understand why soda-lime furnaces are way bigger in terms of size and pull: around 200-250 tonne per day, whereas borosilicate furnaces deal with around 10 – 80.
Therefore, it would not be economically advisable to invest in borosilicate furnaces of such huge dimensions and short lifetime, whereas for soda-lime these are currently employed.

2.3.1: End port furnace

As for the energy efficiency index:

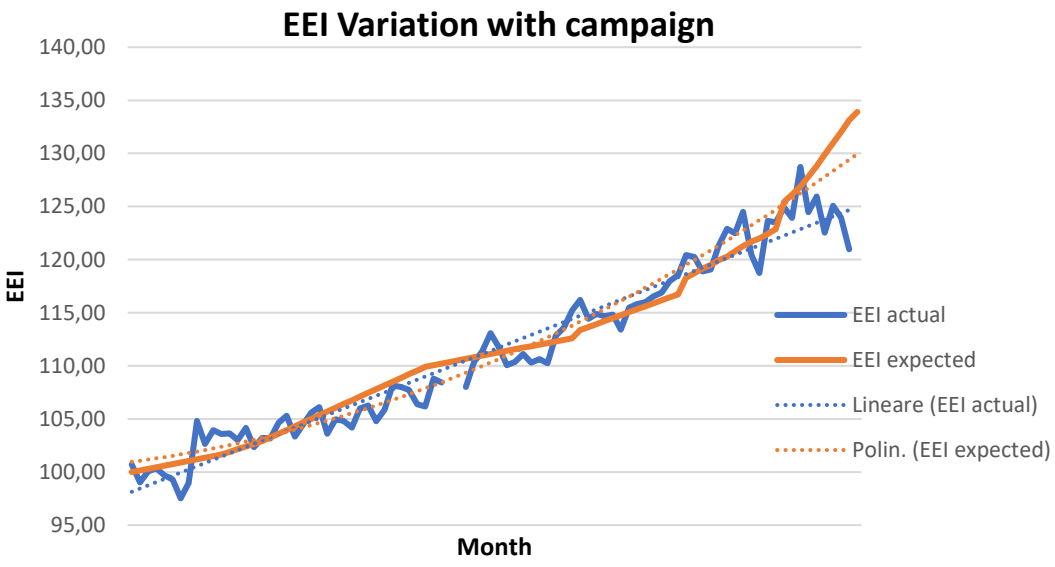

Figure 23 *- EEI end port furnace*

For what concerns the expected behaviour, end port furnaces show linear trend for most of their life. Towards the end instead, EEI increases faster.
Regarding the actual behaviour, fluctuations are expected due to changes in furnace operating conditions. However, the curve is reasonably close to its expected behaviour, which is good and desirable.

Dealing with the energy balance, it holds that:

$$Q_{ee} + Q_{ng} = Q_{s,l,h} + Q_{r,p} + Q_{ex}$$

[2. 14]

Again $Q_{s,l,h} + Q_{r,p}$ are evaluated against pull and cullet, and data are shown in the table and plot below. The range considered is:

$$\begin{cases} 25 < \text{cullet } \% < 70 \\ 115 < \text{pull } \left[\frac{\text{ton}}{\text{d}}\right] < 170 \end{cases}$$

$Q_{s,l,h} + Q_{r,p} \left[\frac{kWh}{kg_{glass}}\right]$										
PULL	**CULLET [%]**									
[ton/d]	**25**	**30**	**35**	**40**	**45**	**50**	**55**	**60**	**65**	**70**
115	1,05	1,04	1,03	1,02	1,01	1,01	1,00	0,99	0,98	0,97
120	1,03	1,03	1,02	1,01	1,00	0,99	0,98	0,97	0,97	0,96
125	1,02	1,01	1,00	1,00	0,99	0,98	0,97	0,96	0,95	0,95
130	1,01	1,00	0,99	0,98	0,98	0,97	0,96	0,95	0,94	0,93
135	1,00	0,99	0,98	0,97	0,97	0,96	0,95	0,94	0,93	0,92
140	0,99	0,98	0,97	0,96	0,96	0,95	0,94	0,93	0,92	0,91
145	0,98	0,97	0,96	0,95	0,95	0,94	0,93	0,92	0,91	0,90
150	0,97	0,96	0,95	0,95	0,94	0,93	0,92	0,91	0,90	0,89
155	0,96	0,95	0,95	0,94	0,93	0,92	0,91	0,90	0,89	0,89
160	0,96	0,95	0,94	0,93	0,92	0,91	0,90	0,90	0,89	0,88
165	0,95	0,94	0,93	0,92	0,91	0,91	0,90	0,89	0,88	0,87
170	0,94	0,93	0,92	0,92	0,91	0,90	0,89	0,88	0,87	0,86

***Table 7** - $Q_{s,l,h} + Q_{r,p}$ for end port furnace as a function of pull and cullet*

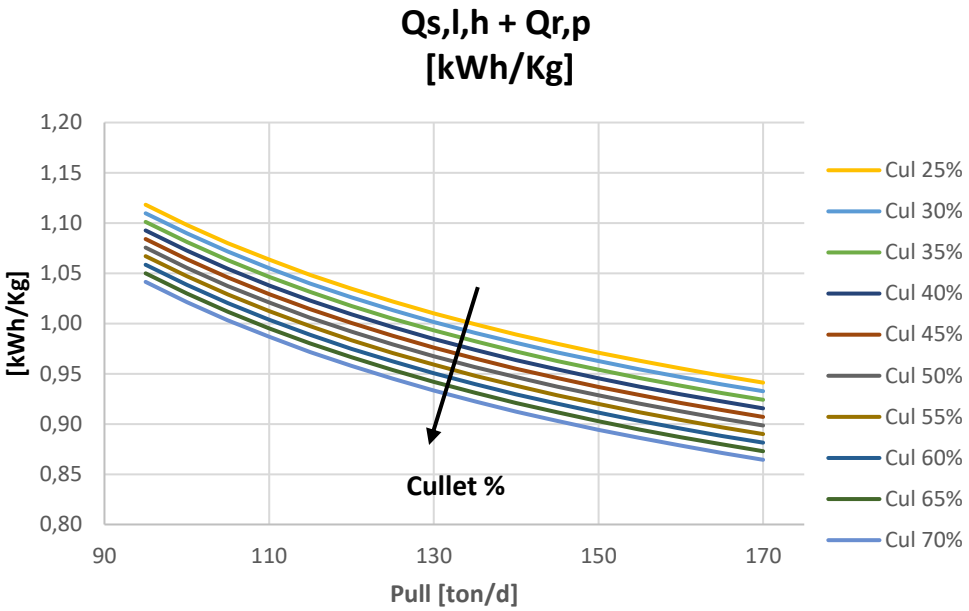

Figure 24 *- $Q_{s,l,h}$ + $Q_{r,p}$ for end port furnace as a function of pull and cullet*

Both cullet and pull play an important role in the energetic demand, which can be reduced either increasing the former or by conducting the furnace at high tonnage.

Second step is to estimate the natural gas demand. Similarly to the case of Cyclope furnace, the fuel consumption has been computed for any pull, cullet and electric input. Out of these data have been extracted those which belong to a tonnage around the design value, for the considered furnace.

Therefore, **Table 8** and plot **Figure 25** show the gas demand around that condition against electric input and cullet:

NG [sm3/d]										
Q EE	**CULLET [%]**									
[kWh/kg]	**25**	**30**	**35**	**40**	**45**	**50**	**55**	**60**	**65**	**70**
0,000	19.006	18.842	18.678	18.514	18.351	18.187	18.023	17.859	17.695	17.531
0,029	18.448	18.284	18.120	17.956	17.792	17.628	17.464	17.300	17.136	16.972
0,058	17.889	17.725	17.561	17.397	17.233	17.070	16.906	16.742	16.578	16.414
0,087	17.331	17.167	17.003	16.839	16.675	16.511	16.347	16.183	16.019	15.855
0,116	16.772	16.608	16.444	16.280	16.116	15.952	15.789	15.625	15.461	15.297
0,145	16.214	16.050	15.886	15.722	15.558	15.394	15.230	15.066	14.902	14.738
0,174	15.655	15.491	15.327	15.163	14.999	14.835	14.671	14.508	14.344	14.180
0,203	15.096	14.933	14.769	14.605	14.441	14.277	14.113	13.949	13.785	13.621
0,233	14.538	14.374	14.210	14.046	13.882	13.718	13.554	13.391	13.227	13.063
0,262	13.979	13.816	13.652	13.488	13.324	13.160	12.996	12.832	12.668	12.504
0,291	13.421	13.257	13.093	12.929	12.765	12.601	12.437	12.273	12.110	11.946

Table 8 *- Natural gas demand for an end port furnace as a function of cullet and electric input at design pull*

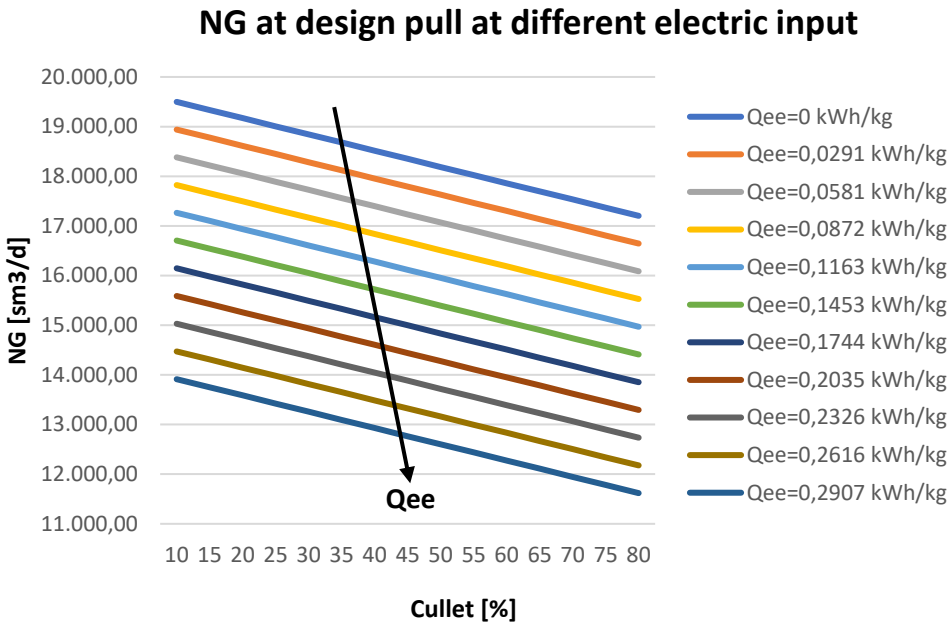

***Figure 25** - Natural gas demand for an end port furnace as a function of cullet and electric input at design pull*

Results are once again aligned with the expectations, as well as with the outcomes of the Cyclope furnace: natural gas demand decreases as cullet and electric input intensify. Besides, a considerable difference lays between each level of booster.

For what concerns the carbon emissions, along the campaign these are the collected data coming from both natural gas combustion and process:

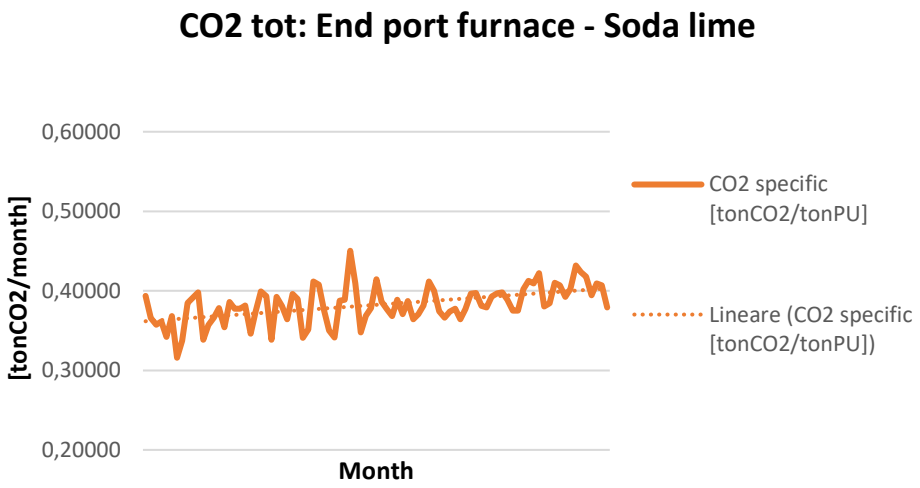

***Figure 26** - specific CO_2 emissions for an end port furnace*

What emerges is aligned with the expectations: both total and specific emissions increase along the campaign, which is a consequence of the furnace ageing inducing a greater fuel consumption.

To conclude, emissions are evaluated, at design pull, against electric input and cullet:

$CO_2 \left[\frac{ton_{CO_2}}{d}\right]$										
Q EE	**CULLET [%]**									
[kWh/kg]	**25**	**30**	**35**	**40**	**45**	**50**	**55**	**60**	**65**	**70**
0,000	56,75	55,15	53,56	51,96	50,37	48,78	47,18	45,59	43,99	42,40
0,029	55,64	54,05	52,45	50,86	49,26	47,67	46,07	44,48	42,88	41,29
0,058	54,53	52,94	51,34	49,75	48,15	46,56	44,96	43,37	41,78	40,18
0,087	53,42	51,83	50,23	48,64	47,05	45,45	43,86	42,26	40,67	39,07
0,116	52,32	50,72	49,13	47,53	45,94	44,34	42,75	41,15	39,56	37,96
0,145	51,21	49,61	48,02	46,42	44,83	43,23	41,64	40,05	38,45	36,86
0,174	50,10	48,50	46,91	45,32	43,72	42,13	40,53	38,94	37,34	35,75
0,203	48,99	47,40	45,80	44,21	42,61	41,02	39,42	37,83	36,23	34,64
0,233	47,88	46,29	44,69	43,10	41,50	39,91	38,32	36,72	35,13	33,53
0,262	46,77	45,18	43,59	41,99	40,40	38,80	37,21	35,61	34,02	32,42
0,291	45,67	44,07	42,48	40,88	39,29	37,69	36,10	34,51	32,91	31,32

***Table 9** - CO_2 emissions for an end port furnace as a function of cullet and electric input at design pull*

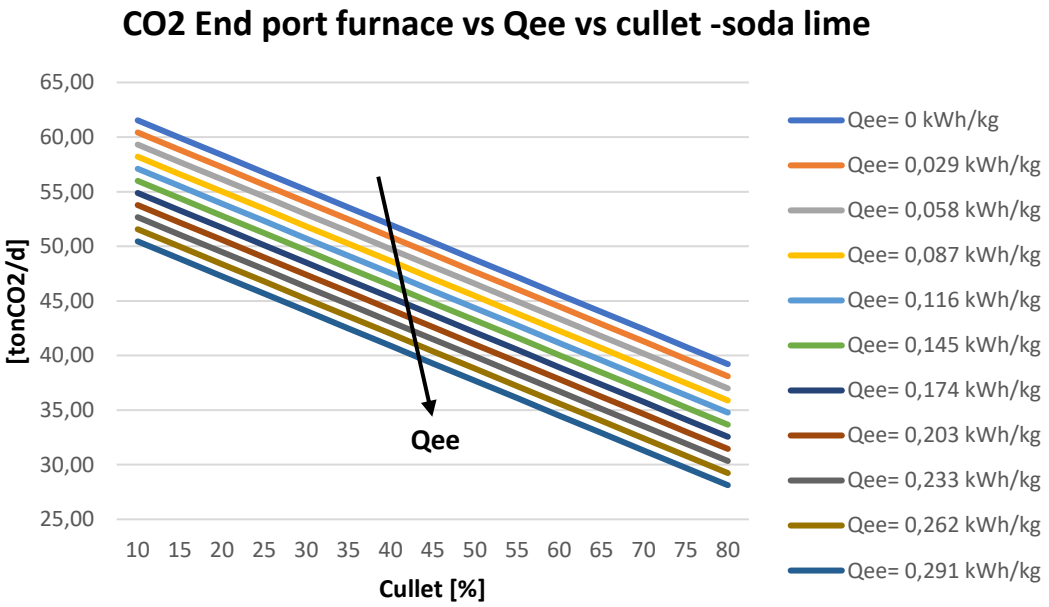

***Figure 27** - CO_2 emissions for an end port furnace as a function of cullet and electric input at design pull*

Once again, the model allows to state the direct CO_2 emissions are strongly related to cullet and boosters, and large amount could be potentially saved by operating at higher electric input.

2.3.2: Unit melter furnace

The energy efficiency index plot is shown below:

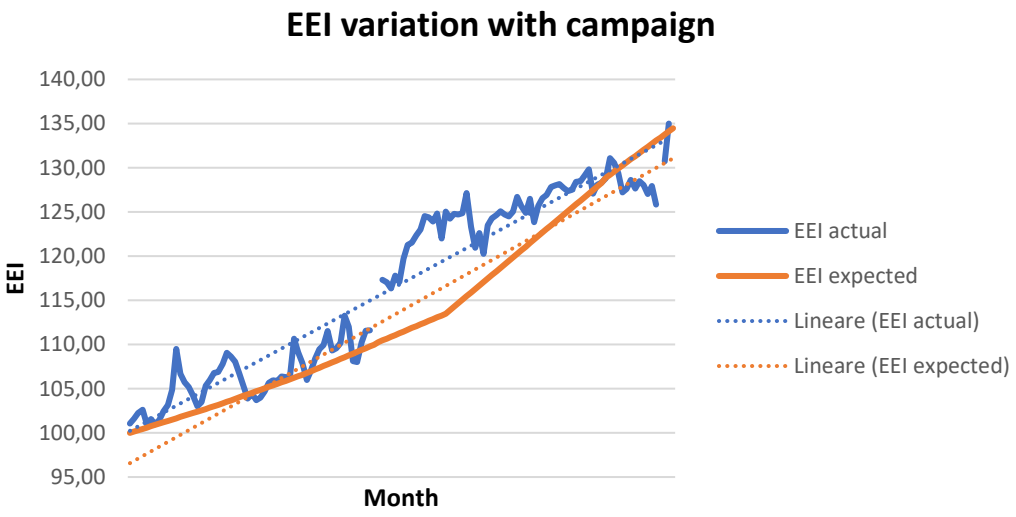

Figure 28 *- EEI unit melter furnace*

The trend is expected linear, with a slope that increases significantly after the half of the furnace lifetime. Even though the actual behaviour turns out to be above the expected with a not negligible fluctuation tendency, which is likely a consequence of the furnace conduction due to changes in the production plan, the trend line - blue dotted line – is parallel to that of the expected behaviour. This confirms the goodness of the forecasts of the furnace energetic behaviour of the unit melter.

For what concerns the heat balance instead, it holds:

$$Q_{ee} + Q_{ng} = Q_{s,l,h} + Q_{r,p} + Q_{ex}$$

[2. 15]

Again $Q_{s,l,h} + Q_{r,p}$ are evaluated against pull and cullet, whose values are taken in the range:

$$\begin{cases} 25 < \text{cullet } \% < 70 \\ 115 < \text{pull } \left[\frac{\text{ton}}{\text{d}}\right] < 170 \end{cases}$$

$Q_{s,l,h} + Q_{r,p} \left[\frac{kWh}{kg_{glass}}\right]$										
PULL	**CULLET [%]**									
[ton/d]	**25**	**30**	**35**	**40**	**45**	**50**	**55**	**60**	**65**	**70**
115	1,05	1,04	1,03	1,02	1,02	1,01	1,00	0,99	0,99	0,98
120	1,03	1,03	1,02	1,01	1,00	0,99	0,99	0,98	0,97	0,96
125	1,02	1,01	1,00	1,00	0,99	0,98	0,97	0,97	0,96	0,95
130	1,01	1,00	0,99	0,98	0,98	0,97	0,96	0,95	0,95	0,94
135	1,00	0,99	0,98	0,97	0,96	0,96	0,95	0,94	0,93	0,93
140	0,98	0,98	0,97	0,96	0,95	0,95	0,94	0,93	0,92	0,92
145	0,97	0,97	0,96	0,95	0,94	0,94	0,93	0,92	0,91	0,91
150	0,97	0,96	0,95	0,94	0,93	0,93	0,92	0,91	0,90	0,90
155	0,96	0,95	0,94	0,93	0,93	0,92	0,91	0,90	0,89	0,89
160	0,95	0,94	0,93	0,93	0,92	0,91	0,90	0,89	0,89	0,88
165	0,94	0,93	0,93	0,92	0,91	0,90	0,89	0,89	0,88	0,87
170	0,93	0,93	0,92	0,91	0,90	0,89	0,89	0,88	0,87	0,86

***Table 10** - $Q_{s,l,h} + Q_{r,p}$ for a unit melter furnace as a function of pull and cullet*

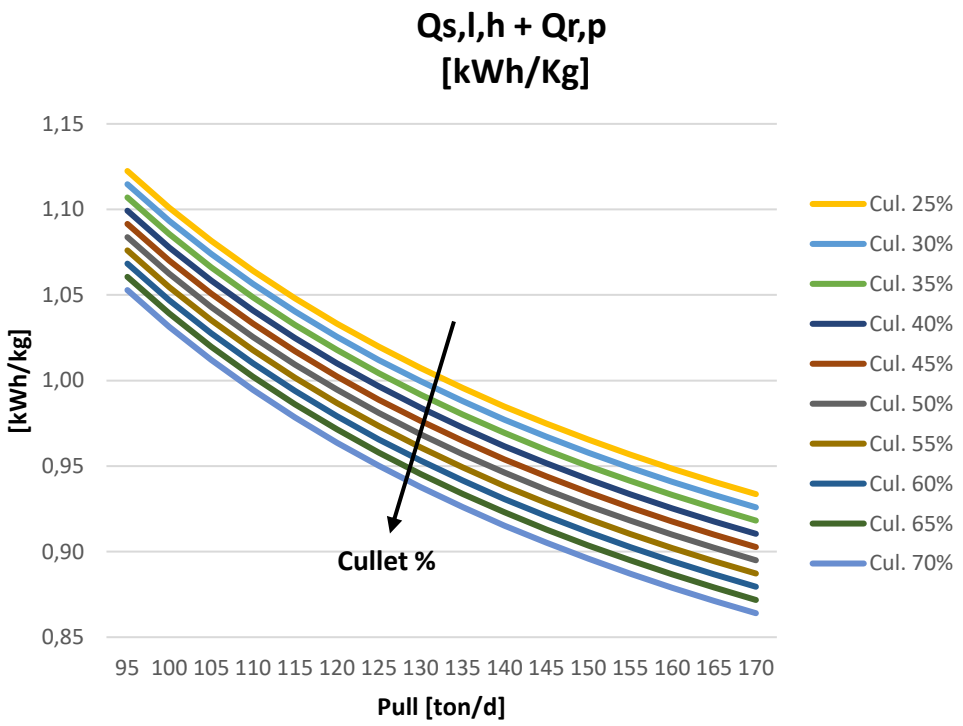

***Figure 29** - $Q_{s,l,h} + Q_{r,p}$ for a unit melter furnace as a function of pull and cullet*

Once again, as cullet and pull increase the specific heat decreases.

The following step is to determine the natural gas demand, which is done for any pull, electric input and cullet. The results shown are referred to the consumption evaluated at the design pull for the furnace and are first collected into the hereinafter table and then plotted:

NG [sm3/d]										
Q EE	CULLET [%]									
[kWh/kg]	25	30	35	40	45	50	55	60	65	70
0,000	22.969	22.789	22.608	22.428	22.248	22.067	21.887	21.707	21.526	21.346
0,029	22.291	22.111	21.930	21.750	21.570	21.389	21.209	21.029	20.848	20.668
0,058	21.613	21.433	21.252	21.072	20.892	20.711	20.531	20.351	20.170	19.990
0,087	20.935	20.755	20.574	20.394	20.214	20.033	19.853	19.673	19.492	19.312
0,116	20.257	20.077	19.896	19.716	19.536	19.355	19.175	18.995	18.814	18.634
0,145	19.579	19.399	19.218	19.038	18.858	18.677	18.497	18.317	18.136	17.956
0,174	18.901	18.721	18.541	18.360	18.180	18.000	17.819	17.639	17.458	17.278
0,203	18.223	18.043	17.863	17.682	17.502	17.322	17.141	16.961	16.781	16.600
0,233	17.545	17.365	17.185	17.004	16.824	16.644	16.463	16.283	16.103	15.922
0,262	16.867	16.687	16.507	16.326	16.146	15.966	15.785	15.605	15.425	15.244
0,291	16.189	16.009	15.829	15.648	15.468	15.288	15.107	14.927	14.747	14.566
0,320	15.511	15.331	15.151	14.970	14.790	14.610	14.429	14.249	14.069	13.888

Table 11 *- Natural gas demand for a unit melter furnace as a function of cullet and electric input at design pull*

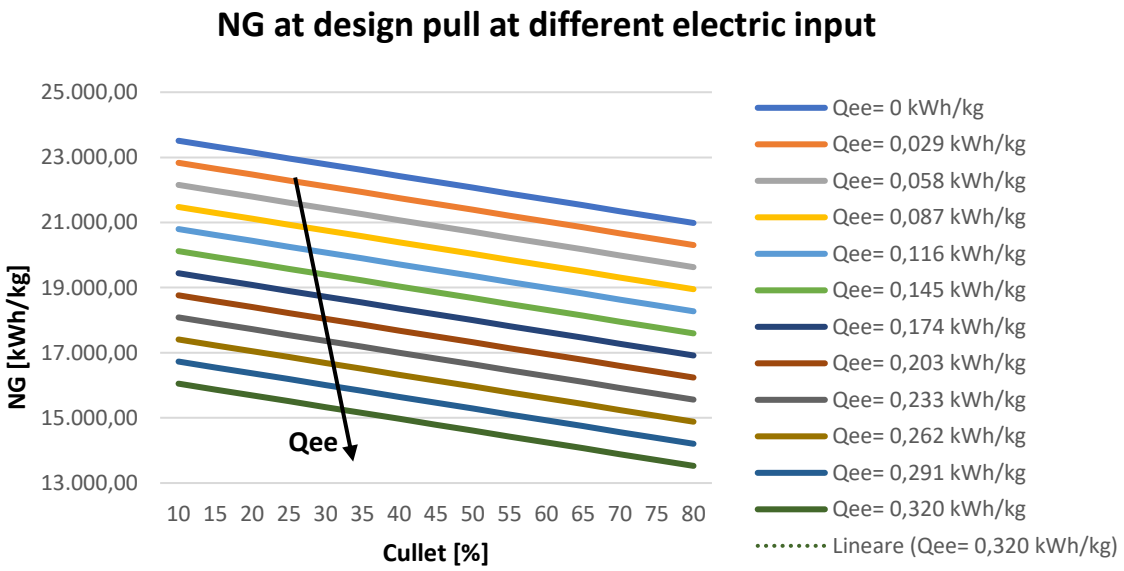

Figure 30 *- Natural gas demand for a unit melter furnace as a function of cullet and electric input at design pull*

Coherently with what one could expect, fuel consumption linearly decreases as cullet, as well as electric input, are increased.

Carbon emissions along the campaign were as shown:

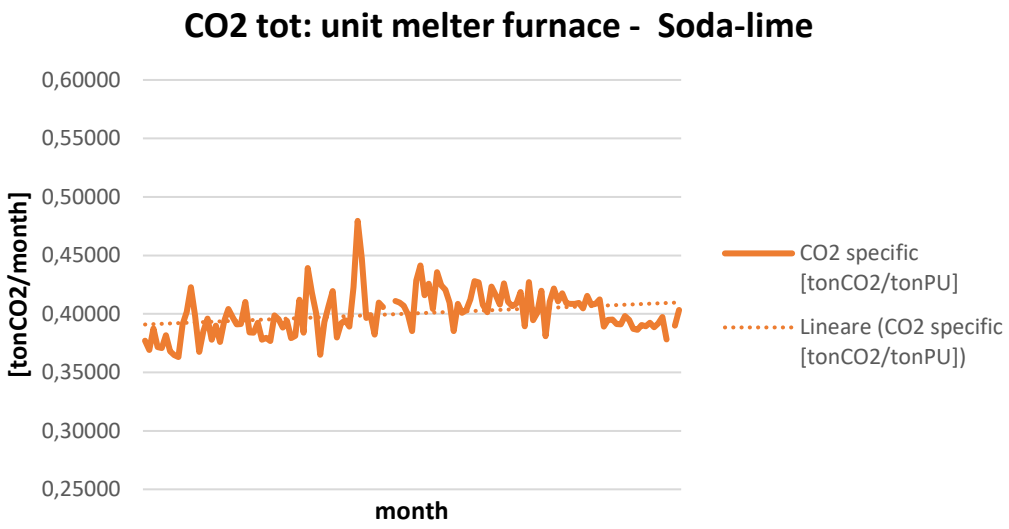

***Figure 31** - specific CO_2 emissions for a unit melter furnace*

Rather fluctuating emissions are registered for both total and specific emissions, which is to be expected as a consequence of the wide oscillations seen in the energy efficiency index, to which correspond a fluctuation of the natural gas burnt too and therefore of the emissions. Besides, the trend is increasing among the campaign as a consequence of the ageing and the increase in energetic demand.

To conclude, emissions are evaluated, at fixed design pull, against electric input and cullet:

$CO_2 \left[\frac{ton_{CO_2}}{d}\right]$										
Q EE	**CULLET [%]**									
[kWh/kg]	**25**	**30**	**35**	**40**	**45**	**50**	**55**	**60**	**65**	**70**
0,000	64,48	62,86	61,24	59,62	58,01	56,39	54,77	53,15	51,53	49,91
0,029	63,13	61,52	59,90	58,28	56,66	55,04	53,42	51,81	50,19	48,57
0,058	61,79	60,17	58,55	56,93	55,32	53,70	52,08	50,46	48,84	47,22
0,087	60,44	58,83	57,21	55,59	53,97	52,35	50,73	49,12	47,50	45,88
0,116	59,10	57,48	55,86	54,24	52,63	51,01	49,39	47,77	46,15	44,53
0,145	57,75	56,14	54,52	52,90	51,28	49,66	48,04	46,43	44,81	43,19
0,174	56,41	54,79	53,17	51,55	49,93	48,32	46,70	45,08	43,46	41,84
0,203	55,06	53,44	51,83	50,21	48,59	46,97	45,35	43,73	42,12	40,50
0,233	53,72	52,10	50,48	48,86	47,24	45,63	44,01	42,39	40,77	39,15
0,262	52,37	50,75	49,14	47,52	45,90	44,28	42,66	41,04	39,43	37,81
0,291	51,03	49,41	47,79	46,17	44,55	42,94	41,32	39,70	38,08	36,46
0,320	49,68	48,06	46,45	44,83	43,21	41,59	39,97	38,35	36,74	35,12

***Table 12** - CO_2 emissions for a unit melter furnace as a function of cullet and electric input at design pull*

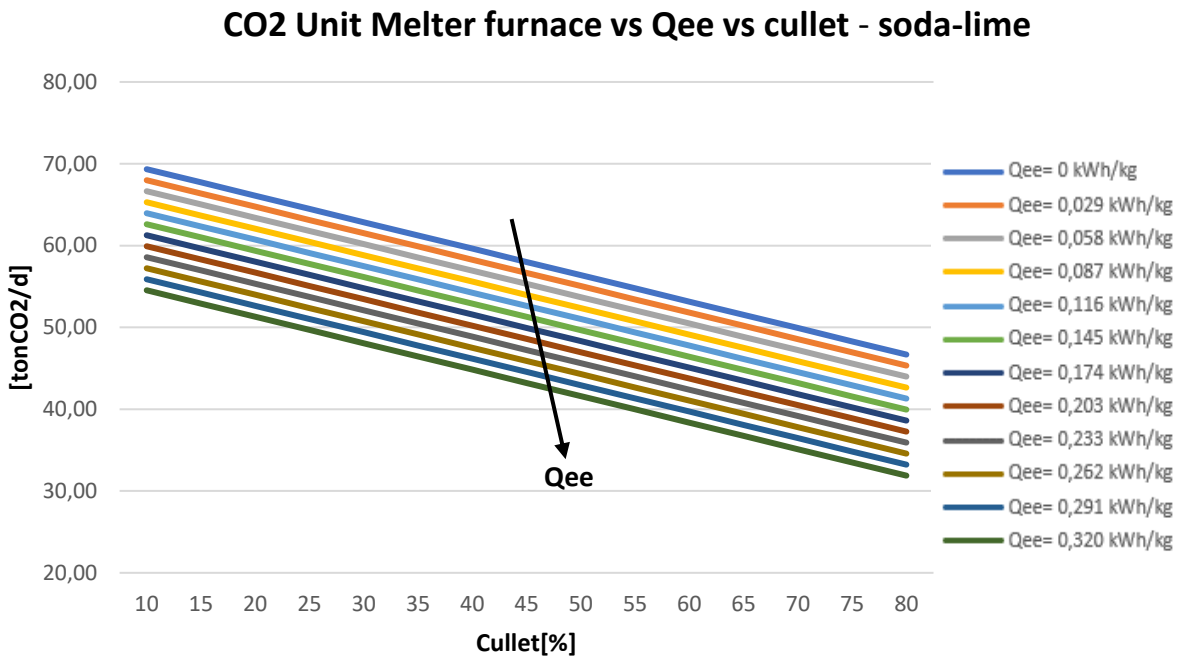

***Figure 32** - CO_2 emissions for a unit melter furnace as a function of cullet and electric input at design pull*

The carbon emissions are expected to be linearly decreasing as cullet and electric input increase. The trend resembles that of natural gas, so that it is possible to state that both fuel and CO_2 could be cut quite significantly if the furnace was conducted with greater electric input and, possibly, high share of cullet.

3. Furnaces comparison for different types of glass

3.1: Approach and method

Within this chapter furnaces are being compared one against the others, on the basis of the data, calculations and plots presented in chapter 2. Again, the idea is to directly compare furnaces producing the same type of glass so to come up with a clear overview of the energetic demand of different technologies and, possibly, to assess which one has a better performance in terms of heat demand and carbon emission.
To conclude, electric and hybrid furnaces are considered: the goal is to show why the former are still not economically competitive with the last years conditions of electricity, natural gas and carbon tax prices.

The discussion is structured as follows:

- Energy efficiency index EEI for different furnaces
- CO_2 emissions for different furnaces
- Heat input Q_{tot} for same glass production (boro/soda-lime) for different furnaces at fixed pull by varying cullet and electric input
- Electric vs hybrid furnace: specific operating cost due to energy supply and carbon emissions

Let's deepen these points.

3.1.1: Energy efficiency index EEI for different furnaces

The idea is to plot on the same plane the EEI of the four furnaces such that it is clear the dynamic behaviour of each along the lifetime, for both expected and actual trends.

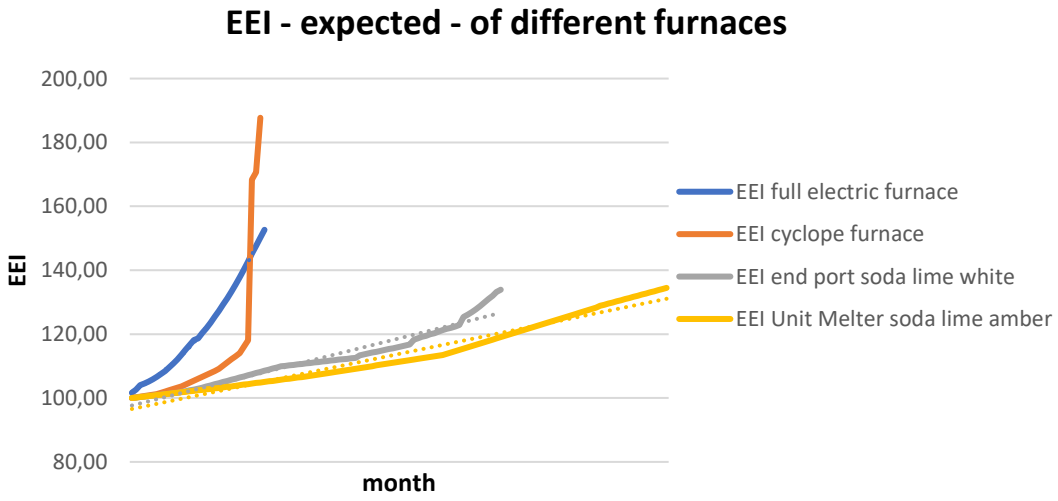

***Figure 33** - Expected EEI for different furnaces*

Trends are those already observed in chapter 2, but it is now immediate to notice that borosilicate glass furnaces (electric, Cyclope), despite a way shorter lifetime, exhibit a way faster worsening of the EEI. Such an expected behaviour is so extreme that soda-lime furnaces (end port, unit melter) might reach a lower EEI at the time of their disposal. On the other way around, it is possible to state that such a shorter lifetime of borosilicate glass furnaces is indeed due to such a poor development of the index.
Actual trends, plotted just below, resemble the estimated tendencies:

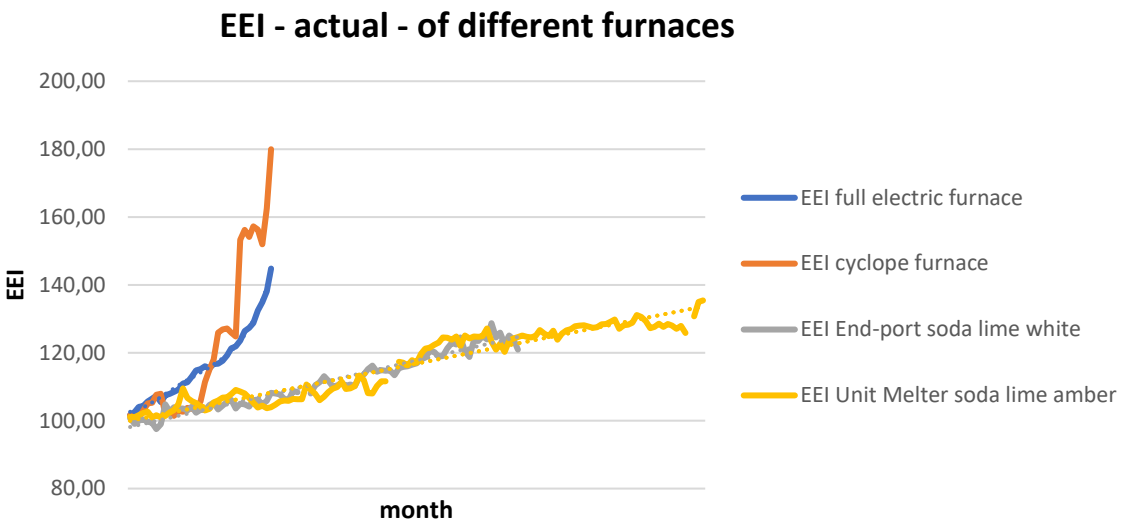

Figure 34 *- Actual EEI for different furnaces*

3.1.2: CO_2 emissions for different furnaces

Direct specific carbon emissions already plotted in chapter 2 for each furnace are now gathered together on the same plane such that it is possible to compare them easily.

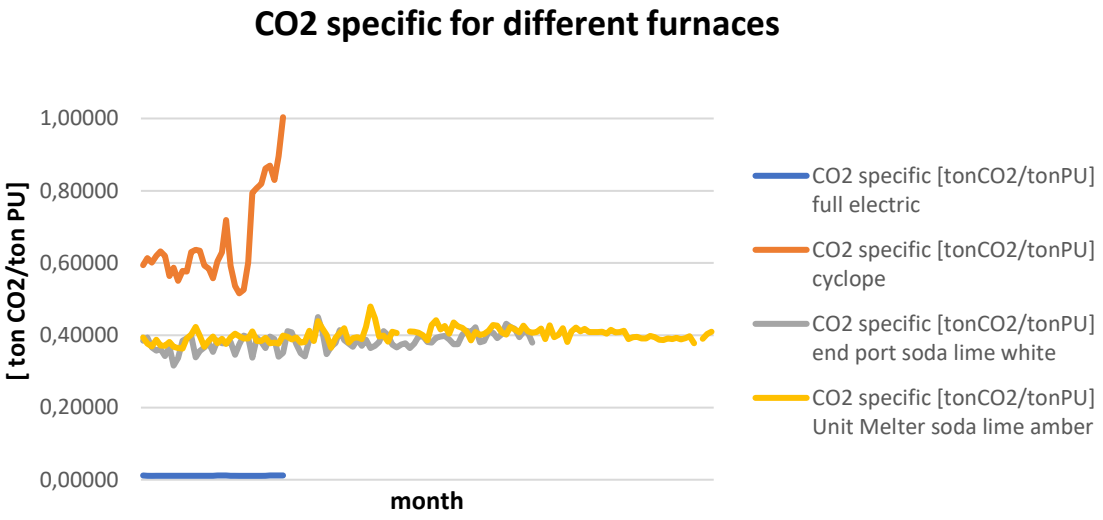

Figure 35 *- specific CO_2 emissions for a unit melter furnace*

The evidence shows that Cyclope furnace has a way higher carbon intensity than end port and unit melter, mainly due to a lower pull, whereas electric furnace has only emissions due to raw materials containing carbonates, and it is basically a negligible yet not avoidable term.

3.1.3: Heat input Q_{tot} for same glass production for different furnaces at fixed pull by varying cullet and Q_{ee}

The goal is to establish the heat input of each furnace for a given glass production, when pull is fixed at the design tonnage for that furnace, as a function of cullet and electric input.
Therefore, for the borosilicate glass the electric and Cyclope furnaces are compared whereas for the soda-lime the end port and unit melter.
On the basis of the electric input, which is considered as a given value, and exploiting the data collected in the tables of chapter two regarding the natural gas required to close the heat balance of each furnace under specific operating conditions, it was possible to establish the total heat input Q_{tot} required:

$$Q_{tot} = Q_{ee} + Q_{ng} \qquad [3.\ 1]$$

$$Q_{tot}\left[\frac{kWh}{kg_{glass}}\right] = \frac{\dot{V}\left[\frac{sm^3}{d}\right] \cdot LHV\left[\frac{kWh}{sm^3}\right]}{Pull\left[\frac{kg_{glass}}{d}\right]} + Q_{ee}\left[\frac{kWh}{kg_{glass}}\right] \qquad [3.\ 2]$$

With Q_{ee} computed as explained in section 2.2.1:

$$Q_{ee} = Q_{s,l,h} + Q_{r,p} \qquad [3.\ 3]$$

Then, the values obtained have been tabulated and plotted. What emerges is the heat input difference between two alternative furnaces producing the same glass under fixed operating conditions.

For the case of **electric** and **Cyclope,** outcomes are as follows:

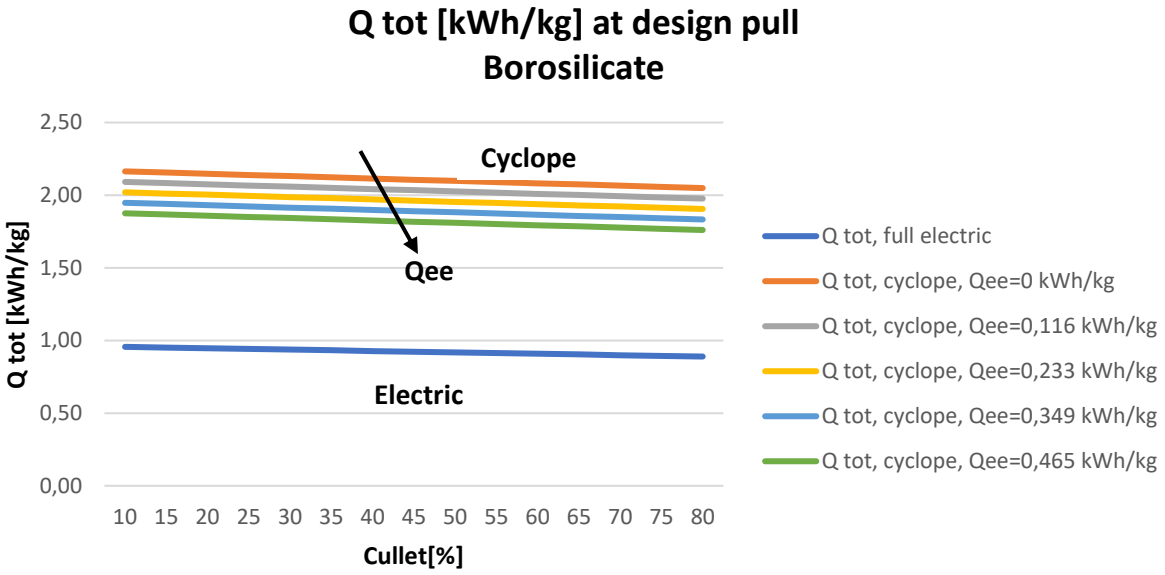

***Figure 36** - total heat input for electric and Cyclope furnace as a function of cullet and electric input, at design pull*

The most relevant information that can be extracted from the plot is on the significant difference in the total heat input between Cyclope and electric furnace, which can even overcome the 100%. Qualitatively, this should not be seen as an unexpected result if one considers that full electric achieves a better heat transfer, being the electrodes submerged in the melting glass. Moreover, the absence of exhaust gases from combustion allows to avoid the loss of a great amount of energy. Therefore, it is reasonable to expect that electric furnaces allow to save a good share of energy for producing the same output.

For the case of **end port** and **unit melter** instead:

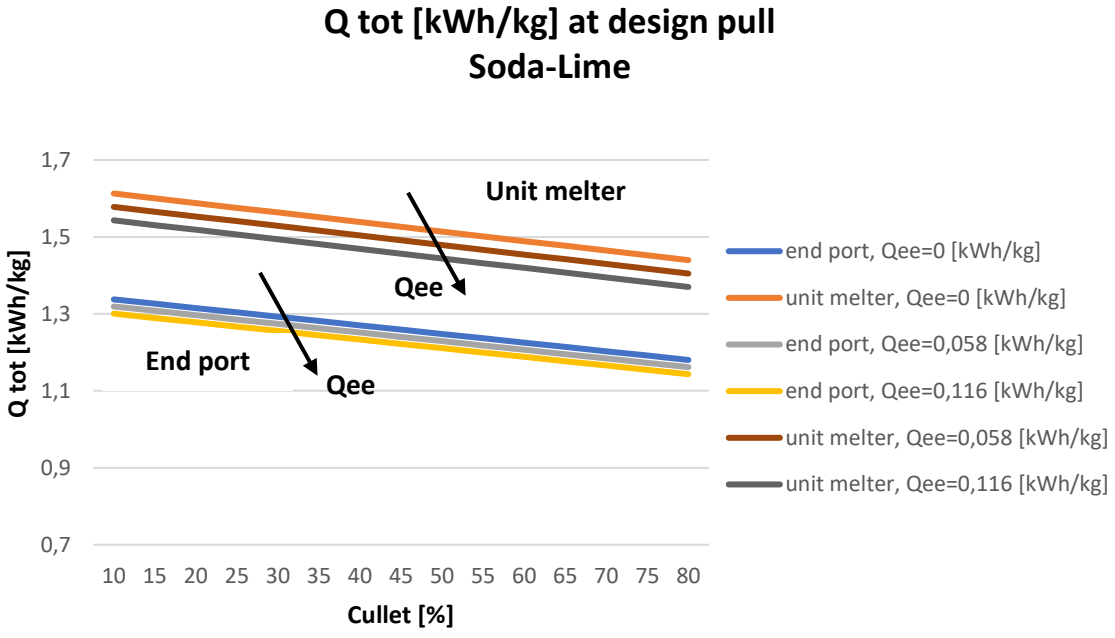

***Figure 37** - total heat input for end port and unit melter furnace as a function of cullet and electric input, at design pull*

What emerges is a clear confirm of the higher thermal efficiency of the end port over the unit melter. Indeed, for instance, the former is characterized by an enhanced value of R, which represents the heat recovery efficiency of the regenerator. Thus, the consequence is that unit melter furnaces require a lower total heat input than unit melter. Therefore, from the energetic viewpoint the end port can be considered as a step forward technology in the hybrid systems panorama.
It is quite straightforward that to an increase of the electric input corresponds a reduction of Q_{tot} , for the abovementioned reasons.

3.1.4: Electric vs hybrid furnace: economic competitiveness and overall carbon emissions

Within this section it is taken into account the difference between electric and hybrid furnaces (Cyclope) in terms of operating cost due to energy supply and carbon emissions. The focus is to try to explain why the hybrid technology, despite being more complex in terms of structure and emissions, is still leading ahead of the full electric.
Furthermore, it is briefly shown the overall carbon footprint of both the furnaces by computing the sum of direct and indirect carbon emissions.
The approach is to observe the trend between 2014 – 2020, in order to justify why full electric has not yet replaced hybrid technology in the recent past[17].
Data regarding costs of natural gas and electricity for industrial customers are taken from ARENA [11], [12] whereas of CO_2 from SENDECO2 [13]:

Year	Natural gas [€/sm3]	Electricity [€/kWh]	Carbon tax [€/tonCO2]
2014	0,3333	0,1538	5,96
2015	0,3046	0,1384	7,68
2016	0,2575	0,1358	5,32
2017	0,2516	0,1298	5,83
2018	0,2878	0,1043	15,88
2019	0,2800	0,1257	24,84
2020	0,2297	0,1082	24,75
Class of consumption	$26.000 < \frac{ksm^3}{year} < 104.000$	$20.000 < \frac{MWh}{year} < 70.000$	

***Table 13** - natural gas, electricity and CO_2 prices between 2014-2020 for industrial customers*

The method employed for the analysis is the following: once set the pull around the design value, compute the operating costs of energy, by means of the estimated volumes of natural gas for given electric input as well as direct emissions due to combustion and raw materials[18] (determined in chapter 2) for each of the considered year, at variable cullet. The outcome is the specific cost for glass production:

[17] From the operating cost perspective. No considerations are here made on other issues such as quality
[18] Electric furnace only has emissions due to raw materials.

$$\text{Cost}\left[\frac{€}{\text{kg}_{\text{glass}}}\right] = \frac{\dot{V}\left[\frac{\text{sm}^3}{\text{d}}\right]\cdot \text{Price}\left[\frac{€}{\text{sm}^3}\right] + \text{EE}\left[\frac{\text{kWh}}{\text{d}}\right]\cdot \text{Price}\left[\frac{€}{\text{kWh}}\right] + \text{CO}_2\left[\frac{\text{ton}_{\text{CO}_2}}{\text{d}}\right]\cdot \text{Price}\left[\frac{€}{\text{ton}_{\text{CO}_2}}\right]}{\text{pull}\left[\frac{\text{kg}_{\text{glass}}}{\text{d}}\right]}$$

[3. 4]

The second step is different for the two technologies:

- **Electric:** consider the average value among the different cullet, such that a unique number is obtained for the year

- **Hybrid:** consider the average value among the different cullet, whereas for the electric input the two opposite operating conditions are chosen, that means null and 0,465 kWh/kg corresponding to the 25% of the energy input, which is definitely a huge share for a hybrid furnace. Even though such a level is never achieved in practice, it has been nevertheless taken into account in order to simulate how such a high share of electricity consumption would impact on the operating cost of the system

Results are tabulated and plotted:

Year	Electric furnace	Hybrid furnace	
		0 kWh/kg	0,465 kWh/kg
	[€/kg]	[€/kg]	[€/kg]
2014	0,142	0,076	0,121
2015	0,128	0,070	0,110
2016	0,125	0,059	0,101
2017	0,120	0,058	0,098
2018	0,096	0,070	0,094
2019	0,116	0,073	0,105
2020	0,100	0,062	0,090

***Table 14** - specific cost for energy and emissions of electric and hybrid furnaces in last years*

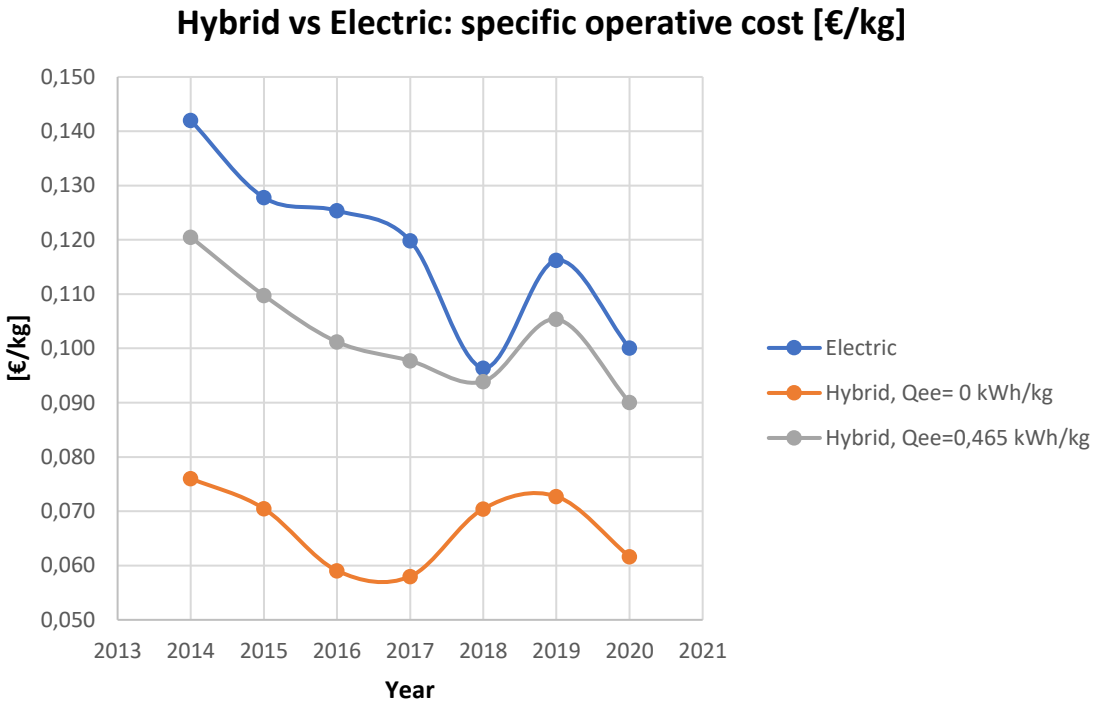

***Figure 38** - specific cost for energy and emissions of electric and hybrid furnaces in last years*

What emerges is that the operating cost of full electric has been steadily above those of hybrid, despite the fluctuation in natural gas, electricity and carbon tax prices. Not only: the cost for the full combustion approach, in 2017, was even half of full electric.
The takeaway message is that in past years there were not the conditions for an overtaking of full electric on hybrid systems: from the specific costs perspective, the former have not achieved competitiveness yet.
Such an environment is most likely going to turn around in the future, as carbon tax has finally been set on a continuous rise after the stagnation between 2012 and 2017, which is mandatory in order to meet the ambitious goals of decarbonization set by the European Union. Indeed, the average price of CO_2 in 2021 was around $54\ \frac{€}{\text{ton}_{CO_2}}$ with even higher values in the very last months.
However, it must be said that an increase in carbon price will also reflect on those of gas and electricity, as well as on final product and customers, therefore it is not that easy to predict how fast these prices will allow such a transition. What is granted is that, wearing the pants of an energy intensive industry, it was not really possible to fully switch on electric, at these conditions.

Lastly, it is interesting to spend few words on the overall carbon footprint of the two furnaces by considering not only the direct emissions, but also the indirect ones which are those associated with the gross production of electricity. This is pursued by applying the *emissive factor,* which represents the average carbon emission in [gCO_2/kWh] within the energetic mix[19] of Italy. By considering the data made available regarding the energetic consumption of the electric furnace and of the Cyclope and relying on the following emissive factor in the corresponding years, the overall carbon footprint of both the systems have been assessed:

[19] It accounts for both fossil fuel and renewable power generation

Year	Emissive factor
	[gCO_2/kWh]
2017	317,4
2018	297,2
2019	277,3

Table 15 *- Emissive factor for electricity production*

Electric	Cyclope
[tonCO_2/campaign]	**[tonCO_2/campaign]**
9.000-13.000	**13.000-17.000**

Table 16 *- Overall carbon footprint of electric and Cyclope furnaces*

The represented ranges are indicative but also useful as they can provide a clear measure of how far an electric furnace from is being emission-free. Or, at least, these can recall that it is not enough to eventually switch to the electric furnace at some point in the future as the issue would anyway pop up as an indirect consequence of electricity production. Hopefully, their impact could potentially be lowered in the upcoming years (decades) as long as the renewable share rises sufficiently in the energetic mix of the Country (or other technologies with higher thermal efficiencies).

4. Decarbonization options

A wide variety of technologies are potentially employable for the sake of enhancing the decarbonization of the glass sector. The current chapter wants to go briefly through the most relevant in order to provide the reader with an overview and discuss to what extent these can effectively mitigate the carbon emissions.
By critically analysing the available literature it was possible to determine the most promising technologies or, at least, to discover those on which studies, pilot projects and efforts should keep on focusing. As a matter of fact, indeed, some of them are already being employed in other sectors, thus making their readiness level suitable for glass furnaces as well, whereas other are still under development and therefore not immediately employable.
Waste heat recovery, *fuel switch* and *process optimization in combustion* are the three areas of concern.

4.1: Waste heat recovery

Huge exergy is stored in the exhaust gas[20] of a glass furnace in the form of thermal power, especially when combustion is operated with air. The most efficient way to exploit it is to install regenerative chambers in which flue gases are cooled down from about 1500 °C to 470 °C, whereas combustion air is heated from ambient temperature to about 1300 °C thus leading to a strong cut in fuel demand. Such a configuration is actually state of art, especially for end port furnaces. An alternative solution, less efficient, is to employ recuperators (metallic) which however cannot exploit the same ΔT on flue gases side and neither achieve 1300 °C on air side. Such a solution is employed on unit melter furnaces. The opposite situation is observed in the case of oxy-fuel furnaces, where no heat recovery is accomplished at all.
Even though regenerative towers allow to achieve up to 70% of heat recovery, flue gases leaving the regenerator are still pretty warm. However, downstream processes such as de-dusting by means of electrostatic precipitation set the lowest temperature, as these devices are usually operated in a temperature window between 180-280 °C.
In order to enhance the waste heat recovery, a number of solutions could be implemented: *heat-to-power* and *thermo-chemical heat recovery*.

4.1.1: Heat - to - power

This is a commonly employed approach to recover thermal energy from exhaust gases. As an example, in combined power plants the flue gases leaving the gas turbine supply the heat required by a bottoming cycle (such as a Rankine cycle) to further produce electricity. The same principle can be reproduced on glass furnaces, and a wide variety of solutions (in terms of thermodynamic cycle, equipment and configuration) could be investigated.
These will be dealt with in details in chapter 5.
As an anticipation, it can be expected that not huge enhancements will be achieved because of a low ΔT exploitable and limited flow rates. However, the produced power (either electric or mechanical[21]) can be

[20] Electric furnaces do have flue gases due to process emissions, but not of interest for the sake of heat recovery
[21] In the form of compressed air, which is massively used in glass plants

directly exploited within the plant thus leading to economic saving from electricity bill as well as carbon emission reduction from power generation plants.

4.1.2: Thermochemical heat recovery

An innovative approach consists in exploiting the large amount of thermal power to activate endothermic chemical reactions. The purpose is to produce an energetic vector with a higher thermal content to be burnt directly in the combustion chamber such that a reduction in natural gas consumption can be pursued.
A possibility is to activate the steam reforming SMR reactions of methane (namely steam reforming and water gas shift) to obtain syngas, which is a mixture of H_2, CO, CO_2, H_2O and unreacted CH_4. SMR is actually a well-established technology which is largely employed at industrial level for the production of H_2: up to the 50% of the world hydrogen production comes from this technology [14]. In order to achieve high H_2 purity at levels of 99% on molar basis [15], pressure swing adsorption units PSA are employed.
Unfortunately, such a technique is not carbon-free: in order to decarbonize it, carbon capture and storage CCS should be considered thus making it *"blue hydrogen".* Whether this path will be taken or not is still something under discussion, considering the difficulties not only in the carbon capture itself but also the transportation to the final site of storage such as dismissed wells or underground caves. However, projects in these regards are being undertaken such as the HyNet in the north-west of UK, which claims to achieve potentially over 25 million tonnes of carbon savings per year [16].

Getting back to the SMR of natural gas, it is basically given by the combination of the two following reactions:

$$CH_4 + H_2O \rightarrow CO + 3H_2 \qquad \Delta H_{sr} = 206 \ \frac{kJ}{mol}$$

$$CO + H_2O \rightarrow CO_2 + H_2 \qquad \Delta H_{wgs} = -41 \ \frac{kJ}{mol}$$

Being the overall enthalpy of reaction $\Delta H = 165 \ \frac{kJ}{mol}$, with positive sign stating that heat must be supplied from an external source (endothermic). In traditional applications it would be coming from combustion of fossil species such as natural gas, whereas for the particular case of glass furnaces the heat source would be the exhaust gases.
This is a rather innovative configuration applied in the field, and applications in real plants are not present in literature. However, projects in this regard are under development: an example is the *Life Sugar Project*[22] [17], supported by the Executive Agency for Small and Medium-sized Enterprises (EASME) of the European Commission. According with this initiative, which is currently at the mock-up testing stage, the expected results are the achievement of a 10/15% energy consumption reduction for glass melting and consequent carbon emissions, leading toward a more sustainable production of glass. Moreover, this represents one of the very first experiment of combustion with alternative fuel to natural gas or oil, which will provide insights on possible consequences on the product quality. This aspect of fuel switch is further addressed in the following sub-chapter 4.2.

[22] Partecipants are Stara Glass, KT, Johnson Matthey, Stazione sperimentale del vetro, Università degli studi di Genova

The thermodynamic assessment of thermochemical heat recovery is discussed in a specific chapter (6), where the modelling of furnace, reactor and heat exchangers have been undertaken on the basis of chemical equilibrium, mass and energy balance.

4.2: Fuel substitution

With *fuel substitution* it is meant the replacement of traditional and conventional fossil fuels such as natural gas or oil with CO_2 – neutral energy carriers, in the light of reducing the impact on environment. The heat required would still be supplied by means of combustion, therefore not significant changes on the equipment and furnace structure are to be expected. The main concerns are related to the unknown and unpredictable consequences on the glass quality because of the different fuel, moreover its actual availability at competitive prices as well as the lack of a widespread infrastructure are major uncertainties that prevent such an alternative approach for decarbonisation to be easily implementable immediately.
The most promising choices are *biogas* and *blue/green hydrogen*.

4.2.1: Biogas

It is produced by means of anaerobic digestion of biomass. The result is a mixture of methane (50-70% vol.), carbon dioxide and traces of other components. It is considered as CO_2 – free if seen from a life cycle point of view: indeed, all the carbon released during combustion has been subtracted from the environment with the organic matter growth.
According with [18], tests have been conducted over the co-firing option in an existing glass furnace. With an energy content from biogas up to 30%, results state that not quality issues were reported nor damages on the equipment or refractories. Even though the type of glass was not specified, it is at least reassuring that such a switch would be technically feasible and already viable with the current equipment and furnace structure.
Because of limits in the supply of biogas, it would be advisable to operate with a co-firing approach which would contribute to emission reduction anyhow.
Unfortunately, biogas price is still not competitive and, together with the absence of a distribution grid, do not contribute to its deployment. Even though the market volume is steadily increasing, with an overall value of 70 bn USD in 2018 and growth forecasts of +7% by 2025 [19], it is likely insufficient to boost its expansion into the glass world unless carbon allowances and/or natural gas costs rise sufficiently.

4.2.2: Hydrogen

The prerequisites for the transition to hydrogen as energy carrier are mainly two. First, it must be produced with the lowest environmental impact, therefore *blue* (fossil fuel based such as SMR, with CCS) or *green* (water electrolysis exploiting renewable electricity) are the choices. Second, it must become economically competitive with fossil fuels.
The development of a “hydrogen economy” is mandatory for the achievement of these two requirements, comprising not only its production but also its distribution and storage. On the one hand, in order to minimize the specific costs for production and transportation, large-scale facilities should be expected because of

economy of scale. On the other, those for large storage plants appear to be higher as capacity increases. Because of a lower volumetric energy density with respect to natural gas[23], the existing infrastructure is not suited for hydrogen storage nor transportation: in order to supply the same energy content indeed, natural gas requires three times lower volume. Another issue is the "hydrogen embrittlement" for which hydrogen can attack the metallic structure of pipelines and storage vessels at high pressures and low temperatures, leading to failures and leakages, such that specific materials not susceptible to the phenomenon are required. Different transmission methods exist, among which four have been analysed from a techno-economic viewpoint [20] and summarized in **Table 17**:

Transmission Type	Pipeline	Tube trailer	Liquid – road	Liquid – ships
Suitability	Short, medium, and large distance transfer of large and very large quantities in a gas state	Short distance gas state transfer	Short and medium distance transfer of large volumes of fuel	Very large quantities of gas for international transportation
Investment Costs	\$200,000-\$1,000,000 per km depending on the terrain	Around \$300,000+ per truck	\$300,00-\$400,000 per truck	\$465,000,000-\$620,000,000 for each LH_2 barge
Operating and Maintenance costs	Around \$0.03 per kg for pipeline compressors	Driver labour at around 18 \$ h^{-1}	Driver labour at around 18 \$ h^{-1}	Crew labour and fuel consumption costs unknown
Efficiency	Over 99.2% per 100 km	94% per 100 km	99% per 100 km (liquefaction efficiency is around 75%)	0.3% boil-off per day
Capacity	Up to 100 tons h^{-1} (3.9 GW)	Up to 400 kg per truck	Up to 4000 kg per truck	Up to 10,000 tons per shipment
Energy required	Electricity required for pipeline compressors	Vehicle fuel consumption	Vehicle fuel and liquefaction energy consumption	Transport fuel
Advantages	Large and very large quantities can be transported to any distance with high efficiency, low running costs, and very low variable expenses. This method also provides storage and buffering possibilities	Small scale deployment possibilities	Larger volumes than gas transportation	International transportation of massive quantities for long distances
Disadvantages	Relative expensive investment costs and requirement of the very large amount of hydrogen delivery to be justified	Small scale delivery per vehicle, energy inefficiency, short-distance transportation	Costs and inefficiency of liquefaction and boil-off product losses	There isn't any industrial experience of shipping LH_2. It's not feasible until large supply and demand exist. Boil-off losses are more significant than road transport
Total transmission cost (\$ kg^{-1} $100km^{-1}$)	\$0.10-\$1.00	\$0.50-\$2.00	\$0.30-\$0.50	\$1.80-\$2.00

***Table 17** - Hydrogen transportation*

Despite the huge investments costs, it turns out that the most economically convenient approach is via pipeline (lowest *total transmission cost)*, as it allows to deliver large flow rates for hundreds of km without compromising the initial energy content of the energy vector and with low operating costs and maintenance. More expansive and less efficient[24] solutions, such as tube trailers[25] or liquefied hydrogen, could potentially be employed in the introductory phase while demand is still growing and both production and distribution network are under enhancement.

From a technical viewpoint, hydrogen combustion represents a challenge: higher flame temperature, different flame lengths and velocities, increased water content in flue gases. All these aspects are important to be addressed since they may play a role in the product quality, as the heat transfer properties could be different from those of natural gas, for instance. In this regards, experiments are being conducted. Among the others, the NSG Group[26] has taken on a 100% hydrogen trial for three weeks long in 2021 [21], showing up good results. Other tests such as the already introduced *Life Sugar Project* will provide further insights on the hydrogen behaviour within glass furnaces.

Therefore, following up the evidence coming from tests, it is legitimate to state that H_2 is a good candidate for the glass sector decarbonisation. It is likely that in the event of a transition towards hydrogen, for a

[23] Natural gas has about three times higher energy volumetric density than hydrogen

[24] Due to compression, liquefaction and boil-off

[25] Tracks hauling compressed H_2 into long cylinders (20 m) at high pressure (greater than 180 bar)

[26] World leader architectural glass producer

successful market ramp up co-firing with natural gas will be the first step, at least until the infrastructure as well as its production capacity have been developed.

4.3: Process optimization in combustion

Other actions and choices could potentially be taken in order to increase the glass melting efficiency, thus leading to a specific consumption and operating costs reduction.
By considering the combustion process, the **air-fuel ratio** plays an important role in both energy consumption and pollutant emission: on one hand, a high value allows to fully burn the fuel and therefore minimize the CO content in flue gas, besides larger NO_x are expected due to a greater amount of nitrogen in the furnace chamber. On the other, a low value increases the amount of fuel and CO in the exhausts (uncomplete combustion) while reducing the NO_x content. From an energetic viewpoint, lower air-fuel ratios are beneficial because of lower volumes of air that would be heated instead. Therefore, it is of key importance to pursue a trade-off between energetic expenditure and pollutant emissions.
Another choice that can contribute to a reduction of both energetic expenditure and pollutant is the **oxidizer**: oxy-fuel furnaces, as already discussed in the previous chapters, allow to strongly reduce the heat demand thanks to the absence of nitrogen and therefore also the associated NO_x. However, because of a limited flow rate of the exhausts, no heat recovery is typically performed.
To conclude, a further option for optimization of combustion is suggested: ***submerged combustion***. The idea is to replace the burners above the melt with burners submerged, in order to strongly enhance heat transfer, thus promoting convective motions as well as homogenization and reduce the heat loss through the walls. Because of way lower temperatures reached inside the chamber, refractories bricks are replaced with water-cooled metallic walls with the inner face protected from radiation heat by a thin layer of castable refractory. Several tests have been conducted, and some glass manufacturers around the world do employ such a technology. According with the *International Journal of applied glass science* [22], that reports the results of a pilot furnace with pull capacity of 900 kg/h with bottom-submerged burners, important energy savings are potentially achievable as well as of NO_x[27]. However, an important aspect poses serious limitations to the deployment of the technology in the glass manufacturing panorama: low refining capability. Indeed, the glass extracted from the testing furnace was characterized by bubbles of diameters in the range of several millimetres. It follows that, in order to make such a technology competitive in terms of product quality, a dedicated stage of refining must be considered.
Despite this limiting factor, submerged combustion has actually been employed for years in real glass furnaces in east Europe (Ukraine, Belarus) where limited quality is required, such as for the sector of mineral and stone wool. Further studies and design investigations from glass furnace manufacturers across the world are addressing the question on how to properly implement the refining stage. Until this issue will not be solved, it is not likely to foresee submerged combustion applied to high quality glass as for the case of pharmaceutical sector.

[27] Submerged combustion is operated with oxygen as oxidizer

5. Waste heat recovery: heat to power

Chapter five is focused on the analysis of different thermodynamic cycles for heat recovery from waste gasses. Thermodynamic and economic performances of four different heat recovery systems HRSs are evaluated for either compressed air or power generation in order to determine which system is the most attractive when applied to glass furnaces.
The present discussion is based on an in-depth literature research of existing papers, among which stands out the work by P. Danieli, S. Rech and A. Lazzaretto of the University of Padova "*Supercritical CO_2 and air Brayton-Joule versus ORC systems for heat recovery from glass furnaces: performance and economic evaluation*" [23], which conducted a study for both on-design and off-design[28] of two end-port glass furnaces of different sizes (small/medium) comparing alternative configurations of Joule-Brayton cycles and Organic Rankine Cycles ORC. For the sake of this work, the "small size" system is considered (150 ton/d) as it is the closest to the average operating conditions of Bormioli Pharma. The authors have also addressed the case of a bigger system, exceeding the 300 ton/d.

After the cycle description, comprehensive of the process flow diagram together with its operative conditions, the methods for the analysis are briefly discussed in order to clarify how the authors have addressed the modelling, optimization as well as the definition of the main performance parameters. The thermodynamic analysis is completed with the economic evaluation in terms of return on the investment ROI, which tells how many years are required to recover the initial expenditure.

5.1: HRS

As anticipated, four are the cycles of interests:

- Open loop, air JB cycle
- Closed loop, sCO_2 JB cycle
- Closed loop, sCO_2 JB cycle with combustion air preheating
- Organic Rankine cycle

5.1.1: Open loop, air JB cycle

The system is an externally heated gas turbine, with air as working fluid being heated by the furnace waste gases in a counter current gas-gas heat exchanger, which replaces the well-known combustion chamber of traditional Joule-Brayton cycles.
Air is first compressed at 5 bar and 245,8°C after which it enters the gas-gas heat exchanger where it is heated up to 591,1°C. Secondly, air undergoes expansion in the turbine reaching ambient pressure at 341,7°C. At this conditions, air is fed into the regenerative chambers where it undergoes the typical thermal cycle of an end port furnace. At the furnace outlet, after being cooled in the regenerative chambers, flue gases are extracted at 641°C making their entry into the heat exchanger, and will be released at 290°C.

[28] Off-design simulations accounting for ambient temperature variation and furnace deterioration

The system can be either used to produce compressed air or electric power: in the first case, a share of the total flow rate is bled and used as industrial feed stream for the factory demand, whereas the remaining part is the exact amount which allows the turbine to produce the mechanical power required to drive the compressor. In the other situation instead, no bleeding occurs and the system operates to maximize the power obtainable from the expander, which will also drive the electric generator.
Here below the plant layout and the T-s diagram[29] are depicted, with the corresponding thermodynamic conditions and mass flow rate in design conditions:

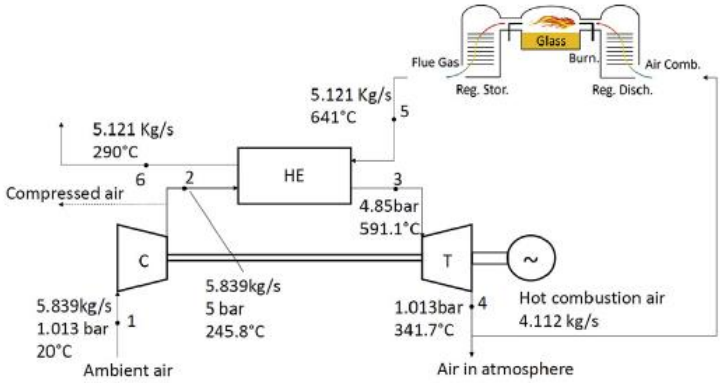

Figure 39 *- Open loop, air JB cycle*

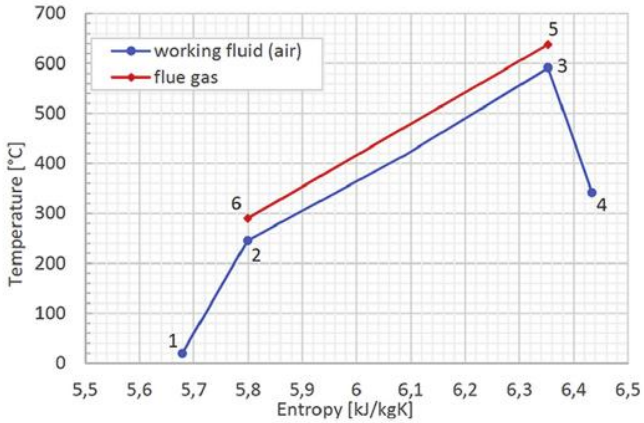

Figure 40 *- T-s diagram open loop air JB cycle*

5.1.2: Closed loop, sCO_2 JB cycle

The system is an externally heated closed loop gas turbine with CO_2 as working fluid, operating in supercritical conditions (T_{cr} = 30,97°C, p_{cr} = 73,77 bar). The CO_2, downstream the compressor (201,5 bar), is first heated in a regenerator from 66,41°C to 177,6°C exploiting the thermal power still available at the turbine outlet, thus increasing the thermal efficiency of the system, and then in the flue gases heat

[29] Entropy scale referred to working fluid only (air)

exchanger: CO_2 reaches 363,1°C whereas waste gases are cooled from 470 to 212,6°C. A cooler is also installed such that the correct design temperature is granted at the compressor inlet: 32°C.
Once again, either electric power or compressed air can be produced by adding an additional dedicated compressor at the same turbine shaft.
Hereinafter plant layout and T-s diagram[30] are provided, with the thermodynamic conditions and mass flow rates in design conditions:

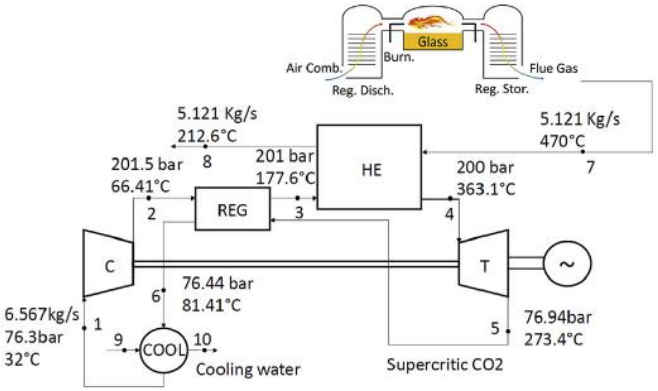

***Figure 41** - Closed loop, sCO_2 JB cycle*

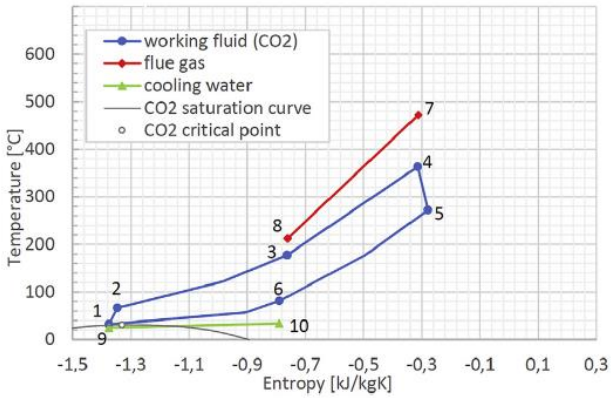

***Figure 42** - T-s diagram closed loop, sCO_2 JB cycle*

5.1.3: Closed loop, $\mathbf{sCO_2}$ JB cycle with combustion air preheating

This solution is a development of the previous one. The focus is on the regenerator of the closed loop cycle: it is the element that sets the working fluid temperature at the primary heat exchanger inlet. The drawback is that the waste gases temperature at its outlet will be set accordingly, and cannot go below that

[30] Entropy scale referred to working fluid only (carbon dioxide)

temperature level, thus compromising the lowest temperature reached by the exhaust gases and therefore reducing the potential heat recovery. To overcome such a limitation, the idea is to install a combustion air preheating unit downstream the regenerator, which enters the regenerative chambers of the furnace at 356,5°C: this basically consists in lifting the temperature levels upwards for both flue gases and carbon dioxide sides, while keeping fixed the temperature in the combustion chamber. Waste gasses would leave the regenerative chambers at 648°C which is a higher temperature than the conventional value of 470°C.
With this modification, the carbon dioxide temperature at the turbine inlet is increased reaching 595,9°C, whereas at the outlet is 489,2°C. At the same time, the conditions at the compressor inlet and outlet would not change with respect to the closed loop, sCO_2 JB cycle.
On the flue gases side, the lowest temperature can go down to 180°C, which is somewhat lower than the 212,6°C of the previous system.
Once again, either electric power or compressed air can be produced by adding an additional dedicated compressor at the same turbine shaft.
Hereinafter plant layout and T-s diagram[31] are provided, with the thermodynamic conditions and mass flow rates in design conditions:

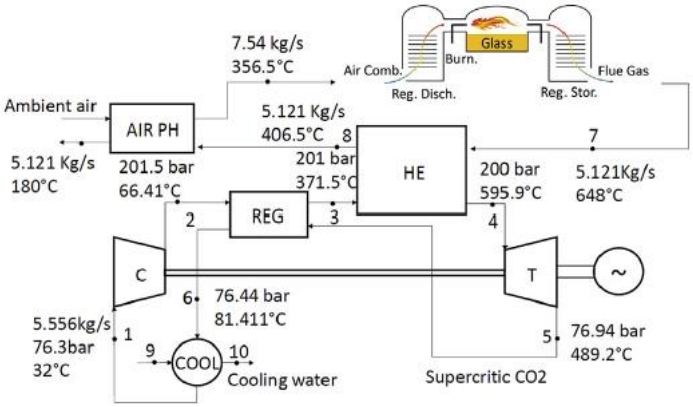

Figure 43 - *Closed loop, sCO_2 JB cycle with combustion air preheating*

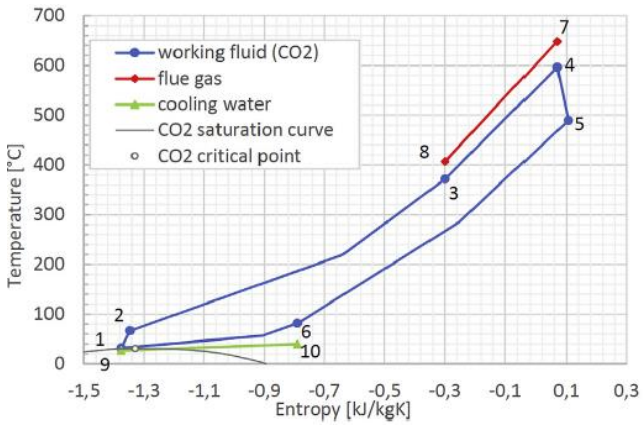

Figure 44 - *T-s diagram closed loop, sCO_2 JB cycle with combustion air preheating*

[31] Entropy scale referred to working fluid only (carbon dioxide)

5.1.4: Organic Rankine cycle

The waste gases and the organic fluid (cyclopentane) are linked with an intermediate closed cycle operating with thermal oil, which is required to transfer heat from the hot source to the working fluid. However, because of issues of chemical deterioration of such thermal oil above 300°C, it follows that the maximum temperature for the cyclopentane cannot overcome this thermal level.
From the working fluid viewpoint, it is first pumped (40,89 bar, 48,22°C) and then preheated in a regenerator up to 102,7°C exploiting the thermal power stored within the superheated organic vapour leaving the turbine (1,334 bar, 179,2°C) before being condensed against air. Then, it undergoes further heating, evaporation and superheating (in dedicated components) thus reaching 279,6°C at the expander inlet. The loop is closed with the working fluid being cooled, condensed and subcooled[32] at 45,37°C and 0,984 bar.
Once again, either electric power or compressed air can be produced by adding an additional dedicated compressor at the same turbine shaft.
Hereinafter plant layout and T-s diagram[33] are provided, with the thermodynamic conditions and mass flow rates in design conditions:

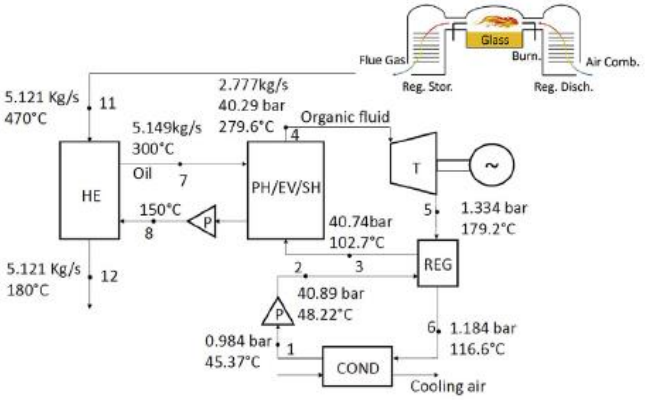

***Figure 45** - ORC*

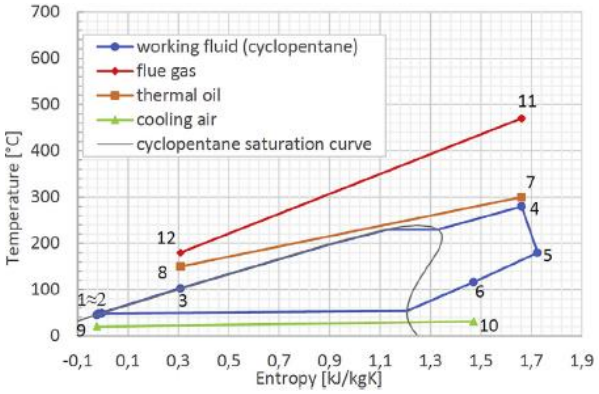

***Figure 46** - T-s diagram ORC*

[32] Subcooling of 3°C is set in order to prevent the formation of biphasic mixture in the pump
[33] Entropy scale referred to working fluid only (cyclopentane)

5.2: Working conditions

The description of the working conditions is discussed after the presentation of the different HRS such that the reader is aware of the layout of each and can more easily understand how these have been set.
The operating conditions of the furnace strongly affect the heat content of the waste gases, and therefore also the efficiency of the HRS. These depend on the presence of the additional air preheating (*Open loop, air JB cycle* and *Closed loop, sCO_2 JB cycle with combustion air preheating*). Indeed, its presence is associated with a higher thermal level of the combustion air that enters the regenerative chambers and, consequently, waste gases will leave the chambers at higher temperature. Such a way of conducing the furnace system is not the traditional one and can be addressed as a modification made necessary to optimize the HRS operativity.
On the other hand, for the two cases with no additional combustion air preheating (*Closed loop, sCO_2 JB cycle* and *Organic Rankine cycle),* the furnace is operated regardless the downstream presence of the HRS thus coinciding with the traditional way of conducing the furnace system.
The choice of the design conditions is made by also considering the ageing of the furnace itself, which has important influence on both flue gas flow rate and temperature: both are expected to increase along the campaign because of a higher fuel demand required to compensate the enhanced heat losses through the furnace structure. With 10-year lifetime, according with the authors the following variations on flue gases leaving the regenerative chambers are foreseen:

- Linear temperature increase of 45°C
- Linear mass flow rate increase of 20%

The design conditions[34] are taken as those at the fifth year of operativity, for both the two cases with additional air preheating and for the other two cases without. These are respectively:

- *Open loop, air JB cycle*: **641°C – 5,121 kg/s**
- *Closed loop, sCO_2 JB cycle with combustion air preheating:* **648°C – 5,121 kg/s**
- *Closed loop, sCO_2 JB cycle:* **470°C – 5,121 kg/s**
- *Organic Rankine cycle:* **470°C – 5,121 kg/s**

These are also reported in the plant layouts available in section 5.1, for each configuration.

5.3: Methods

The section 5.3 provides a brief presentation and discussion of the approach employed by the authors for the modelling of each component, as well as the definition of the performance parameters.

[34] These may be different from furnace to furnace, depending on the type of glass, cullet and electric input. The suggested values are therefore to be taken as a reference

For a complete and in-depth analysis please refer to the original paper available in the bibliography [23].

The behaviour of the HRS components is simulated, at any operative condition, using a steady-state zero-dimensional model. For the sake of the present work, only the *on design* working conditions are simulated even though also the *off design*[35] have actually been analysed.
Turbomachinery components (pumps, compressors and expanders) are modelled on the basis of mass and energy balances, exploiting the efficiencies and performances made available[36] for the *on design* case.
Heat exchangers are also modelled on the basis of mass and energy balances, and the definition of the heat transfer surfaces is pursued by means of the *Delta T mean logarithmic approach* for counter current configurations. In this regard the overall heat transfer coefficient K, thermal power exchanged Q and ΔT_{ml} are set according with the process. In particular, K is computed by means of thermodynamic correlations, which require the estimation of the properties of both working fluid and exhaust gases. For this purpose, it is required to assign thermodynamic and geometric variables such as flow rates, inlet/outlet temperatures of both fluids, inlet pressures, internal and external tube diameter as well as tube lengths and numbers. An iterative procedure is implemented to compute the geometric parameters of the tubes such that given constrains are respected, for example the pressure losses must be kept within acceptable limits.
It is straightforward that each HRS will be characterized by different assigned values and operating conditions of the equipment.

The optimization of the design solution has been pursued by maximizing the function *mechanical power output* $P_{mec}(\boldsymbol{x})$, as a function of the array **x** containing all the variables, through the imposition of the condition g (**x**) = 0, where g(**x**) represents the set of equations of the design model for each HRS. Therefore, the mathematical problem consists in finding **x** that maximizes $P_{mec}(\boldsymbol{x})$. This task has been carried out through the implementation of the software EES® (engineering equation solver).

For what concerns the performance parameters, here is their definition:

- Thermal efficiency of the HRS: $\boldsymbol{\eta_{th}} = \frac{\mathbf{P_{mec}}}{\mathbf{Q_{in}}}$
- Total efficiency of the HRS[37]: $\boldsymbol{\eta_{tot}} = \frac{\mathbf{P_{mec}}}{\mathbf{Q_{av}}}$
- Heat recovery coefficient[38]: $\boldsymbol{\phi} = \frac{\boldsymbol{Q_{in}}}{\boldsymbol{Q_{av}}} = \frac{\boldsymbol{h_{in}-h_{out}}}{\boldsymbol{h_{in}-h_{out,180°C}}}$
- Glass furnace + HRS thermal efficiency: $\boldsymbol{\eta_{th,furn}} = \frac{\boldsymbol{Q_{glass}}+\mathbf{P_{mec}}}{\boldsymbol{m_{fuel}\cdot LHV}+\boldsymbol{P_{el}}}$

With h_{in}, h_{out} referred to the flue gases. Note that ϕ represents the ability of the HRS to exploit all the available thermal power of the exhaust gases, by cooling it down to 180°C, which is the lowest temperature that can be reached to avoid acid condensation in the filters. Q_{glass} is representative of the heat input absorbed by the glass.

[35] Accounting for ambient temperature variation and furnace ageing
[36] See the Appendix in the original document
[37] Q_{av} is the thermal power of the flue gases between the inlet temperature and the lowest temperature allowable (180°C)
[38] Note that $\eta_{tot} = \eta_{th} \cdot \phi$

5.4: Results

Both thermodynamic and economic performances are evaluated within the paper in terms of net power output, efficiencies and return on investment ROI respectively, and hereinafter are summarized.

5.4.1: Thermodynamic performances

Let's now evaluate the results of the optimized, on design simulations for each HRS whose thermodynamic conditions are shown in the flowsheets for each configuration.
These are shown in **Table 18**:

	Symbol	Unit	Air Brayton-Joule cycle	Standard sCO_2 cycle	sCO_2+air PH cycle	ORC
Net power output [kW]	P_{net}	[kW]	183.9	321.8	473.3	359
Working fluid mass flow rate	$\dot{m}_{wf}$	[kg/s]	5.839	6.567	5.556	2.777
Heat source temperature	T_{gas}	[°C]	641	470	648	470
Thermal efficiency	η_{th}	[−]	0.084	0.204	0.307	0.203
Heat recovery coefficient	ϕ	[−]	0.772	0.892	0.531	1
Heat recovery efficiency	η_{tot}	[−]	0.064	0.182	0.163	0.203
Furnace + HRS thermal efficiency	$\eta_{furnace+HRS}$	[−]	0.367	0.378	0.391	0.382

***Table 18** - Design performances of each HRS*

What emerges is that the highest net power output extractable is 473,3 kW achieved by the *Closed loop, sCO_2 JB cycle with combustion air preheating*. Moreover, this is the HRS that also maximizes the thermal efficiency reaching the 30,7%. On the other hand, this is the cycle which exhibits the lowest heat recovery coefficient (53,1%): this is something expected because, even though the flue gases are indeed cooled down to the lower limit of 180°C, not the entire thermal power is actually given to the working fluid since it is partly employed to preheat the combustion air in the downstream preheating unit. The three other cycles instead do not have any additional recovery unit to preheat the combustion air downstream, so they can achieve higher heat recovery coefficient. The best (100%) is obtained by the ORC which manages to fully cool down the waste gases by exchanging with the thermal oil.
Even though *Closed loop, sCO_2 JB cycle with combustion air preheating* has a limited heat recovery coefficient, it does not mean that it has a worse capability of recovery as the share of thermal power which is not exchanged with the HRS is supplied to the combustion air preheating unit. This finds proof in the *furnace + HRS thermal efficiency* which is the highest: 39,1%. As a reference, according with the authors, the furnace thermal efficiency (without air preheating downstream the HRS) is around 35%.

5.4.2: Economic performances

For what concerns the economic considerations, the authors have compared the four HRS in terms of ROI on four different scenarios:

1. Production of compressed air

2. Production of compressed air with energy efficiency incentives
3. Production of electricity
4. Production of electricity with energy efficiency incentives

In order to determine the ROI, equation [5. 1] has been used:

$$F_0 - \sum_{y=1}^{PBP} F_y \cdot (1+k)^{-y} = 0$$

[5. 1]

Where F_0 represents the investment cost, whereas F_y is the cash flow in the considered year and k is the discount rate.
The approach employed for the costs calculation, known as "Module Costing Technique MCT" by Turton et al. [24], takes into account both direct (equipment, foundations, structural supports, piping, insulation, fireproofing, electrical devices etc.) and indirect (freight, insurance, taxes, construction overhead, contractor engineering expenses etc.) costs. However, O&M is not included. Unfortunately, because of the quite recent and innovative development of CO_2 systems, the cost of turbomachines is estimated between a minimum and a maximum value. To account for this variability, both the scenarios have been evaluated.
MCT is organized as follows:

$$\mathrm{C_{BM}} = \mathrm{C_p^0} \cdot \mathrm{F_{BM}}$$

[5. 2]

Where $\mathrm{C_{BM}}$ is the *bare module equipment cost*, $\mathrm{C_p^0}$ is the *purchased cost for base conditions*[39] and $\mathrm{F_{BM}}$ is the *bare module cost factor*. In order to incorporate the equipment material and pressure though, it is proposed a further equation that replaces $\mathrm{F_{BM}}$:

$$\mathrm{F_{BM}} = \mathrm{B_1} + \mathrm{B_2} \cdot \mathrm{F_M} \cdot \mathrm{F_P}$$

[5. 3]

Where $\mathrm{B_1}$, $\mathrm{B_2}$ are coefficients material - specific and $\mathrm{F_M}$, $\mathrm{F_P}$ account respectively for material and pressure. Moreover, for a more detailed description of $\mathrm{F_P}$ correlation [5. 4] can be used:

$$\log_{10}\mathrm{F_P} = \mathrm{C_1} + \mathrm{C_2} \cdot \log_{10}\mathrm{P} + \mathrm{C_3} \cdot (\log_{10}\mathrm{P})^2$$

[5. 4]

Eventually, data for the *purchased cost for base conditions* of equipment, at ambient temperature and using carbon steel, were fitted to equation [5. 5]:

[39] Common material and near ambient pressure

$$\log\left(C_p^0\right) = K_1 + K_2 \cdot \log(A) + K_3 \cdot (\log A)^2$$

[5. 5]

Again, K_1, K_2 and K_3 are equipment specific constants whereas A is the equipment cost attribute.
Once the size, material and operating pressure of each component are known the overall cost can be computed by applying these equations whose coefficients are provided directly by MCT and listed in table A10 in the Appendix of the original paper and here below reported in **Table 20** for the sake of completeness, together with the list of the equipment for each HRS (**Table 19**). Note that the list of coefficients is the result of a survey conducted by equipment manufacturers.
The choice of applying the MCT approach is based on the fact that it is able to account for changes in process parameters such as materials of construction and operating pressures. The drawback is that it does not allow to differentiate between direct and indirect cost and neither between material, labour and installation: the output of the model is the overall module equipment cost.

	Air Brayton-Joule cycle system	Standard sCO_2 cycle system	sCO_2 + air PH cycle system	ORC system
Compressor	✓	✓	✓	
Turbine	✓	✓	✓	✓
Flue gas heat exchanger	✓	✓	✓	✓
Regenerator		✓	✓	✓
Preheater				✓
Evaporator				✓
Superheater				✓
Air cooled Condenser				✓
Cooler		✓	✓	
Cooling tower		✓	✓	
Fans				✓
Air preheater			✓	
Air compressor (compressed air production)		✓	✓	✓
Pump				✓
Electrical generator	✓	✓	✓	✓

***Table 19** - components of each HRS*

Component	Size	K_1, K_2, K_3	C_1, C_2, C_3	B_1, B_2	F_M	F_P	F_{BM}
Air compressor	W [kW]	2.2897 1.3604 -0.1027	0 0 0	/	/	1	1.5
sCO_2 compressor	W [kW]	2.2897 1.3604 -0.1027	0 0 0	/	/	1	2 3.3
Air turbine	W [kW]	2.7051 1.4398 -0.1776	0 0 0	/	/	1	1.4
sCO_2 turbine	W [kW]	2.7051 1.4398 -0.1776	0 0 0	/	/	1	2.9 4.2
ORC pump	W [kW]	3.3892 0.0536 0.1538	-0.3935 0.03967 -0.00226	1.89 1.35	1.5	0.46	2.8
ORC turbine	W [kW]	2.2476 1.4965 -0.1618	0 0 0	/	/	1	13.8
Air/flue gas HE	A [m^2]	4.3247 -0.303 0.1634	0 0 0	1.63 1.66	6.7	1	12.7
Combustion air preheater	A [m^2]	4.3247 -0.303 0.1634	0 0 0	1.63 1.66	1	1	3.3
sCO_2/flue gas HE	A [m^2]	4.3247 -0.303 0.1634	13.1467 -12.657 3.0705	1.63 1.66	4.8	1.9	16.8
Thermal oil/flue gas HE	A [m^2]	4.3247 -0.303 0.1634	0 0 0	1.63 1.66	1	1	3.3
ORC HE and regenerator	A [m^2]	4.3247 -0.303 0.1634	0.03881 -0.11272 0.08183	1.63 1.66	1.2	1.5	4.5
sCO_2 regenerator	A [m^2]	4.6656 -0.1557 0.1547	0 0 0	0.96 1.21	1	1	2.2
Air cooled condenser	A [m^2]	4.0336 0.2341 0.0497	0 0 0	0.96 1.21	1	1	2.2
sCO_2 cooler	A [m^2]	4.3247 -0.303 0.1634	-0.4045 0.1859	1.63 1.66	1.05	2	5.1
Fans (air cooler condenser)	$\dot{V}$[m^3/s]	3.1716 -0.1373 0.3414	0 0 0	/	1	/	5
Fans (cooling tower)	$\dot{V}$[m^3/s]	3.1716 -0.1373 0.3414	0 0 0	/	1	/	3.8
Electrical generator	W [kW]	1.956 1.7142 -0.2282	0 0 0	/	1	/	1.5

***Table 20** - MCT coefficients*

After having discussed about the approach employed for the cost estimation, it is possible to move to the economic results in order to assess which HRS is the most convenient in terms of ROI. **Table 21** summarizes these results:

	ROI - compressed air [years]	ROI - compressed air + incentives [years]	ROI - electrical power [years]	ROI - electrical power + incentives [years]
Open loop, air JB cycle	9,9	8,4	10,5	8,9
Closed loop, sCO2 JB cycle (min)	8,5	7,2	8,2	6,9
Closed loop, sCO2 JB cycle (max)	9,5	8	9,2	7,8
Closed loop, sCO2 JB cycle with combustion air preheating (min)	7,3	6,1	6,9	5,9
Closed loop, sCO2 JB cycle with combustion air preheating (max)	8	6,8	7,7	6,5
ORC	7,5	6,4	7,2	6,1

***Table 21** - HRS economic performances*

What emerges is that, for each HRS, the ROI are quite high. The most competitive HRS seems to be the *Closed loop, sCO_2 JB cycle with combustion air preheating* if the lowest cost for CO_2 turbomachines is considered. In this scenario, the production of electricity shows the lowest ROI: 5,9 years. However, the uncertainty on the cost for CO_2 equipment suggests that other HRS may be more convenient, such as the ORC which is instead well known and available in the market. Also for ORC the most competitive solution is the production of electricity with a ROI of 6,1 years.
Note that the production of electricity is the most convenient choice because it avoids the additional purchase of dedicated and expensive air compressors. Only for *Open loop, air JB cycle* they would not be required, because such a cycle operates with air as working fluid thus making the compressed air production the best choice for this specific cycle.
The *Open loop, air JB cycle* and *Closed loop, sCO_2 JB cycle* are not comparable in terms of competitiveness with *Closed loop, sCO_2 JB cycle with combustion air preheating* nor with *ORC* as way higher ROI are expected.

It is worth it to mention that, once the investments are repaid, these HRS allow to continuously generate positive income until the furnace lifetime in the form of both saving on electricity bills and incentives.

Eventually, it is interesting to notice the cost allocation for the two most competitive solutions:

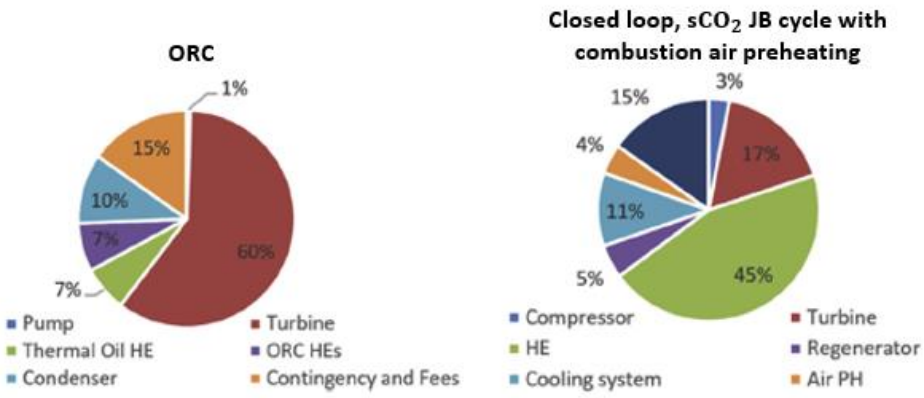

***Figure 47** - Cost allocation*

For the ORC the biggest share is allocated to the turbine, up to the 60%. On the contrary, for the *Closed loop, sCO_2 JB cycle with combustion air preheating* the major role is played by the waste gasses-CO_2 heat exchanger which accounts for the 45% of the overall investment.

5.5: Summary

To sum up, chapter 5 wants to provide an assessment of alternative thermodynamic cycles to the well-established Organic Rankine Cycle in the field of heat recovery from medium temperature heat sources, such as the case of waste gasses leaving end port regenerative chambers.
Referring to the simulation conducted over an end port furnace with a pull of 150 ton/d, which is the closer case for the interest of Bormioli Pharma, and keeping fixed its operating conditions, by considering three alternatives to the ORC it is possible to state that the highest thermodynamic performances are achieved with the *Closed loop, sCO_2 JB cycle with combustion air preheating*: 473,3 kW of net power output and 30,7% of thermal efficiency. The ORC is the second-best solution with 359 kW and 20,3%. However, the situation mixes up when economic performances are considered: due to the uncertainty on the equipment costs for CO_2-JB cycles, the ORC seems to be still the best choice both for the comparable ROI and, most importantly, due to its high level of readiness and availability in the market.
To conclude, *closed loop, sCO_2 JB cycle with combustion air preheating* may become a valid alternative to ORC if the cost of CO_2 turbomachines remain close to the lowest values assumed, while the innovative *Open loop, air JB cycle* and *Closed loop, sCO_2 JB cycle* are less attractive due to lower performances and high costs of the equipment which bring their ROI to unaffordable levels.

6. Waste heat recovery: steam methane reforming

Chapter six aims at developing the thermodynamic model of an end port glass furnace with the additional presence of the steam methane reforming unit. The goal is to determine first whether this technology applied to this type of glass furnace is physically feasible and to what extent it would be possible to exploit the thermal power of the exhaust gasses in order to produce an energy vector (syngas) to be directly burnt, thus saving fuel and carbon emissions in the glass melting process. Secondly, an economic analysis of the project is carried out by applying the Net Present Value NPV approach in order to provide an esteem on the investment profitability along its lifetime.
The choice of end port furnace is suggested by the fact that no existing literature is available on this specific system and, at the same time, Bormioli Pharma employs such a furnace, so this could be useful as a reference for a future and potential application of the technology.

6.1: Approach and method

The approach consists in the modelling, from the energetic viewpoint, of the furnace on the basis of *mass* and *energy balances*, together with *chemical equilibrium* applied to all the undergoing reactions (combustion, reforming and water gas shift). By doing so, the thermodynamic assessment of the system is addressed.
The first step is the realization of the base-model of the existing furnace (no SMR), to be validated against a pre-existing model built up by Bormioli Pharma supplier: this represents the basis on which the SMR unit would be installed.
The second step, once the base-model is validated, is to add the SMR thus obtaining the final system configuration.
The operating principle for the reformer is to exploit the waste gasses thermal power to activate the endothermic reactions of steam methane reforming in order to generate a higher energy content mixture (syngas) which will then be burnt in the furnace chamber: the process is controlled by setting, as an input for the model, the share of energy that the hydrogen within the syngas will replace thus leading to a saving in natural gas consumption.
The system is designed such that the flue gases leaving the furnace regenerative chambers provide not only the power required by the endothermic reactions, but also the thermal power needed to supply the mixture of superheated vapour and methane at the thermodynamic conditions at which these reactions are operated. Therefore, exhaust gasses will first enter the reactor followed by a heat recovery steam generator in parallel with a methane preheating heat exchanger before eventually being sent to the filters. The precise system configuration will be detailed in sub-chapter 6.3.
Once the thermodynamic design of the system is concluded, it is possible to move towards the sizing of each component in terms of exchanged powers and surfaces of heat transfer by applying the method of the *mean logarithmic temperature difference*, for which the overall heat transfer coefficients have been taken from literature.
The last step consists in the economic assessment of the system by applying the NPV method. Therefore, cash flows have been computed assuming as incomes the savings from natural gas consumption and carbon emissions which are expected as a result of the SMR. Detailed description will follow in section 6.5.
The applied procedure is run on several cases: first of all, it is of key relevance the ***share of energy*** that the hydrogen within the syngas would replace from natural gas, and different shares have been considered in this regards. Moreover, also the operating conditions of the furnace in terms of ***pull*** and ***electric input*** have

been considered as variables, given their relevance on the energy input required. Therefore, a sensitivity analysis is operated on these figures.
Moreover, the economic analysis also includes sensitivity considerations especially for what concerns the ***heat transfer coefficients*** in the heat exchanger design, as well as ***prices of natural gas and carbon emission***.
All the modelling activity is carried out by means of Microsoft Excell.

6.2: Furnace modelling without SMR

Within sub-chapter 6.2 the description of the base-model of the existing furnace is taken on.

The domain for the modelling is sketched in **Figure 48**:

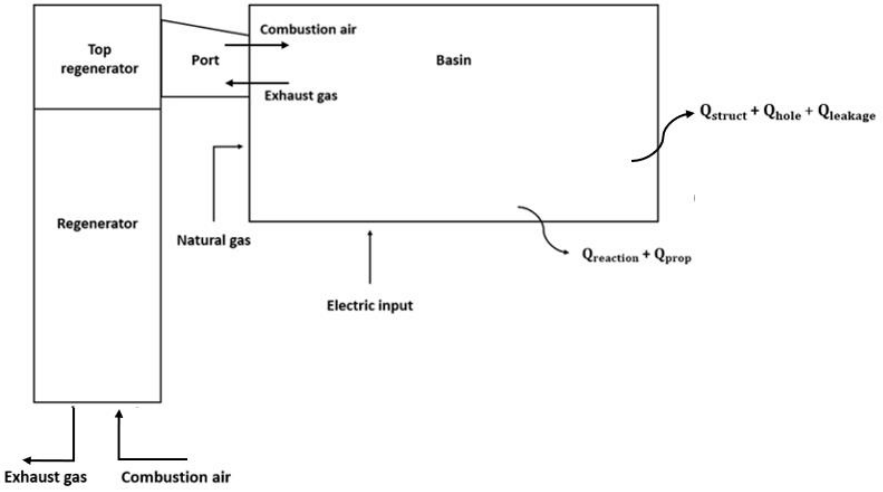

Figure 48 *- Furnace base-model domain*

The relevant streams are depicted, where combustion air and exhaust gasses are shown both at the basin (preheated combustion air – hot flue gases) and regenerator (cold combustion air – warm flue gases) borders, whereas natural gas is supplied at the reference conditions. For what concerns $Q_{s,l,h}$, this heat stream is limited to the heat leakage from the basin (not from ports/top regenerators/regenerator).

6.2.1: Input and variables

The base-model is run at fixed conditions, especially for what concerns *pull* and *cullet*: the first is set equal to the design value, on which the pre-existing model, used as reference for the validation, is tuned. Cullet is also set to the average value both for the base-model and the final configuration[40] (with SMR). For what concerns the *electric input EE,* it is set equal to 0,116 kWh/kg[41] for the validation step.

[40] Despite being important, cullet is not taken as a variable in order to simplify the modelling
[41] Electric input is set to a value, however in the model it can be modified easily as it is a free parameter

It is interesting to point out that the overall heat input Q_{tot} is taken as a known value: it comes indeed from the analysis of the state-of-art carried out in the previous chapters 2 and 3, more specifically from the assessment of the overall heat demand for each class of furnace (see **Figure 37**[42]).
The reference conditions for the energy balances are 298 K and 1 bar.
For sake of simplicity, natural gas is assumed to be composed only by methane.
Table 22 hereinafter provides an insight on the model inputs:

Pull	Q_{tot}	Cullet	EE	T_{ref}
$\frac{ton}{d}$	$\frac{kWh}{kg}$	[%]	$\frac{kWh}{kg}$	[K]
Design value	1,187	Design value	0,116	298

***Table 22** - Inputs and variables for base-model*

The furnace heat balance is expressed via [6. 1]:

$$Q_{tot} = Q_{ee} + Q_{CH_4} \qquad [6.\ 1]$$

The electric input from kWh/kg is converted into kW:

$$EE[kW] = \frac{EE\left[\frac{kWh}{kg}\right] \cdot Pull\left[\frac{kg}{d}\right]}{24\left[\frac{h}{d}\right]} \qquad [6.\ 2]$$

From the furnace energy balance, the heat input required from methane is computed, in terms of kW:

$$Q_{CH_4}[kW] = \frac{Q_{CH_4}\left[\frac{kWh}{kg}\right] \cdot Pull\left[\frac{kg}{d}\right]}{23^{43}\left[\frac{h}{d}\right]} \qquad [6.\ 3]$$

The next step is to compute the flow rate of methane, whose LHV has been determined by applying the enthalpies of formation at normal conditions $\Delta H_{f_i}^0(298\ K)$ to the methane combustion:

[42] The plot refers to 140 ton/d, but it is useful as reference to understand how Q_{tot} has been computed
[43] Because of the switch in the regenerator chambers, burners are stopped for 1 minute at each switch: burners operate 23 h/d

$$CH_4 + 2O_2 = CO_2 + 2H_2O$$

$$LHV_{CH_4} = -\Delta H_r^0(298\ K) = \sum_i v_i \cdot \Delta H_{f_i}^0(298\ K)$$

Where the $\Delta H_{f_i}^0(298\ K)$ of the relevant species (also those relevant for the SMR) are reported in **Table 23**, whereas v_i represents the stoichiometric coefficient of the i-th species:

Component	$\Delta H_{f_i}^0(298\ K)$
-	$\left[\frac{J}{mol}\right]$
CH4	-74900
O2	0
N2	0
H2	0
CO	-110600
CO2	-393800
H20	-242000

Table 23 - $\Delta H_{f_i}^0(298\ K)$

As a result, it holds:

$$LHV_{CH_4} = 802900\ \left[\frac{J}{mol}\right] = 50{,}18\ \left[\frac{MJ}{kg}\right]$$

Eventually, the molar and mass flow rate con be computed:

$$n_{CH_4}\left[\frac{mol}{s}\right] = \frac{Q_{CH_4}[\,kW\,]}{LHV_{CH_4}\left[\frac{J}{mol}\right]} \qquad [6.\ 4]$$

This value represents the amount of fuel that satisfies the demand.

6.2.2: Heat balance on the furnace

Mass and energy balances are written with the approach of the *extent of reaction* ε_j, where j stands for j-th reaction taking place in the system and i stands for the i-th species[44]:

$$n_{i,\,out}\left[\frac{mol}{s}\right] = n_{i,\,in}\left[\frac{mol}{s}\right] + \sum_{j}^{NR} v_{i,j} \cdot \varepsilon_j \left[\frac{mol}{s}\right] \qquad [6.\ 5]$$

$$\sum_{i}^{n} H_{i,in}[W] = \sum_{i}^{n} H_{i,out}[W] + \sum_{j}^{NR} \varepsilon_j \left[\frac{mol}{s}\right] \cdot \Delta H^{\circ}_{r_j}(T_r)\left[\frac{J}{mol}\right] \qquad [6.\ 6]$$

The expression of the enthalpy flux can be written as [6. 7]:

$$\sum_{i}^{n} H_i[W] = \sum_{i}^{n} n_i \left[\frac{mol}{s}\right] \cdot \left[h_{i,ref}[W] + \int_{T_{ref}}^{T} C_{p_i}\left[\frac{J}{mol \cdot K}\right] dT\right] \qquad [6.\ 7]$$

For what regards the $C_{p_i}\left[\frac{J}{mol \cdot K}\right]$, the polynomial relationship [6. 8] was employed to account for temperature dependency:

$$C_{p_i}\left[\frac{J}{mol \cdot K}\right] = R\left[\frac{J}{mol \cdot K}\right] \cdot \left(a_i + b_i \cdot T + c_i \cdot T^2 + \frac{d_i}{T^2}\right) \qquad [6.\ 8]$$

The values for the parameters a, b, c and d are taken from reference [25], while reported in **Table 24**:

Component	T_{max}[45] [K]	a	b	c	d
CH4	1500	1,702E+00	9,081E-03	-2,164E-06	0,000E+00
O2	2000	3,639E+00	5,060E-04	0,000E+00	-2,270E+04
N2	2000	3,280E+00	5,930E-04	0,000E+00	-4,000E+03
H2	3000	3,249E+00	4,220E-04	0,000E+00	8,300E+03
CO	2500	3,376E+00	5,570E-04	0,000E+00	-3,100E+03
CO2	2000	5,457E+00	1,045E-03	0,000E+00	-1,157E+05
H20 vap	2000	3,470E+00	1,450E-03	0,000E+00	1,210E+04

***Table 24** - Heat capacity equation constants*

[44] In case of no reaction, such as heat exchange processes, $\varepsilon = 0$

[45] It is important to choose a set of constants compatible with the high temperatures reached in the furnace chamber

Before writing down the heat balance on the furnace, it is necessary to specify that the assumption of *complete combustion* is considered, which means that the fuel is entirely reacted: no methane nor carbon monoxide is expected in the exhaust gases. To cope with these simplifying conditions, an air-to-fuel ratio higher than the actual one has been employed which means that combustion is simulated with a greater excess of oxidizer. In particular:

$$\alpha = \frac{n_{air}}{n_{CH_4}} = 11$$

$$e\,[\%] = \frac{\alpha - \alpha_{st}}{\alpha_{st}} \cdot 100 = 15{,}55\%$$

Lastly, an air humidity of 50% is assumed. The amount of water vapor in the combustion air is computable by means the two equations [6. 9]:

$$\begin{cases} R.H. = \dfrac{y_{H_2O} \cdot p}{p_{sat_{H_2O}}(298K)} \\ y_{H_2O} = \dfrac{n_{H_2O}}{n_{air}} \end{cases}$$

[6. 9]

Finally, the heat balance on the furnace basin can be written as:

$$H_{in} + EE + n_{CH_4} \cdot LHV_{CH_4} = H_{out}(T_{out}) + Q_{s,l,h} + Q_{r,p}$$

[6. 10]

As external data for the resolution of the heat balance, $Q_{s,l,h} + Q_{r,p}$ are taken from the pre-existent furnace model made available by Bormioli Pharma supplier. These values would not be otherwise computable, and they are set equal to 49,89% of the overall heat input ($H_{in} + EE + n_{CH_4} \cdot LHV_{CH_4}$). Note that such a value is only valid if referred to the considered domain (furnace basin): if another control volume was to be considered, then this 49,89% would not be a reliable esteem anymore.

By setting $T_{in_{air}} = 1300°C$ for the preheated combustion air entering the furnace basin from the port, which is a typical value, the heat balance is solved in the unknown $T_{out_{ex}}$ which represents the temperature of the exhaust gases leaving the furnace chamber (not the temperature within the basin itself), after having set a guess value. This is pursued by imposing the objective function $f_{obj}(T_{out_{ex}})$ [6. 11] and employing the *Goal Seek Function* in Excell:

$$f_{obj}(T_{out_{ex}}) = H_{in} + EE - H_{out}(T_{out}) + n_{CH_4} \cdot LHV_{CH_4} - Q_{s,l,h} - Q_{r,p} = 0$$

[6. 11]

At this point the furnace is characterized in term of temperatures, streams compositions and power fluxes.

6.2.3: Heat balance on the regenerator

When considering the regenerator chambers, the only unknown variable is the outlet temperature of the flue gasses which leave the chambers. The other three streams are completely known (composition and temperatures) as a consequence of the resolution of the energy balance on the furnace basin.
Therefore, by assuming a heat transfer efficiency for the chambers equal to η_{reg}[46] $= 0{,}95$ and by imposing objective function [6. 12], the temperature at which the exhaust gasses leave the domain before making their way to the filters is determined:

$$\mathrm{f_{obj}}\left(\mathrm{T_{out_{regenerator}}}\right) = \eta_{\mathrm{reg}} - \frac{\mathrm{H_{air_{out}}} - \mathrm{H_{air_{in}}}}{\mathrm{H_{ex_{in}}} - \mathrm{H_{ex_{out}}}} = 0 \qquad [6.\ 12]$$

It is interesting to compute both the exchanged power and thermal efficiency of the recovery system:

$$\mathrm{Q_{regen_{exch}}} = \mathrm{H_{air_{out}}} - \mathrm{H_{air_{in}}}$$

$$\eta_{\mathrm{th}}[47] = 100 \cdot \left(1 - \frac{\mathrm{H_{ex_{out}}}}{\mathrm{H_{ex_{in}}}}\right) \qquad [6.\ 13]$$

6.2.4: Model validation

Once the procedure is completed, it is possible to compare the obtained results with the corresponding values computed in pre-existing heat balances built by a Company supplier at the beginning of the furnace campaign. The idea is to determine their *relative percentual error* $err_{rel_{\%}}$:

$$\mathrm{err_{rel_{\%}}} = \left|\frac{\mathrm{x} - \mathrm{x_{model}}}{\mathrm{x}}\right| \qquad [6.\ 14]$$

Where x stands for the generic variable from the pre-existing heat balance, whereas x_{model} represents the one computed within this work.
If these $\mathrm{err_{rel_{\%}}}$ are sufficiently low, the model is considered to be close to the real system behaviour and therefore it is validated.

[46] It tells how much power get lost during the process of heat exchange (to walls, structure, environment, …)
[47] It tells to what extent the recovery system exploits the overall thermal energy of the waste gases

In **Table 25** it is possible to observe which are the compared variables as well as the outputs from the current model, together with the corresponding $\mathrm{err}_{\mathrm{rel}_{\%}}$:

Variable	Pre-existing	Model	$\mathrm{err}_{\mathrm{rel}_{\%}}$
$\mathbf{H_{in}[kW]}$	3.674,42	3.970,85	**8,07**
$\mathbf{H_{out}[kW]}$	5.651,16	5.835,38	**3,26**
$\mathbf{T_{out_{ex}}[K]}$	1.755,00	1.847,16	**5,25**
$\mathbf{T_{out_{regenerator}}[K]}$	761,00	787,36	**3,46**
$\boldsymbol{\eta_{th}[\%]}$	69,14	71,63	**3,61**
$\mathbf{Q_{tot_{furnace}}[kW]}$	11.255,81	11.638,18	**3,40**

***Table 25** - Model outputs and validation*

Noticing that all the errors are well below the 10%, the model is considered validated.

6.3: Furnace modelling with SMR

At this point, it is possible to add the SMR unit to the furnace domain. **Figure 49** represents the process flow diagram of the system:

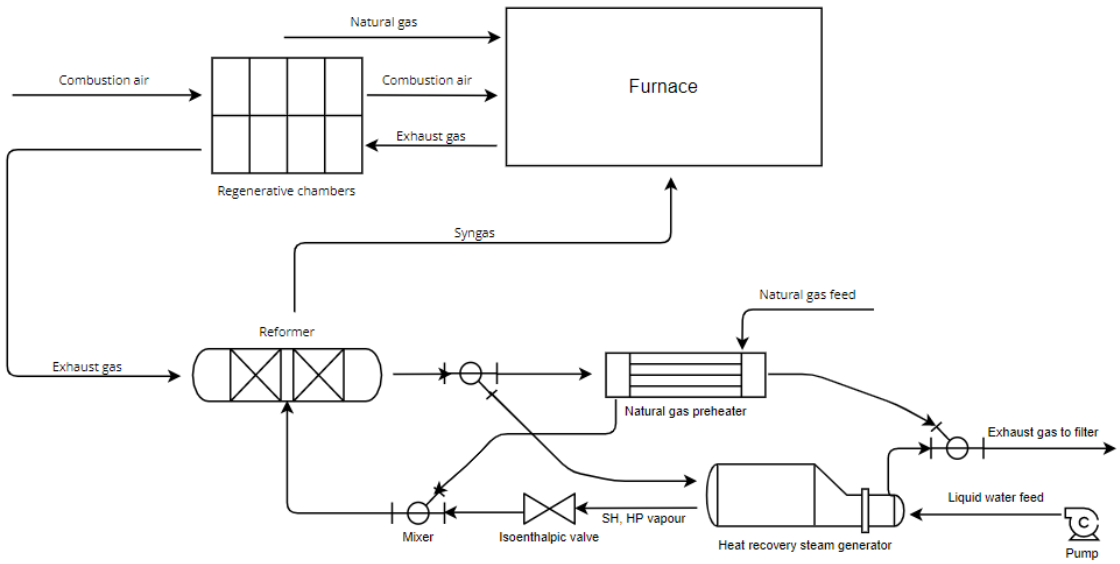

***Figure 49** - Process flow diagram furnace + SMR unit*

The SMR unit system is composed of:

- Reformer reactor
- Natural gas (methane) preheater
- Heat recovery steam generator
- Isoenthalpic valve
- Valves
- Feed/recirculation pumps
- Mixers

As shown in the diagram, the system would be placed downstream the regenerator chambers thus exploiting the residual thermal power of the flue gasses, whose temperature must be sufficiently higher than the temperature level set by the chemical equilibrium on the steam reformer which is, as an anticipation, equal to 850K[48] and it represents the temperature at which the steam reforming reactions occur as well as the value at which the syngas leaves the reactor.
The exhaust gases are initially sent to the reformer reactor, where they lose a first amount of thermal power. Secondly, by means of a valve the flow rate is splitted into two different streams of different rates: one is fed to the heat recovery steam generator HRSG where superheated vapor is produced, whereas the other is fed to the methane preheating heat exchanger. These two exhausts flow rates, having the same temperature[49], are then reunited in the downstream mixer before eventually being sent to the filters.
On the water side, it is fed to the HRSG at the reference temperature (298 K) and at a pressure of 20 bar: this choice is due to the necessity of reducing as much as possible the size of the HRSG and, at the same time, of pursuing a matching[50] between hot source (gases) and cold source (water) which is as good as possible. On the other hand, as an anticipation, the reforming reactions are operated at the lowest pressure possible of 1 bar[51]. Therefore, an isoenthalpic valve is placed such that the superheated steam, which can be considered as ideal gas due to the high temperature and moderate pressure, is expanded without reducing neither its enthalpy nor its temperature. The following step is the mixing of vapor and methane, which are now brought at the same thermodynamic conditions (T, p): the resulting mixture is the feed stream which is eventually fed to the reactor.
The reactor output will be syngas at 850 K, which will be burnt into the furnace chamber. It is reasonable to expect that a couple of dedicated burners would be placed approximately at 3/4 of the basin length, one per each side, resembling some kind of post-combustion. However, their position and number are not accounted in the thermodynamic simulation.

6.3.1: Input and variables

The furnace model accounts for different *pull*, which is therefore a variable for the system, whereas as anticipated the *cullet* is fixed at the design value. The *electric input EE* is also a variable, but just as a reference 0,116 kWh/kg can be employed. The corresponding $\mathrm{Q_{tot}} = \mathrm{Q_{ee}} + \mathrm{Q_{comb}}$ is computed as stated in sub-chapter 6.2.1.
The same reference conditions of 298 K and 1 bar are chosen for the energy balances.

[48] How to compute this value will be explained in section 6.3.2
[49] This is a constraint imposed when computing their flow rates
[50] Higher pressure leads to higher evaporation temperature: hot-cold sources get closer on the T-Q diagram
[51] This will be explained later on when addressing the SMR reactor design (section 6.3.2)

Table 26 sums up the model inputs:

Pull	$Q_{ee} + Q_{comb}$	Q_{tot}	Cullet	EE	T_{ref}
$\frac{ton}{d}$	$\frac{kWh}{kg}$	[kW]	[%]	$\frac{kWh}{kg}$	[K]
135	1,235	10.561,76	Design value	0,116	298
140	1,222	10.830,90			
145	1,210	11.099,98			
150	1,198	11.369,10			
155	1,187	11.638,18			
160	1,177	11.907,30			
165	1,169	12.176,44			
170	1,160	12.443,35			

Table 26 - *Inputs and variables for furnace + SMR unit model*

An important variation with respect to the base-model is on the overall furnace thermal power demand: while for the base-model it was provided in terms of $Q_{tot} = Q_{ee} + Q_{comb}$ from the analysis of the state-of-art accomplished in the firsts chapters, for the complete-model instead (base + SMR unit) it is expressed with [6. 15][52]:

$$Q_{tot}[kW] = H_{in}\ [kW] + EE\ [kW] + \ n_{CH_4}\left[\frac{mol}{s}\right] \cdot LHV_{CH_4}\left[\frac{kJ}{mol}\right] \qquad [6.\ 15]$$

It is comprehensive of the enthalpy flux associated with the preheated combustion air, and it is nothing but the output of the simulation run on the base-model under the same pull, cullet and electric input.

The corresponding values are also available in **Table 26**.
However, the information on $Q_{tot} = Q_{ee} + Q_{comb}$ from the analysis of the state-of-art is nevertheless exploited in parallel for the esteem of the heat to be supplied from combustion (of a generic fuel):

$$Q_{comb}[kW] = \frac{\left(Q_{tot}\left[\frac{kWh}{kg}\right] - \ EE\left[\frac{kWh}{kg}\right]\right) \cdot Pull\ \left[\frac{kg}{d}\right]}{23\left[\frac{h}{d}\right]} \qquad [6.\ 16]$$

At this point, the required thermal power from combustion is determined.

[52] The equation is referred to the base-model: combustion of only methane (no syngas yet)

The knowledge of these two thermal powers is fundamental because they are the fixed elements between the base-model and the complete-model, as they represent the amount of thermal energy that the furnace requires.

Once this is clear, it is possible to go on and set the desired share of energy that the hydrogen within the syngas[53] will provide by means of its LHV: this is the most important variable that can be set, together with the pull.
Therefore, once it has been set, the share of thermal power that both hydrogen and methane would supply is established:

$$\begin{cases} \mathrm{Q_{comb}[kW]} = \mathrm{Q_{CH_4}[kW]} + \mathrm{Q_{H_2}[kW]} \\ \mathrm{Q_{H_2}[kW]} = \mathrm{x\,[\%]} \cdot \mathrm{Q_{comb}[kW]} \\ \mathrm{Q_{CH_4}[kW]} = (1 - \mathrm{x\,[\%]}) \cdot \mathrm{Q_{comb}[kW]} \end{cases}$$

[6. 17]

The next step consists in determining the flow rate of $\mathrm{H_2}$. To do so, its LHV is first computed: it is important to consider that the syngas will leave the reformer reactor at a temperature different from 298 K. Therefore, the LHVs of each species ($\mathrm{H_2}$, CO and unreacted $\mathrm{CH_4}$) will be different from those at reference conditions (298 K). This aspect could be neglected, for sake of simplicity. However, it has been addressed and the correct LHVs have been computed by applying the following relations, where the value of temperature is equal to 850 K:

$$\Delta H_R^0(T) = \Delta H_R^0(T_{REF}) + a_{tot} \cdot (T - T_{REF}) + \frac{b_{tot}}{2} \cdot (T^2 - T_{REF}^2) + \frac{c_{tot}}{3} \cdot (T^3 - T_{REF}^3) + \frac{d_{tot}}{4} \cdot (T^4 - T_{REF}^4)$$

$$a_{tot} = \sum_1^{NC} \upsilon_i \cdot a_i \qquad c_{tot} = \sum_1^{NC} \upsilon_i \cdot c_i$$

$$b_{tot} = \sum_1^{NC} \upsilon_i \cdot b_i \qquad d_{tot} = \sum_1^{NC} \upsilon_i \cdot d_i$$

With:

$$\Delta H_r^0(298\ \mathrm{K}) = \sum_i v_i \cdot \Delta H_{f_i}^0(298\ \mathrm{K})$$

[6. 18]

The intermediate values of a_{tot}, b_{tot}, c_{tot} and d_{tot} are not reported. Moreover, it should be remembered that the fuel heating value is equal and opposite to the ΔH_r^0.

[53] Rather than setting the share of energy supplied by the syngas, it is set that of the hydrogen within the syngas. This is because the LHV of syngas is not known as it depends on its composition, which varies from simulation to simulation

Refer to **Table 23** and **Table 24** respectively for the $\Delta H_{f_i}^0(298\ K)$ and coefficients a_i, b_i, c_i and d_i.

Table 27 sums up the LHV of each species susceptible of combustion within syngas at 850 K (H_2, CO, CH_4):

Component	$\mathbf{LHV(T_{syngas} = 850\ K)}$	$\mathbf{LHV(T_{syngas} = 850\ K)}$
-	$\left[\frac{MJ}{kg}\right]$	$\left[\frac{J}{mol}\right]$
CH4	50,04	-800.726,04
H2	123,51	-247.023,89
CO	10,11	-283.213,93

Table 27 - *LHV species within syngas*

Finally, the H_2 flow rate can be determined:

$$n_{H_2}\left[\frac{mol}{s}\right] = \frac{Q_{H_2}[\,kW\,]}{LHV_{H_2}\left[\frac{J}{mol}\right]}$$

[6. 19]

Contrary to what one would expect, the methane flow rate is not computed on the basis of its LHV and on the remaining share of thermal power (complementary to Q_{H_2}). Indeed, it is at this point that Q_{tot} (output from base-model) is employed. By doing so, it is possible to account for the enthalpy fluxes associated to both preheated combustion air and hot syngas which is fed into the chamber at 850 K. Moreover, the supplementary combustion of unreacted methane and CO enters in the game.
Therefore, the equation [6. 20] represents the heat balance on the furnace basin:

$$H_{in_{air}} + EE + n_{CH_4} \cdot {LHV^{298}}_{CH_4} + {n_{CH_4}}_{syn} \cdot {LHV^{850}}_{CH_4} + n_{H_2} \cdot LHV_{H_2} + n_{CO} \cdot LHV_{CO} + H_{in_{syn}} = H_{out} + Q_{s,l,h} + Q_{r,p}$$

[6. 20]

Obviously, to compute the flow rate of methane (to be supplied as fuel to the furnace) it must first be solved the chemical equilibrium on the reformer reactor, such that the composition of the syngas as well as the demand of methane and water feed for the SMR can be established.

6.3.2: Chemical equilibrium at SMR reactor

In order to study the reactions undergoing in the reactor, the approach of the chemical equilibrium has been applied together with the species mass balance.
First of all, the involved reactions are the *steam reforming* coupled with the *water gas shift*:

$$CH_4 + H_2O \rightarrow CO + 3H_2 \qquad \Delta H_{sr} = 206\ \frac{kJ}{mol}$$

$$CO + H_2O \rightarrow CO_2 + H_2 \qquad \Delta H_{wgs} = -41\ \frac{kJ}{mol}$$

According to literature, in order to obtain a satisfactory methane conversion in terms of mole reacted, a good value for water-to-methane molar ratio needs to be set. Typically, this is between 2 and 4. Accordingly, the following assumptions were made:

1) $\frac{n_{H_2O}}{n_{CH_4}} = 3{,}5$
2) Methane (molar) conversion efficiency: $conv_{CH_4} = \frac{n_{CH_4}^{in} - n_{CH_4}^{out}}{n_{CH_4}^{in}}$ =75%[54]
3) $n_{H_2}\left[\frac{mol}{s}\right]$ computed at previous step

The species mass balance can be written as:

$$n_{i,\,out}\left[\frac{mol}{s}\right] = n_{i,\,in}\left[\frac{mol}{s}\right] + \sum_{j}^{NR} \nu_{i,j} \cdot \varepsilon_j \left[\frac{mol}{s}\right]$$

[6. 21]

For what regards the chemical equilibrium instead, it consists in computing the *equilibrium constant* for each reaction j, by applying the two equations [6. 22]:

$$\begin{cases} K_{eq_j}^{\ 1} = p^{\sum_i^n \nu_i} \cdot \prod_i^n (y_i)^{\nu_i} \\ K_{eq_j}^{\ 2} = e^{\left(-\frac{\Delta G_{R_j}^{\circ}(T_{out})}{R \cdot T_{out}}\right)} \end{cases}$$

[6. 22]

Where *p* is the operating pressure, y_i is the molar fraction of the i-th species in the reactor, $\Delta G_{R_j}^{\circ}(T_{out})$ is the standard Gibbs free energy of reaction j evaluated at the outlet temperature and *R* is the universal gas constant.
For the calculation of the $\Delta G_{R_j}^{\circ}(T_{out})$, the following relationships where used:

[54] The 25% of the methane feed to the SMR is unreacted and therefore burnt in the furnace chamber

Steam reforming

$\Delta H^0_{R,SR}(298K) = +206.3$ kJ/mol

$\Delta G^0_{R,SR}(T) = 53717 - 60.25\,T\ \left[\frac{cal}{mol}\right]$ T is K, 600 K < T < 1500 K

Water Gas Shift

$\Delta H^0_{R,WGS}(298K) = -41.2$ kJ/mol

$\Delta G^0_{R,WGS}(T) = -8514 + 7.71\,T\ \left[\frac{cal}{mol}\right]$ T is K, 600 K < T < 1500 K

Figure 50 *- $\Delta G^{\circ}_{R_j}(T_{out})$ for steam reforming and water gas shift*

For sake of completeness, **Table 28** shows the mass balance on the reactor, where it appears that three unknows are there: x (molar methane feed), ε_{SR} and ε_{WGS} which are the extents of reactions respectively of steam reforming and water gas shift.

Component	$\boldsymbol{n_i^{in}}$	$\boldsymbol{n_i^{out}}$
-	$\left[\frac{\boldsymbol{mol}}{\boldsymbol{s}}\right]$	$\left[\frac{\boldsymbol{mol}}{\boldsymbol{s}}\right]$
CH4	x	$x - \varepsilon_{SR}$
H2O	3,5x	$3{,}5x - \varepsilon_{SR} - \varepsilon_{WGS}$
H2	0	$3\varepsilon_{SR} + \varepsilon_{WGS} = n_{H_2}$
CO	0	$\varepsilon_{SR} - \varepsilon_{WGS}$
CO2	0	ε_{WGS}

Table 28 *- example of species mass balance*

To solve this, let's consider that methane (molar) conversion efficiency as well as the desired hydrogen molar output are known. Hence, it follows that it is possible to reduce the problem to a unique unknown in x (ε_{SR} and ε_{WGS} can be written as functions of only x).

When dealing with the equilibrium constants instead, it appears the variable *pressure p*: if one would write down carefully both $K_{eq_{SR}}$ and $K_{eq_{WGS}}$, it would be clear that the pressure would only appear for the steam reforming, at numerator. From a thermodynamic viewpoint, this means that by operating at higher pressure the chemical equilibrium gets shifted towards the reactants, thus leading to a lower conversion into products (so to keep $K_{eq_{SR}}$ constant)[55]. Hence, in order to avoid this behaviour, it is chosen to operate at low pressure: 1 bar.

[55] In other words, to keep the same conversion rate, at high pressures the equilibrium is reached at higher temperatures. This must be avoided as much as possible due to the limited thermal power that the system can actually exploit!

By writing the equilibrium constants, it also appears that these are functions of the unknown x and of the equilibrium temperature T_{out}, which is also unknown. Hence, the overall problem reduces to a non-linear system of two equations in two unknowns. To solve it, the objective functions [6. 23][6. 24] can be written:

$$f_{obj_1}(x, T_{out}) = \frac{K_{eq_{SR}}^{1}}{K_{eq_{SR}}^{2}} - 1 = 0 \qquad [6.\ 23]$$

$$f_{obj_2}(x, T_{out}) = \frac{K_{eq_{WGS}}^{1}}{K_{eq_{WGS}}^{2}} - 1 = 0 \qquad [6.\ 24]$$

These can be solved numerically by iterative procedure, once two initial guesses are chosen. This was done by means of the Goal Seek Function of Excell.

From this system, the outputs are the required methane molar flow rate needed in order to supply the desired hydrogen molar flow rate and the temperature at the reactor outlet, which is the already mentioned 850 K.
As a consequence, the molar composition of the syngas is also fully determined as well as the extents of reactions of both steam reforming and water gas shift (useful for the heat balances on the reactor).

NOTE: while the methane molar flow rate changes from simulation to simulation as it is a function of desired hydrogen output, the equilibrium temperature instead turns out to be always equal to 850 K.

Figure 51 taken from reference [26] is the schematization of a shell-and-tube steam reformer which could be also employed:

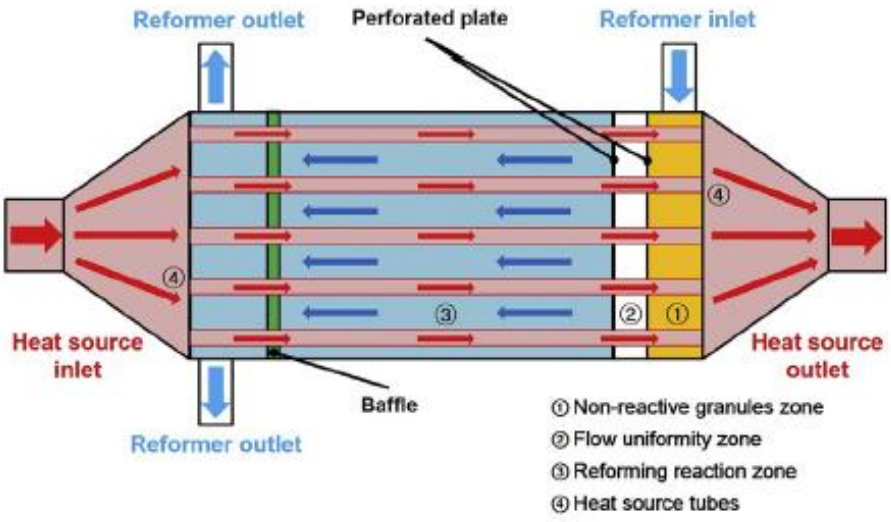

Figure 51 - *Schematic of reformer reactor*

6.3.3: Heat balance on the furnace

It is now possible to focus on the determination of the methane flow rate supply at the furnace. This is achieved by applying objective function [6. 25]:

$$f_{obj_3}(n_{CH_4}) = Q_{tot} - \left(H_{in_{air}} + H_{in_{syn}} + EE + n_{CH_4} \cdot LHV^{298}{}_{CH_4} + n_{CH_4} \cdot LHV^{850}{}_{CH_4} + n_{H_2} \cdot LHV_{H_2} + n_{CO} \cdot LHV_{CO}\right) = 0 \quad [6.\ 25]$$

For what regards the "boundary" conditions (air excess, relative humidity and $(Q_{s,l,h} + Q_{r,p})$[56]), these are just the same as for the base-model. For reference, check on sub-chapter 6.2.2.
The free variable that can be tuned at each simulation is on the temperature of the preheated combustion air $T_{in_{air}}$. At normal operating conditions, it is equal to 1300°C. However, such a level of temperature might not be achievable because of the SMR unit presence downstream the regenerator. Indeed, the higher $T_{in_{air}}$ the better is the heat recovery taking place within the regenerative chambers. As a consequence then, the waste gasses leaving the chamber would be well cooled down (in traditional end port furnaces they are in the range 450-500°C). The fact that the SMR unit is placed downstream means that flue gases must be at a temperature sufficiently higher than 850 K (577 °C): as a reference value, such a difference between these two temperatures is chosen to be higher than 20°C. Therefore, $T_{in_{air}}$ must be set accordingly and it is only acceptable if the above condition is respected, which is something to be checked after the heat balance on the regenerator.
All this considered, it follows that a trade-off between heat recovery in the chambers and in the SMR unit needs to be minded. This is particularly true when low shares of hydrogen production are simulated: $T_{in_{air}}$ can sink down to 1150°C. In such conditions, the main consequence is on the methane demand which increases as $T_{in_{air}}$ decreases. On the other side, when high shares of hydrogen production are simulated $T_{in_{air}}$ can be maintained around normal levels without compromising the capability of the flue gases to provide the required thermal power at the SMR unit.

At this point, all the flow rates are fully determined, and it is possible to set the heat balance on the furnace whose unknown is the waste gasses outlet temperature from the basin. It can be computed with the objective function [6. 26]:

$$f_{obj_4}(T_{out_{ex}}) = H_{in_{air}} + EE + n_{CH_4} LHV^{298}{}_{CH_4} + n_{CH_4{}_{syn}} LHV^{850}{}_{CH_4} + n_{H_2} LHV_{H_2} + n_{CO} LHV_{CO} + H_{in_{syn}} - H_{out} - Q_{s,l,h} - Q_{r,p} = 0 \quad [6.\ 26]$$

6.3.4: Heat balance on the regenerator

By solving the heat balance on the regenerator it is possible to determine the waste gasses outlet temperature from the regenerator chambers, as it is the only unknown variable for this control volume. Moreover, it is at this very step of the resolution procedure that it becomes clear whether the above-set

[56] The assumption of 48,89% of the inlet thermal power is maintained

value of $T_{in_{air}}$ is compatible with the constraint on the temperature difference between exhausts gases and chemical equilibrium (850 K). In case it is not respected, then a lower value of $T_{in_{air}}$ has to be chosen.
By assuming a heat transfer efficiency for the chambers equal to $\eta_{reg} = 0{,}95$, the objective function [6. 27] is imposed:

$$f_{obj_5}\left(T_{out_{reg}}\right) = \eta_{reg} - \frac{H_{air_{out}} - H_{air_{in}}}{H_{ex_{in}} - H_{ex_{out}}} = 0$$

[6. 27]

Thus:

$$T_{in_{air}} \text{ acceptable if } \quad \Delta T = T_{out_{reg}} - 850\ K > 0$$

$$T_{in_{air}} \text{ not acceptable if } \quad \Delta T = T_{out_{reg}} - 850\ K < 0$$

In case the criterion was not respected, then a new $T_{in_{air}}$ would need to be imposed and the procedure would restart from the resolution of $f_{obj_3}(n_{CH_4})$.

Again, it is interesting to compute both the exchanged power and thermal efficiency of the recovery system:

$$Q_{regen_{exch}} = H_{air_{out}} - H_{air_{in}}$$

$$\eta_{th} = 100 \cdot \left(1 - \frac{H_{ex_{out}}}{H_{ex_{in}}}\right)$$

[6. 28]

6.3.5: Heat balance SMR unit

This step of the procedure is focused on the thermodynamic design of the reactor as well as of the steam and methane preheating units.
At this level of accuracy, no distinction is made between methane heat exchanger and HRSG: these are initially modelled as a unique box, as the target of the step is to fully determine the thermodynamic quantities of the involved streams (temperatures, thermal powers), whereas the flow rates are already known.

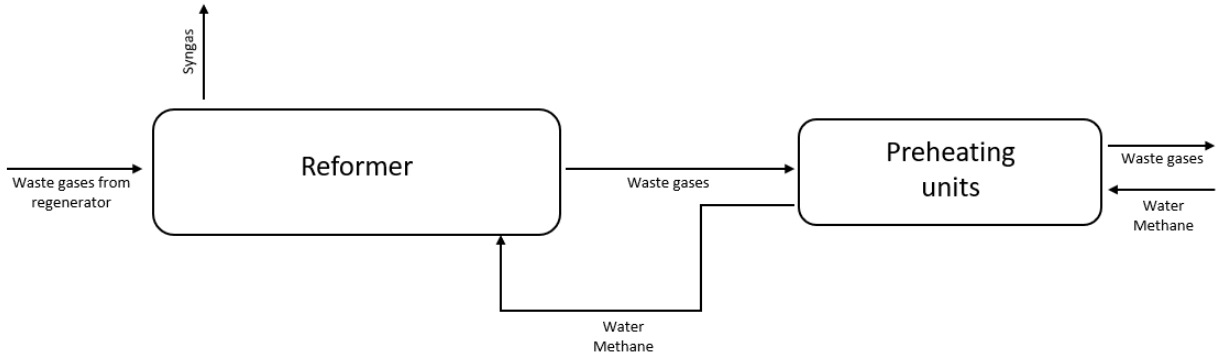

***Figure 52** - SMR unit*

The purpose is to exploit the residual thermal power of the exhaust gases leaving the regenerator to activate the reforming reactions, preheat the methane feed and generate the superheated vapour at 850 K.

From the energetic viewpoint, the heat balances on the overall system (reformer + preheating units), on the reformer and on the preheating units must be verified contemporarily. They are reported in [6. 29][6. 30][57]:

$$H_{ex}^{in} + H_{w,m}^{in} = H_{ex}^{out} + H_{syn} + \varepsilon_{SR} \cdot \Delta H_{R_{SR}}^{0}(850\ K) + \varepsilon_{WGS} \cdot \Delta H_{R_{WGS}}^{0}(850\ K) + n_{CH_4} R \int_{T_{in_r}}^{850} C_p dT + n_{H_2O} R \int_{T_{in_r}}^{850} C_p dT$$

[6. 29]

$$H_{ex}^{in} + H_{w,m} = H_{ex} + H_{syn} + \varepsilon_{SR} \cdot \Delta H_{R_{SR}}^{0}(850\ K) + \varepsilon_{WGS} \cdot \Delta H_{R_{WGS}}^{0}(850\ K) + n_{CH_4} R \int_{T_{in_r}}^{850} C_p dT + n_{H_2O} R \int_{T_{in_r}}^{850} C_p dT$$

[6. 30]

$$H_{ex} + H_{w,m}^{in} = H_{ex}^{out} + H_{w,m}$$

[6. 31]

Let's discuss the conditions applied on the control volumes.

First of all, the $\Delta H_{r_j}^{0}(850\ K)$ for steam reforming and water gas shift are computed by applying the same procedure explained in sub-chapter 6.3.1 for the calculation of the LHV at 850 K. Their values are hereinafter reported:

Reaction	$\Delta H_{r_j}^{0}(298\ K)$	$\Delta H_{r_j}^{0}(850\ K)$
-	$\left[\frac{J}{mol}\right]$	$\left[\frac{J}{mol}\right]$
Steam Reforming	206.300,00	223.559,56
Water gas shift	-41.200,00	-36.190,04

***Table 29 –** Reaction enthalpies for steam reforming & water gas shift*

[57] Note that the sum of the heat balances on reactor and preheating units gives the overall balance

Regarding the integral terms, they account for the last temperature step that methane and vapor feeds need to reach the temperature at which reactions occur, when they leave the preheating units. Indeed, the methane preheating heat exchanger and the HRSG will be designed such that at their outlet the maximum temperature is 490 °C[58].

For what concerns the definition of the enthalpy fluxes of water, it is important to recall that a pressure of 20 bar in the HRSG is set, which should allow to reduce the size of the unit and, at the same time, enhance the matching between hot source and cold source as the evaporation temperature gets increased. To model the new thermodynamic behaviour of water, the relations [6. 32][6. 33] and coefficients in **Table 30** were employed for the estimation of the evaporation temperature[59] and enthalpy[60]:

$$\ln\left(\frac{p_{sat}}{p_c}\right) = A \cdot \left(1 - \frac{1}{\frac{T_{sat}}{T_c}}\right)$$

[6. 32]

$$\Delta H_{evap}(T_{evap}) = \Delta H_{evap}(373\ K) \cdot \left[\frac{1 - \frac{T_{evap}}{T_c}}{1 - \frac{373\ K}{T_c}}\right]^{0,38}$$

[6. 33]

T_c	p_c	A	$\Delta H_{evap}(373\ K)$
[K]	[bar]	[-]	$\left[\frac{J}{mol}\right]$
647	221	7	33.672,44

***Table 30** - Water properties*

The unknown variables in such a domain are two temperatures, both on waste gases side: the intermediate one (between reactor and preheating unit) and at the system outlet (lowest thermal level for the entire system).
These can be computed by setting the two objective functions [6. 34[6. 35] to be solved in series (heat balances on reactor and preheating units):

$$f_{obj_6}(T_{ex}) = H_{ex}^{in} + H_{w,m} - H_{ex}(T_{ex}) - H_{syn} - \varepsilon_{SR} \cdot \Delta H_{R_{SR}}^{0}(850\ K) - \varepsilon_{WGS} \cdot \Delta H_{R_{WGS}}^{0}(850\ K) - n_{CH_4} R \int_{T_{in_r}}^{850} C_p dT - n_{H_2O} R \int_{T_{in_r}}^{850} C_p dT = 0$$

[6. 34]

[58] Design approach and constraints fully explained in section 6.4
[59] Antoine equation
[60] Watson equation

From f_{obj_6} the intermediate temperature is computable.

$$f_{obj_7}\left(T_{ex}{}^{out}\right) = H_{ex} + H_{w,m}^{in} - H_{ex}^{out}\left(T_{ex}{}^{out}\right) - H_{w,m} = 0$$

[6. 35]

From f_{obj_7} the waste gases outlet temperature is determined: this basically is representative of how much the overall heat recovery system (regenerative chambers + SMR unit) is able to exploit. The goal of the system is to have it as low as possible. In general, it cannot go beyond a given value because of the presence of filters, which operate at around 280 °C (electrostatic filter) – 180 °C (baghouse filter) to avoid acid condensation. Therefore, these represent the threshold for any recovery system applied to a glass furnace.

6.3.6: Heat balance on HRSG and methane preheater

Once these two temperature levels are established, it is possible to split the control volume representing the HRSG and methane preheater, which operate in parallel, in order to characterize their thermodynamic features in terms of flow rates (waste gasses side) and exchanged thermal powers. Refer to **Figure 49** for the precise flow diagram.

First of all, let's address the exhaust gasses flow rates in the HRSG and methane preheater, respectively. These have been computed by imposing the following constraints:

- The waste gasses flow rate leaving the reactor is not equally splitted among HRSG and methane preheater, however their molar composition is fixed
- Superheated vapor and methane feeds reach the same outlet temperature of 490 °C
- The two waste gasses flow rates at HRSG and methane preheater outlet are at the same temperature $T_{ex}{}^{out}$

Therefore, the two flow rates have been computed by setting a heat balance on HRSG [6. 36] and methane preheater [6. 37]:

$$n_{ex}^{HRSG} = \frac{n_{H_2O} \cdot \left[C_{p_{liq}}^{H_2O} \cdot \left(T_{evap} - 298\right) + \Delta H_{evap} + R\int_{T_{evap}}^{490} C_{p_{vap}} dt\right]}{\sum_i^n y_i \cdot C_{p_i} \cdot \left(T_{ex} - T_{ex}{}^{out}\right)}$$

[6. 36]

$$n_{ex}^{meth.PH} = \frac{n_{CH_4} \cdot R\int_{25}^{490} C_p dt}{\sum_i^n y_i \cdot C_{p_i} \cdot \left(T_{ex} - T_{ex}{}^{out}\right)} = n_{ex} - n_{ex}^{HRSG}$$

[6. 37]

It is now possible to determine the operating conditions for the HRSG in terms of exchanged powers as well as flue gasses temperatures in each section (economizer, evaporator, superheater). To do so, let's consider its T-Q diagram:

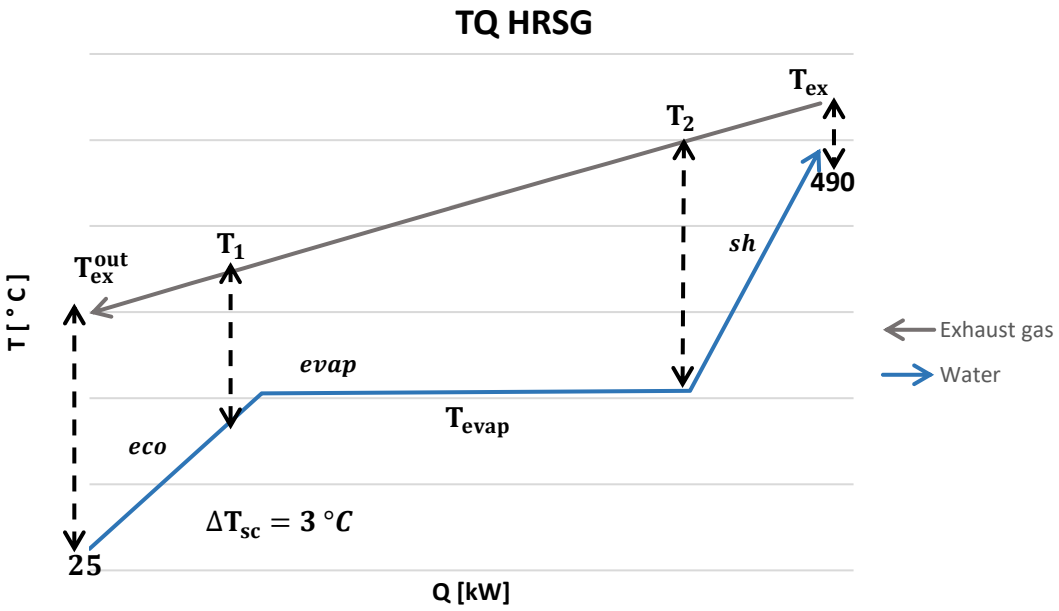

***Figure 53** - TQ diagram HRSG*

Water is fed at the HRSG inlet at the reference conditions. In the economizer, water is heated up close to its evaporation temperature: a sub-cooling temperature difference ΔT_{sc} equal to 3 °C is imposed which should avoid the formation of a two-phase mixture within the economizer tubes. Water is then supplied with the evaporation duty in the evaporator and finally superheated vapor is produced within the superheater. From the water side, all temperatures are known such that it is also possible to compute the corresponding exchanged thermal powers:

$$Q_{eco}\ [W] = n_{H_2O} \cdot C_{p_{liq}}^{H_2O} \cdot \left(T_{evap} - \Delta T_{sc} - 298\right) \qquad [6.\ 38]$$

$$Q_{evap}\ [W] = n_{H_2O} \cdot \Delta H_{evap} \qquad [6.\ 39]$$

$$Q_{sh}\ [W] = n_{H_2O} \cdot R \int_{T_{evap}}^{490} C_{p_{vap}} dt \qquad [6.\ 40]$$

From the exhaust gasses side instead, temperatures T_1(economizer inlet) and T_2 (superheater outlet) need to be computed to fully characterize the waste gases side ($T_2 > T_1$). This is pursued by applying the two objective functions [6. 41][6. 42], representative of heat balances on economizer and evaporator respectively:

$$f_{obj_8}(T_1) = Q_{eco} - (H_{ex}(T_1) - H_{ex}^{out}) = 0$$

[6. 41]

$$f_{obj_9}(T_2) = Q_{evap} - \left(H_{ex}(T_2) - H_{ex}(T_1)\right) = 0$$

[6. 42]

To check on the accuracy of the procedure, the overall heat balance on the HRSG can be implemented, which must be always satisfied:

$$H_{ex} - H_{ex}^{out} = Q_{eco} + Q_{evap} + Q_{sh}$$

[6. 43]

Eventually, the methane preheating thermal duty can be computed by means of [6. 44]:

$$Q_{CH_4}[W] = n_{CH_4} \cdot R \int_{25}^{490} C_p dt$$

[6. 44]

6.3.7: Schematized procedure

The implemented procedure is schematized in **Figure 54**:

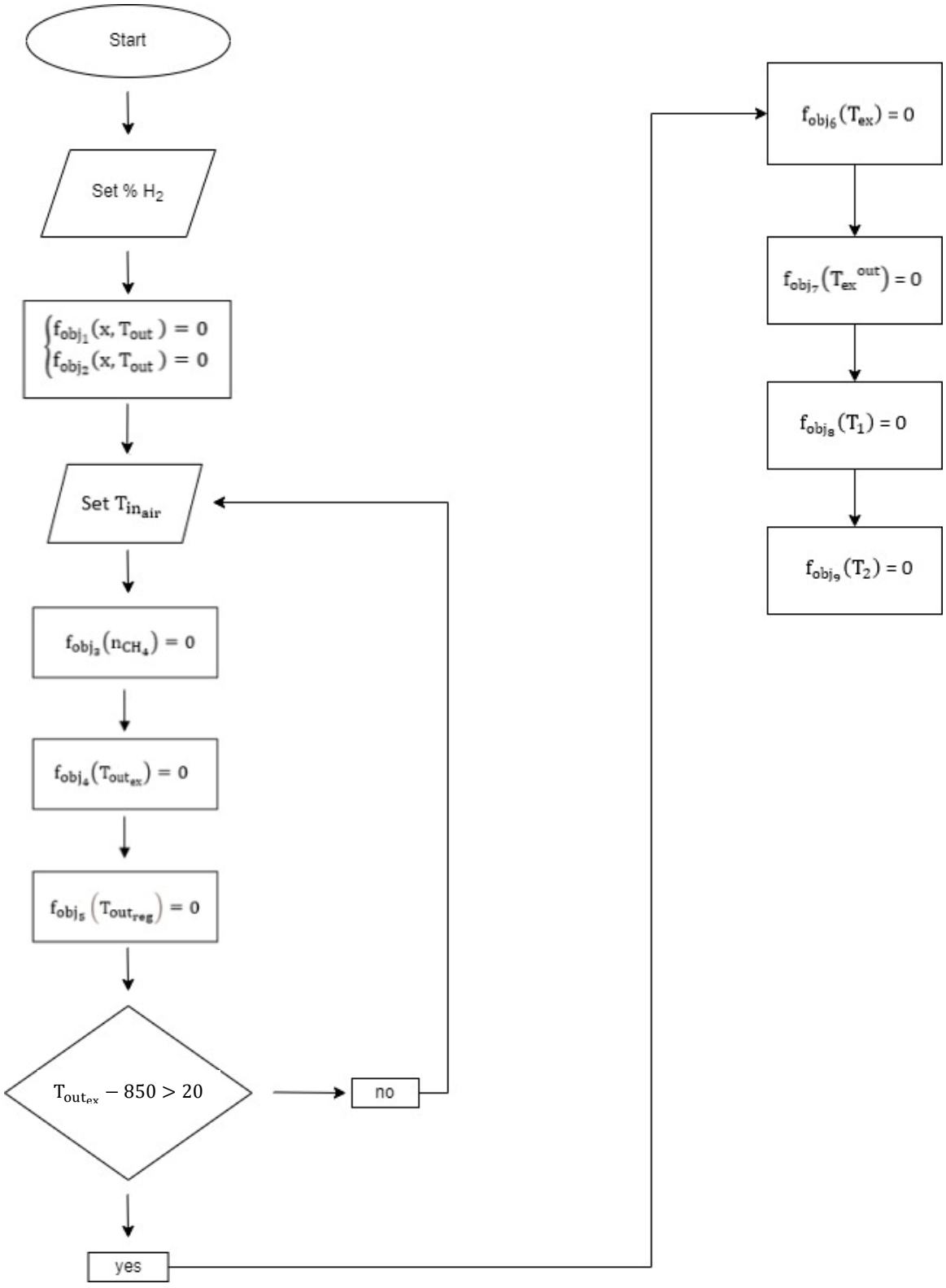

Figure 54 - *Procedure block flow diagram*

6.4: Methane preheater and HRSG sizing

Once the thermodynamics has been carried out and all the temperature profiles as well as thermal powers are established, it is possible to move on the sizing of the heat exchangers.

6.4.1: Methane preheater

For the case of the methane preheater, it is designed by applying the approach of the *logarithmic mean temperature difference:*

$$Q_{CH_4}[\,W\,] = U\left[\frac{W}{m^2K}\right] \cdot A[\,m^2\,] \cdot \Delta T_{ml}[\,K\,] \qquad [6.\ 45]$$

Where *U* is the *overall heat transfer coefficient* and *A* is the *surface of heat exchange* on waste gasses side, which is the parameter that is going to be defined by means of the current analysis.
For what regards U, a literature review has been performed in order to estimate its value. Indeed, in order to compute it precisely, the rigorous approach would require the detailed knowledge of geometric and fluid dynamic parameters which are however not available at this level of design. Therefore, the current approach is seeking more a range within the final size would fall rather than defining the final and precise surface A.
According with literature [27], [28] typical values of U for gas-gas heat exchangers are in the range:

$$U \in [5, 40]\ \frac{W}{m^2K}$$

To account for the uncertainty on U, a sensitivity analysis is carried out by taking first 5 and then 40 such that a reliable esteem on the likely range for A is provided.
Obviously, this will then reflect on the heat exchanger cost.

For the definition of ΔT_a and ΔT_b refer to the hereinafter heat exchanger T-Q diagram, whereas the thermal duty Q_{CH_4} has been computed above.

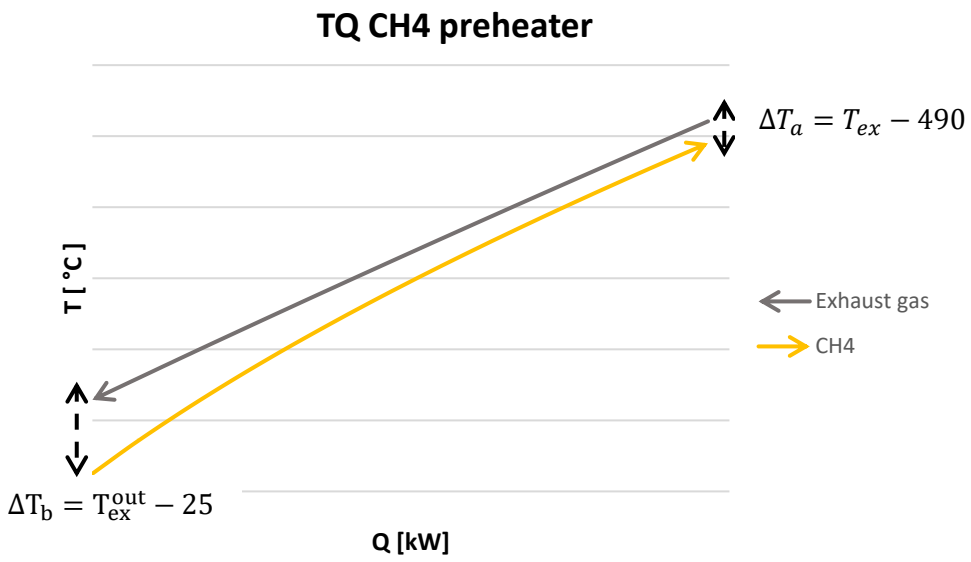

Figure 55 *- TQ diagram methane preheater*

6.4.2: HRSG

The design of the steam generator has been carried out by a Company supplier, on the basis of the outcomes obtained from the thermodynamic modelling. These are, in particular, the flow rates of water and exhaust gases within the HRSG, the thermal powers exchanged (in economizer, evaporator and superheater), the temperature profile for water and waste gases as well as the pressure of the superheated vapor.

Initially, the idea was to set up the unit consisting of economizer, evaporator and superheater with water inlet at 20 bar and 25°C (reference temperature) and vapour outlet at same 20 bar and temperature as close as possible to the 850 K. However, following up a discussion with the supplier, it has been decided to apply two changes:

1. Water at the unit inlet (25°C) is first pumped to 4 bar and then preheated with a flow rate of superheated vapour, which is bled at the outlet conditions, to about 120 °C. At these conditions (subcooled liquid), water is fed to a physical deaerator where the most volatile species are extracted. This is necessary because of sulphur oxides traces in liquid water at low temperature which would affect the economizer bundle, thus leading to a fast degradation of the economizer itself, being SO_2 at 20 bar and low temperature below the dew-point curve[61].
   At this point, water is pumped to 20 bar. Because of the limited temperature difference from the saturation, it has been decided to not employ the economizer and to directly feed the water stream to the evaporator, followed by the superheater.

2. The outlet temperature of superheated steam is relevant not only for the thermodynamic of the process, but also for the choice of the metals of the superheater. It is suggested a maximum outlet temperature of 490 °C which would allow to operate safely with a commercial steel P22. For higher

[61] Sulphur oxide would condensate and react with water into sulphurous acid, highly corrosive for common metals

temperatures instead, more peculiar metals should be employed. Hence, the outlet temperature of the vapor is set to 490°C

Therefore, the HRSG unit has been set up with these expedients. Note that, according with the designer, because of the important amount of dust in the flue gases, it was not possible to adopt finned surfaces which would have made it possible to reduce quite significantly the heat transfer area, thanks to an enhanced heat exchange efficiency.

6.5: Results and sensitivity

Within this section of the chapter the results that can be deduced from the model are discussed. The idea is to analyse separately the outcomes: first will be proposed the potential savings, with respect to the base-model, in terms of CH_4 and CO_2 , together with the sensitivity analysis on pull and electric input. The goal is not only to identify whether all the $\%H_2$ are able to bring to satisfactory savings, but also to establish at which percentage the highest performance is obtained, and if this is really achievable or technological limitations exist.
Then, the heat exchanger design is tackled with the corresponding sensitivity analysis on the variable U, evaluated on the most remarkable operating conditions.
Last, the economic assessment of the project is presented, tuned on the most promising solutions.
The overall process is expected to bring to the individuation of those configurations which are able to maximize the thermodynamic and economic performances. Thanks to the sensitivity analysis carried out on a number of variables, these outcomes are supposed to provide a reasonable esteem, at least within a given margin of error.

6.5.1: Potential CH_4 and CO_2 savings

First of all, let's define the savings:

- $\Delta \mathrm{CH_4} \left[\frac{\mathrm{sm^3}}{\mathrm{y}}\right] = \left(\mathrm{V}_{\mathrm{CH_4}}^{\mathrm{SMR}} - \mathrm{V}_{\mathrm{CH_4}}^{\mathrm{no\ SMR}}\right)$
- $\Delta \mathrm{CO_2} \left[\frac{\mathrm{tonCO_2}}{\mathrm{y}}\right] = \left(\mathrm{m}_{\mathrm{CO_2}}^{\mathrm{SMR}} - \mathrm{m}_{\mathrm{CO_2}}^{\mathrm{no\ SMR}}\right)$

These figures, together with the corresponding percentual values, have been computed under different conditions of $\%H_2$, pull and electric input.

For the case of fixed electric input (0,116 kWh/kg) and variable pull, the results are plotted. Note that three levels of pull are taken, indicated as lower, middle and higher:

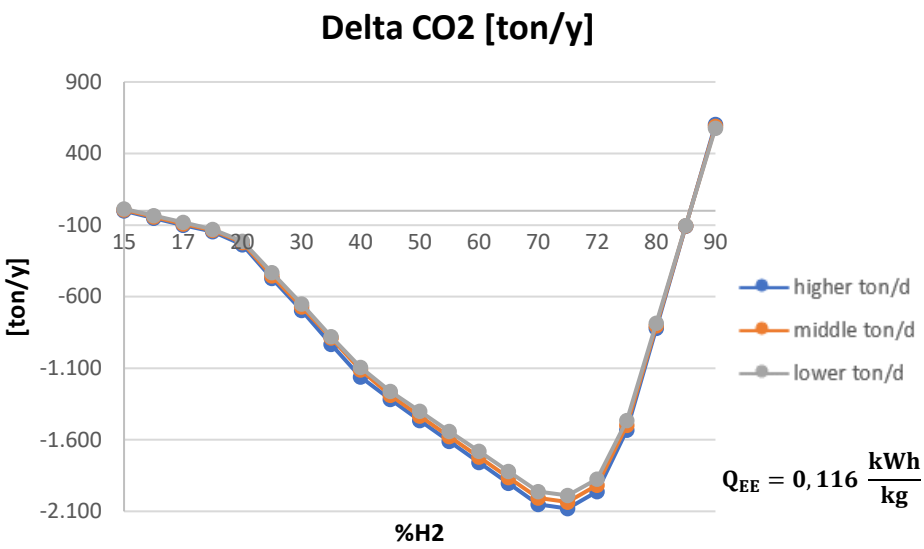

Figure 56 *- Savings in carbon emission against pull [ton/y]*

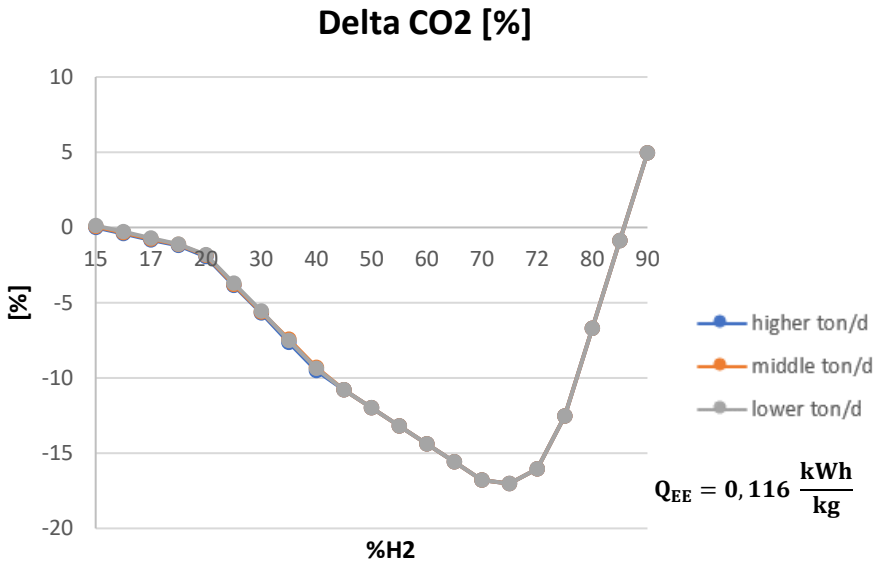

Figure 57 *- Savings in carbon emission against pull [%]*

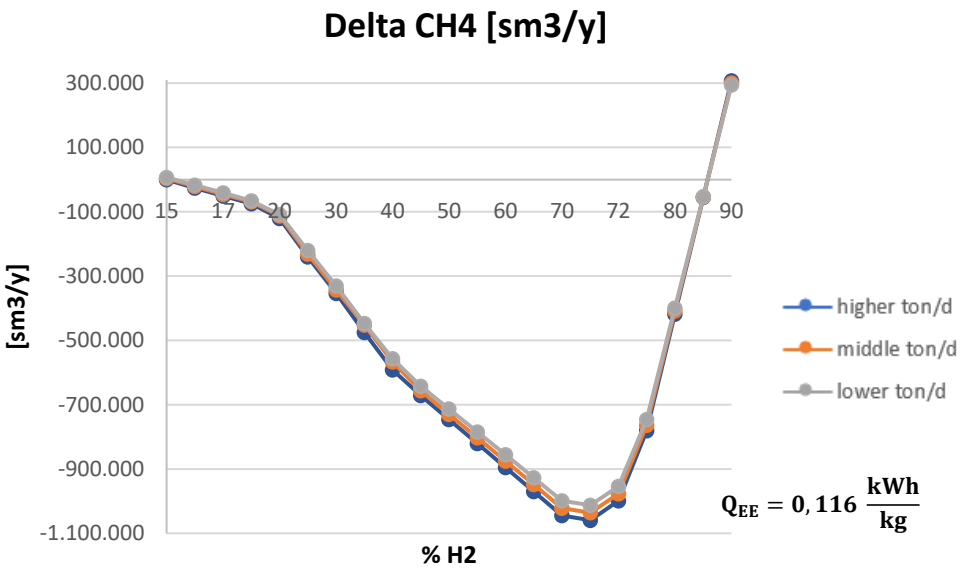

Figure 58 *- Savings in methane demand against pull [sm3/y]*

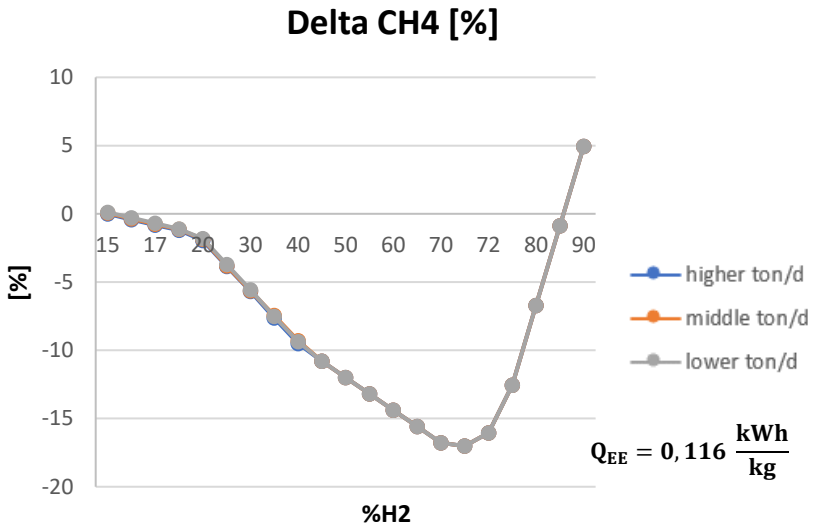

Figure 59 – *Savings in methane demand against pull [%]*

What can be noticed is that a non-monotonic behaviour of both CH_4 and CO_2 is expected. More specifically, a beneficial effect of the system is for $\%H_2$ between 16 and 85 with a point of maximum in the range 65-75%. Such an outcome holds for all the three pulls under investigation, with not a major difference in absolute terms (ton/y and sm3/y) and basically same output in relative terms (%).

In order to assess whether such results also hold whit different electric inputs, the same procedure has been repeated. The pull is kept fixed at middle ton/d, whereas the electric inputs are 0,070, 0,093 and 0,116 kWh/kg which correspond to a range of about 400-800 kW:

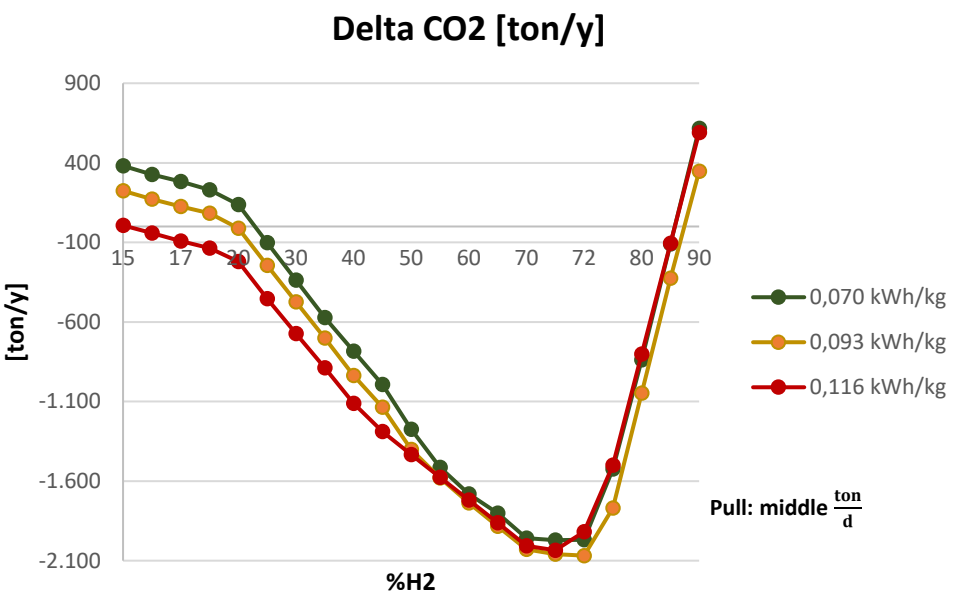

Figure 60 *- Savings in carbon emissions against ee [ton/y]*

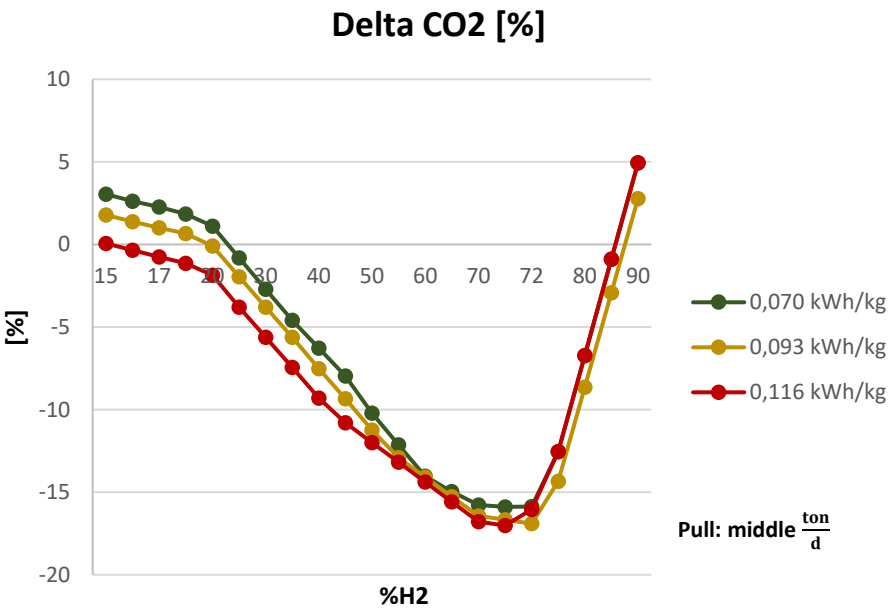

Figure 61 *- Savings in carbon emissions against ee [%]*

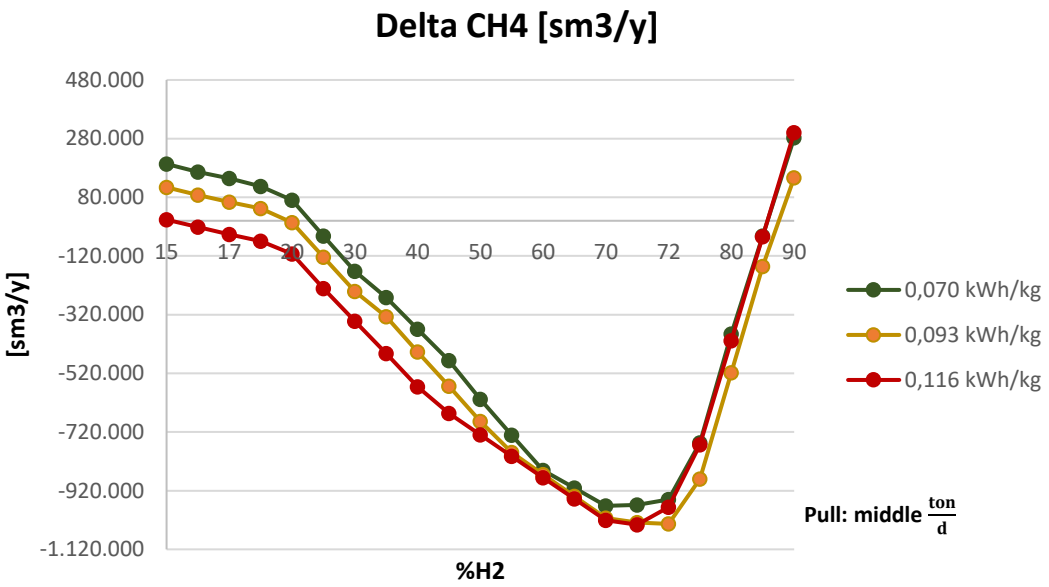

Figure 62 *- Savings in methane demand against ee [sm3/y]*

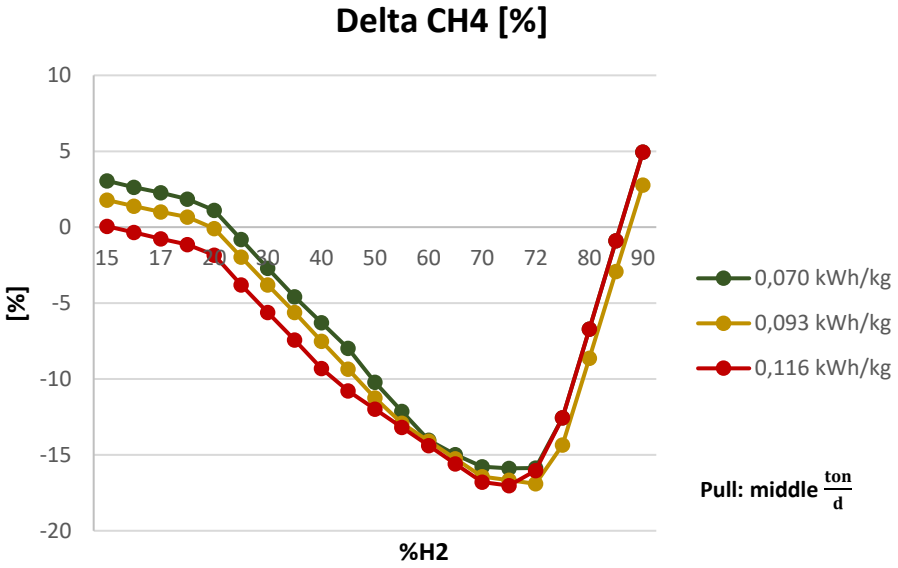

Figure 63 *- Savings in methane demand against ee [%]*

The behaviour is qualitative the same as for the sensitivity on the pull, however the differences between the three electric inputs are stronger, especially at the lowest share of H_2: The lower is the electric input, the higher is the $\%H_2$ able to give a beneficial result. On the other hand, at high shares (>60%) the difference is marginal. For what concerns the optimum though, it is confirmed to belong to the range 65-75%, with rather small differences both from absolute (ton/y and sm3/y) and relative (%) viewpoint.

From these two scenarios then, it is possible to state that the model is able to provide a positive effect on fuel demand and carbon emissions only within a window of H_2 share, which is roughly between 16-85%. Within these values, a maximum is reached around 65-75%.
However, the last question is yet to be addressed: are there any technological limitations on the possibility to adopt such high shares? From a thermodynamic perspective, the main limitation is coming from the temperature at which the exhaust gases would leave the system (${T_{ex}}^{out}$), before being sent to the filter. It is indeed the presence of the filter the major limitation, since it is the component that sets the flue gases lowest temperature within the process and, therefore, the heat recovery that can be achieved by the system. According with the type of filter, these are the limiting temperatures:

- Electrostatic filter: T=280 °C
- Baghouse filter: T=180 °C

If these technological constraints were imposed, it would follow that it might not be possible to achieve those 65-75% able to optimize the system. This is indeed the situation, as such high shares would be reached, for each of the run simulations, with ${T_{ex}}^{out}$ that goes beyond these thresholds. What would be then the technologically feasible hydrogen share, able to maximize the savings? Results show the following output, for each simulation:

- 40-45 $\%H_2$, for electrostatic filter
- 55-60 $\%H_2$ for baghouse filter

Accordingly, the estimated savings are those shown in the plots. It is also provided a table that summarizes the results for respectively electrostatic and baghouse filter, expressed in terms of relative percentual error. This is supposed to tell the degree of uncertainty of the model on the results:

$$\mathrm{err}_{\mathrm{rel}_{\%}} = \left|\frac{x_{max} - x_{min}}{x_{max}}\right| \qquad [6.\ 46]$$

For each of the four figures ($\Delta CO_2\left[\frac{ton}{y}\right]$, $\Delta CH_4\left[\frac{sm^3}{y}\right]$, $\Delta CO_2\ [\%]$ and $\Delta CH_4\ [\%]$) the relative percentual error is computed for both the cases of electrostatic and baghouse filter. Moreover, it is determined for the results of the sensitivity analysis on pull and electric input separately: this should highlight how much these figures are sensible to these variables.
For the sake of clearness, the procedure followed is the reported:

1. For each plot, set the hydrogen share
2. Select the three corresponding values of the y-axis
3. Individuate the minimum and maximum values

4. Compute $\mathrm{err}_{\mathrm{rel}_{\%}}$ between these two values

The outcomes are hereinafter reported:

Electrostatic $\mathbf{T_{lim} = 280°C}$	$\boldsymbol{\Delta CO_2}$	$\boldsymbol{\Delta CO_2}$	$\boldsymbol{\Delta CH_4}$	$\boldsymbol{\Delta CH_4}$
Sensitivity	$\left[\frac{\mathbf{ton}}{\mathbf{y}}\right]$	[%]	$\left[\frac{\mathbf{sm^3}}{\mathbf{y}}\right]$	[%]
Pull	±5,7 %	±2,0 %	±5,8 %	±2,0 %
Electric input	±40,0 %	±32,0 %	±50,0 %	±32,0 %

***Table 31** - relative percentual error on results for the case of electrostatic filter*

Baghouse $\mathbf{T_{lim} = 180°C}$	$\boldsymbol{\Delta CO_2}$	$\boldsymbol{\Delta CO_2}$	$\boldsymbol{\Delta CH_4}$	$\boldsymbol{\Delta CH_4}$
Sensitivity	$\left[\frac{\mathbf{ton}}{\mathbf{y}}\right]$	[%]	$\left[\frac{\mathbf{sm^3}}{\mathbf{y}}\right]$	[%]
Pull	±4,4 %	±1,0 %	±4,4 %	±1,0 %
Electric input	±14,0 %	±16,0 %	±18,0 %	±16,0 %

***Table 32** - relative percentual error on results for the case of baghouse filter*

It can be deduced that the model has a limited sensibility on the pull, given the low relative percentual errors (<6%) for both the cases of electrostatic and baghouse filters. On the other hand, the electric input turns out to be a variable which introduces an important uncertainty on results (up to 50%), especially for the case of the electrostatic filter. This is also evident from the plots, as the curves are way more apart.

In general, it holds that results are not only more attractive when the baghouse filter is considered, but also more stable with respect to variations in pull and electric input.

6.5.2: Heat exchangers size

Also in the heat exchanger sizing the approach is to discuss the effect of different variables on the surface of heat exchange. The main variable of interest in this regard is the value of the *overall heat transfer coefficient U,* which is supposed to range between 5 and 40 $\frac{\mathrm{W}}{\mathrm{m^2K}}$. The extremes of the interval are taken for the purpose. In addition, also the effect of pull and electric input has been evaluated, such that an overall esteem on the degree of uncertainty can be addressed.

Figure 64 and **Figure 65** represent the outcome of the sizing: the first shows the surface dependency on pull and U at fixed electric input, whereas the second is about electric input and U a fixed pull.
The values of pull and electric input under assessment are the same as the previous.

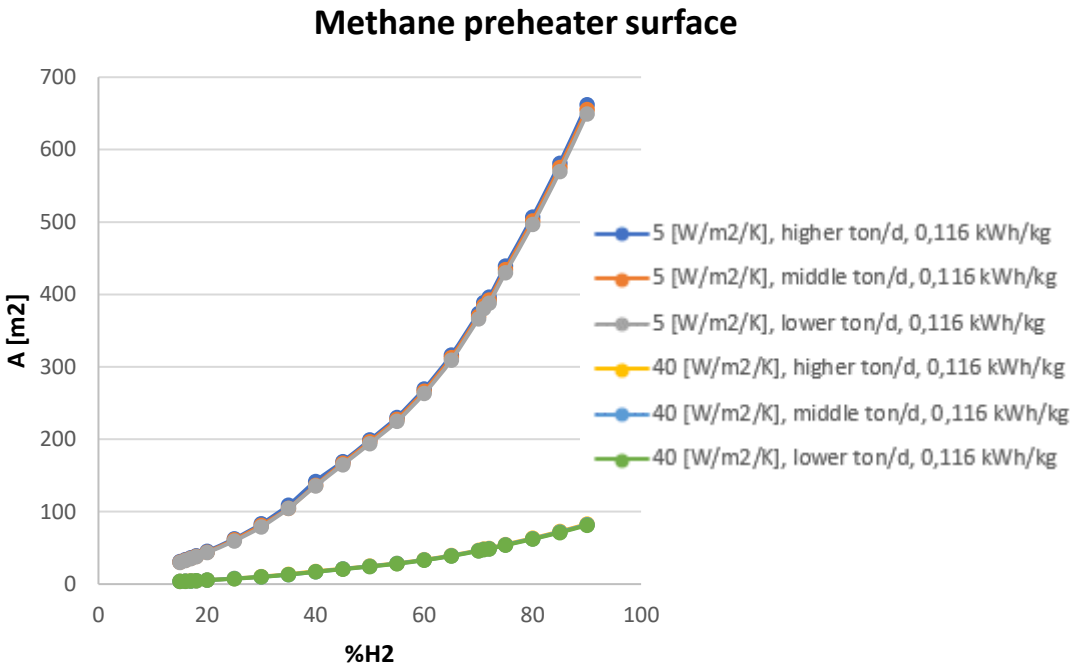

***Figure 64** - Methane preheater surface against U, pull at fixed ee*

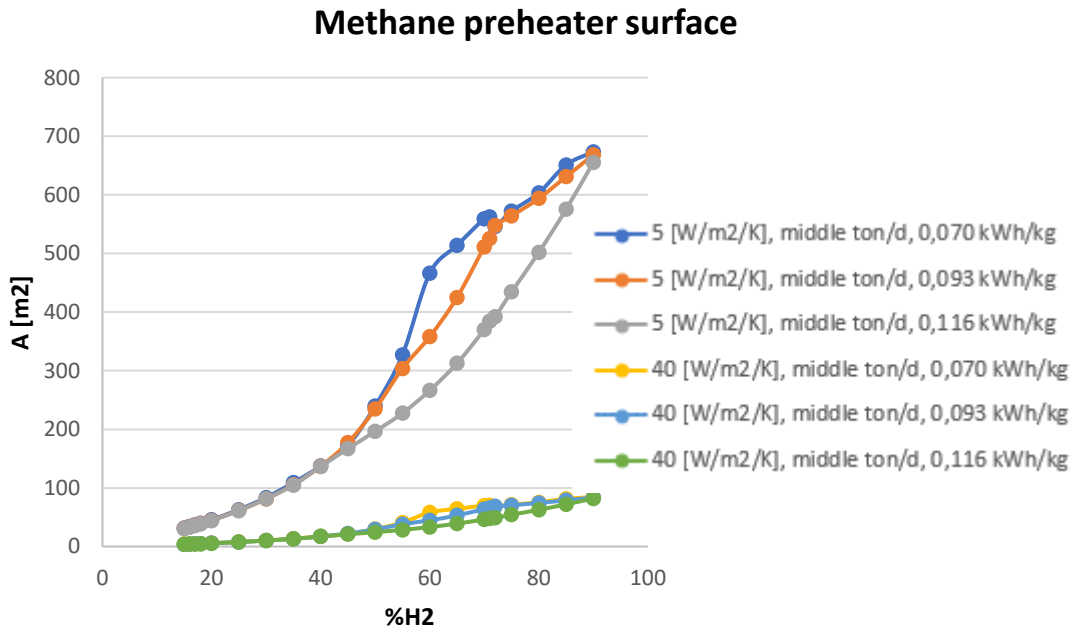

***Figure 65** - Methane preheater surface against U, ee at fixed pull*

The results tell that U is definitely a major variable that must be considered, as strong differences are to be expected when it undergoes significant changes. It appears that, ranging from 5 to 40 $\frac{W}{m^2K}$, the surface increases 8 times: this shall not be unexpected, given the linearity of the mean logarithmic temperature difference approach with respect to U.
What about the influence of pull and electric input? It appears that pull is not actually significantly influencing the heat exchanger sizing, considering that the curves in **Figure 64** are almost overlapped.
This is not true for the electric input. Once again, it plays an important role, at least at high hydrogen shares and in particular for the case of U=5 $\frac{W}{m^2K}$.

For the sake of the project, the interesting cases are those compatible with the temperature constrain set by the filters. Similarly to what done for the evaluation of the relative percentual error between ΔCH_4 and ΔCO_2, the same procedure has been applied in order to establish the degree of uncertainty of the model with respect to these variables. Results are provided in the tables hereinafter:

Electrostatic $T_{lim} = 280°C$	**A** $[m^2]$	
	U = 5	**U = 40**
Sensitivity	$\left[\frac{W}{m^2K}\right]$	$\left[\frac{W}{m^2K}\right]$
Pull	±4,6 %	±4,6 %
Electric input	±1,0 %	±1,0 %

***Table 33** - relative percentual error on methane preheater surface for the case of electrostatic filter*

Baghouse $T_{lim} = 180°C$	**A** $[m^2]$	
	U = 5	**U = 40**
Sensitivity	$\left[\frac{W}{m^2K}\right]$	$\left[\frac{W}{m^2K}\right]$
Pull	±2,4 %	± 2,4 %
Electric input	±18,5 %	±18,5 %

***Table 34** - relative percentual error on methane preheater surface for the case of baghouse filter*

According with this evidence, the sizing of the methane preheater is less sensible to the accounted variables, as the relative percentual errors are way lower than those obtained for the savings in fuel and carbon emissions. However, for the case of system operating with a baghouse filter, the electric input is a variable that introduces quite an important uncertainty (18,5%).

6.5.3: Equipment quotation

The cost of each piece of equipment has been estimated, taking into account also the sensitivity analysis performed. The components addressed are:

- Reforming reactor
- Methane preheater
- HRSG
- Couple of additional burners

For the case of the ***reforming reactor***, the approach consisted in searching for a reference [29] able to tell the cost associated with its hydrogen mass flow rate production. Then, correlation [6. 47] is exploited:

$$\frac{C_a}{C_b} = \left(\frac{A_a}{A_b}\right)^n \qquad [6.\ 47]$$

Where C_a, C_b represent the costs while A_a, A_b are the equipment cost attributes[62] and n is an exponent which accounts for the non-linear relationship, which can also be accounted as a "economy of scale" attribute (equipment at twice the capacity of another is less than twice the cost). A typical value for n is 0,6: for this reason, such a correlation is also known as "*six-tenths rule*". In this specific case, C_b and A_b are the cost [€] and hydrogen output $\left[\frac{kg}{h}\right]$ of the reference reactor, respectively.
Once again, the results of the cost estimation are analysed by taking into account different pulls and electric input. **Figure 66** summarizes the reactor expected quotations:

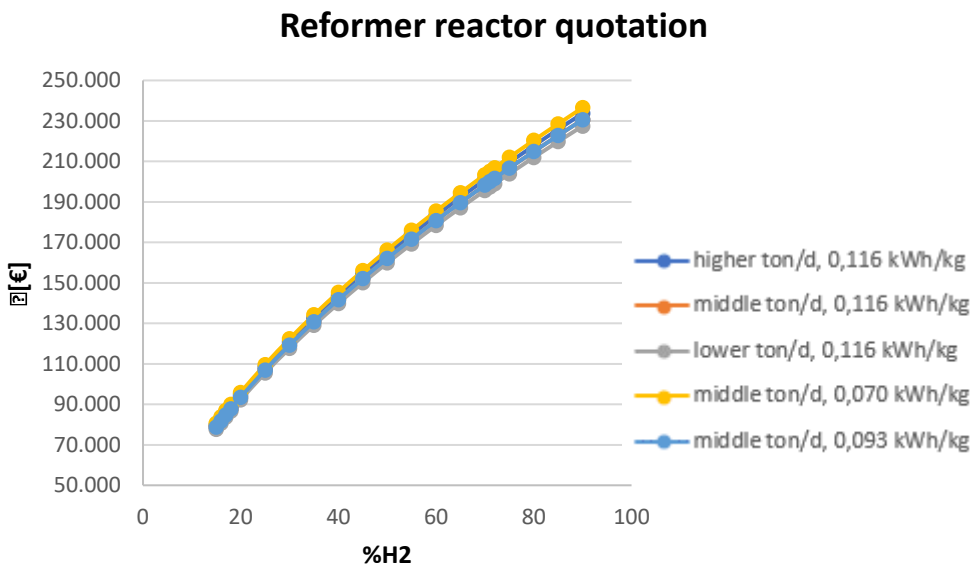

Figure 66 *- Reformer reactor quotation against pull and ee*

[62] As an example, this could be a flow rate output, the power of an equipment or in general any other desired output for the considered system

Almost overlapped curves indicate that the expected cost is basically independent of the two variables. Indeed, by computing the relative percentual error, one would obtain very narrow differences:

Reactor quotation	
Sensitivity	[€]
Pull	±2,7 %
Electric input	±3,8 %

Table 35 *- relative percentual error on reactor quotation*

For what regards the ***methane preheater***, once the size has been established it is a matter of applying a reliable correlation for the quotation. According with reference [24], the six-tenth rule can be linearized. Different authors suggested slightly different coefficients for the tuning[63] of the linearization when applied to the case of a carbon-steel U-tube shell-and-tube heat exchanger, whose results are here reported:

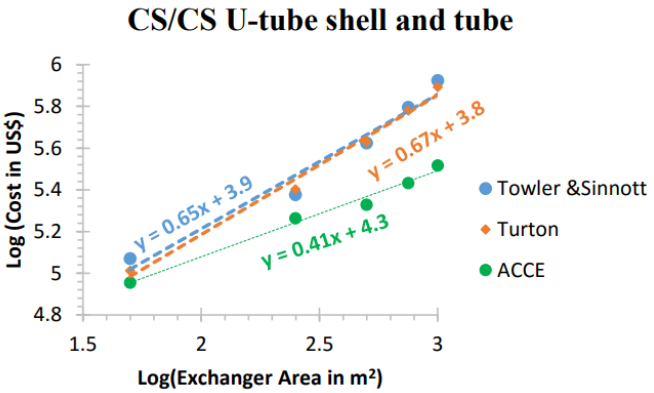

Figure 67 *- Linearization of the six-tenth rule for a U-tube shell and tube heat exchanger [24]*

By applying the Turton[64] 's correlation, the knowledge of the surface of the heat exchange is enough to obtain the corresponding quotation. Once again, this is done by varying pull and electric input on the two different values of U (5 and 40 $\frac{W}{m^2K}$):

[63] Slope and intercept

[64] Same reference as for chapter 5

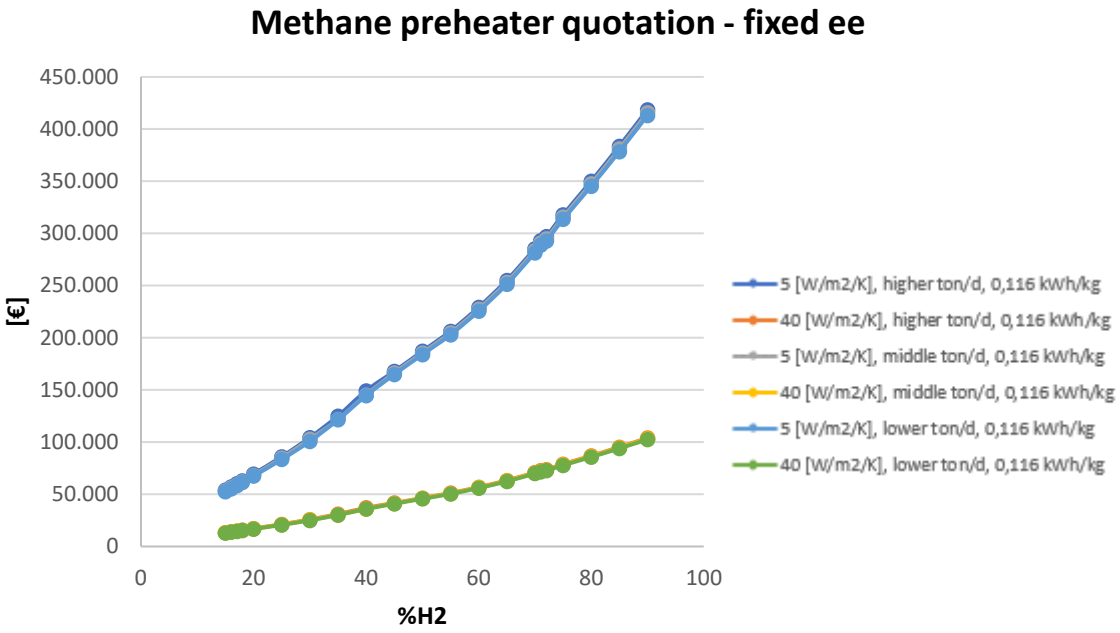

Table 36 - *Methane preheater quotation against U, pull at fixed ee*

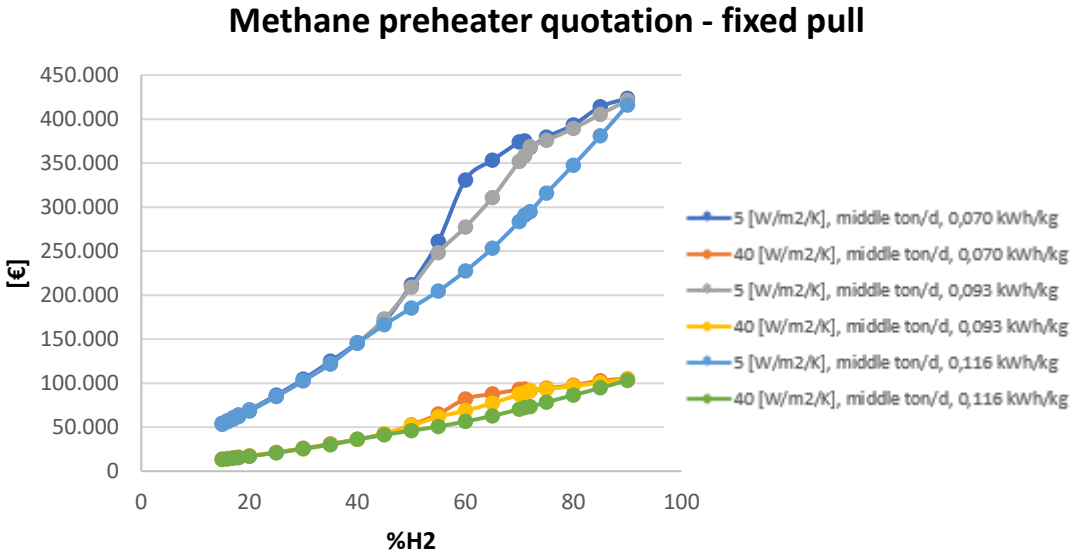

Figure 68 - *Methane preheater quotation against U, ee at fixed pull*

The quotation is basically a scaling of the results achieved in the sizing step, which is confirmed by the curve shapes. The following are the relative percentual errors:

Electrostatic $T_{lim} = 280°C$	A [€]	
	U = 5	U = 40
Sensitivity	$\left[\frac{W}{m^2K}\right]$	$\left[\frac{W}{m^2K}\right]$
Pull	±3,1 %	±3,1 %
Electric input	±0,4 %	±0,4 %

Table 37 - *relative percentual error on methane preheater quotation for the case of electrostatic filter*

Baghouse $T_{lim} = 180°C$	A [€]	
	U = 5	U = 40
Sensitivity	$\left[\frac{W}{m^2K}\right]$	$\left[\frac{W}{m^2K}\right]$
Pull	±1,6 %	±1,6 %
Electric input	± 12,8 %	± 12,8 %

Table 38 - *relative percentual error on methane preheater quotation for the case of baghouse filter*

Limited uncertainties are to be expected.

For what regards the quotation of the ***HRSG***, as anticipated it is provided by a supplier together with its design and sizing. The offer includes, together with the components specified in section 6.4.2, also the circulation and feed pumps, valves and instrumentation, insulation, electric panel and certification H72[65]. The budgetary proposal for the overall set is 415.000 €.
Even though the design was specifically carried out for the solution at 40% of hydrogen share (what would change from case to case would be the involved thermal powers and flow rates), according with the designer of the supplying company there were only slight differences with the other configurations in terms of equipment size and quotation. Therefore, this solution is taken as reference for the HRSG quotation.

Last, for the case of ***burners***, the cost indication comes from a Company supplier. Accordingly, the offer would include a set of two burners, dedicated supports, brackets and pressure gauges. The overall cost would be around 20.000-25.000 €. Moreover, it is suggested a replacement of each burner every three years, which is to be accounted in the cash flow calculation.

[65] Specific certification for pressurized steam generator from waste gasses comprising a number of equipment and instrumentation

6.6: Economic analysis

The very last part of the model wants to address the economic evaluation of the project. For the choice of the most suitable approach, it is considered as relevant the time value of money due to the fact that the investment is projected over a considerable length of time (furnace lifetime, nine years are assumed). Therefore, the *Net Present Value NPV* approach is employed which is not only able to tell whether the investment is profitable (NPV>0), but also how much the company would earn because of its implementation. As an alternative, the *Payback Period PBP* could be implemented. However, it would not provide any information on the project profitability since the cash flows beyond the PBP would not be considered.

The NPV is based on formula [6. 48]:

$$\mathrm{NPV} = \sum_{t=1}^{N} \frac{F_t}{(1+i)^t} - F_0 \qquad [6.\ 48]$$

Where N is the number of years being considered (furnace lifetime around nine years), i is the inflation rate[66], F_t is the cash flow at time t and F_0 is the invested capital.

For what regards the positive cash flow instead, the CH_4 and CO_2 savings with respect to the base-model are considered (furnace without SMR unit). The main uncertainty here is about their prices, which are strongly fluctuating and steadily on a rising path. To smooth down such an unpredictability, a sensitivity analysis is operated. A yearly maintenance expenditure of 2% of the CAPEX is assumed.

This analysis seeks at establishing whether the project is actually feasible in economic terms and which configuration (% H_2) would achieve the highest performance. Similarly to what done in the previous sections, a sensitivity analysis is carried out on the following variables: ***pull, electric input, overall heat transfer coefficient U, price of methane*** and ***price of carbon emission***. The goal is to establish their impact on the NPV of the project. To do so, the idea is to separately evaluate pull and electric input in the same manner as done so far, and in addition to apply the variability of U and price of methane as well as of carbon emission. **Figure 69** should clarify the approach:

[66] A reference value of 1% is used

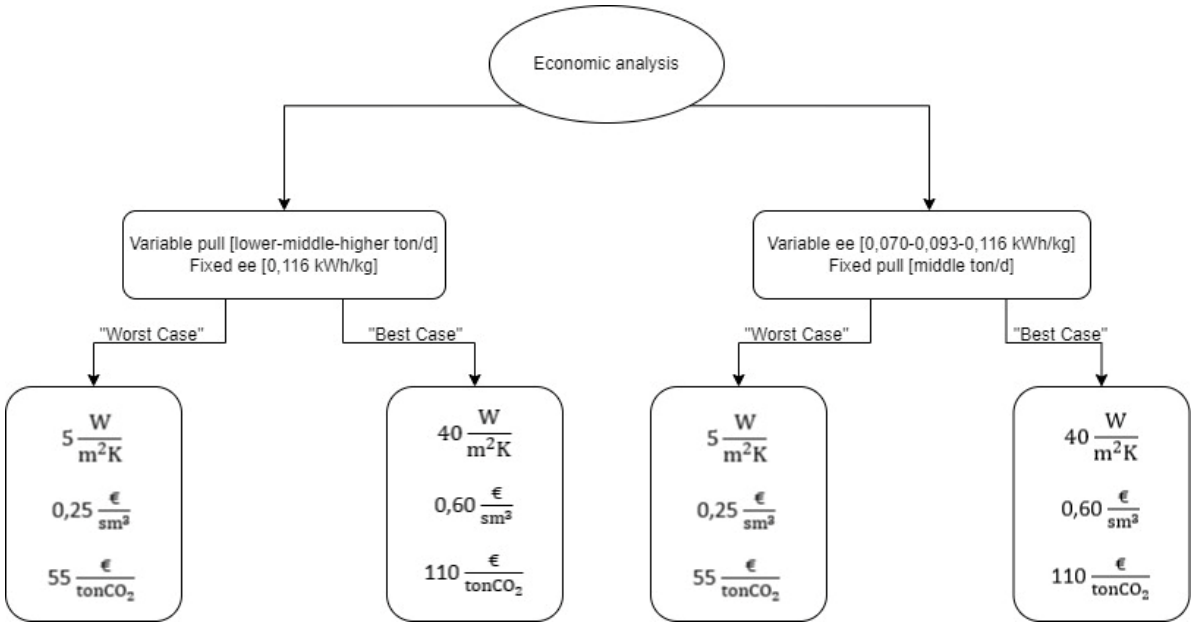

***Figure 69** - Sensitivity structure for economic analysis*

Where "worst case" and "best case" represent the scenarios in which the project would appear the least[67] and the most[68] profitable, respectively.
This should allow on the one hand to establish the influence of pull and electric input, on the other to define the range where the actual NPV should be located for any value of U and methane/carbon prices, as long as these are between 5 and 40 $\frac{W}{m^2K}$, 0,25 and 0,60 $\frac{€}{sm^3}$, 55 and 110 $\frac{€}{tonCO_2}$ respectively.

Once the calculations have been carried out, the results have been collected and plotted. The output is, for each of the twelve cases, the corresponding NPV for each hydrogen share, which is made varying between 15 and 60 %, the latter being the ultimate technologically feasible configuration. Hereinafter the results are provided:

[67] Low U means bigger surface and therefore higher cost, combined with the lowest methane and carbon dioxide savings
[68] high U means smaller surface and therefore lower cost, combined with the highest methane and carbon dioxide savings

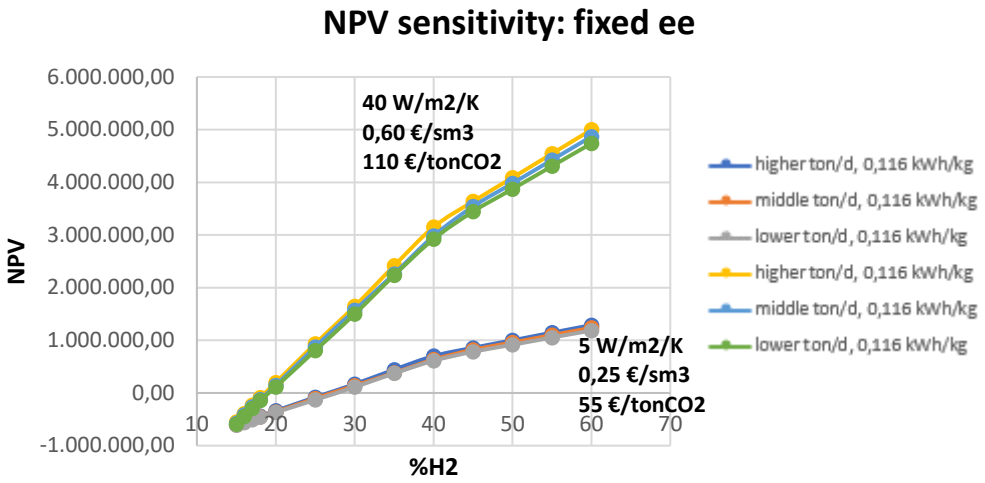

***Figure 70** - NPV sensitivity at fixed electric input*

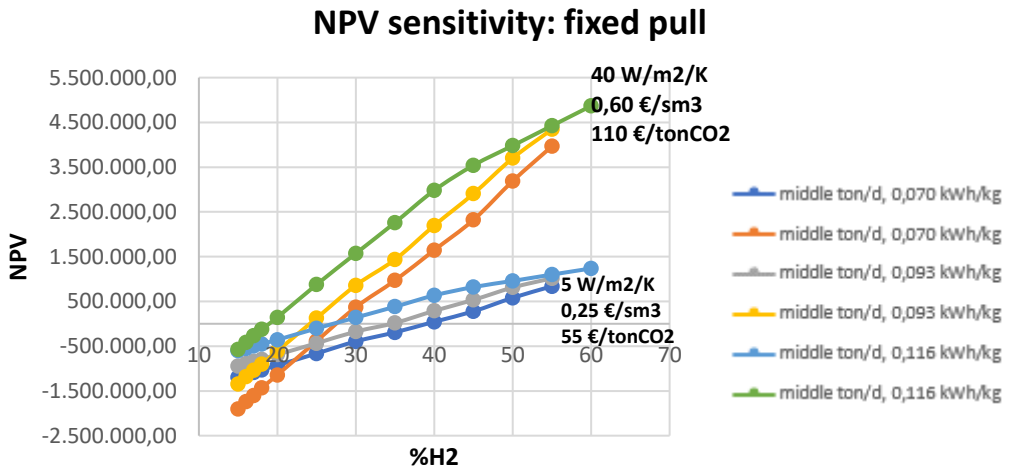

***Figure 71** - NPV sensitivity at fixed pull*

According with the results, it appears that the electric input plays a bigger role also for what regards the NPV. Indeed, stronger differences are foreseen which are reflected both on the minimum hydrogen share that makes the project advantageous and on the NPV itself. Moreover, also note that the "worst" configurations exhibit the lowest profitability and also require a higher % H_2 to ensure a positive NPV.

All being considered, the analysis brings to the conclusion that the NPV at the optimal operating conditions[69] is expected within the ranges:

- Electrostatic filter 40% H_2: 44.824 < NPV [€] < 3.150.312
- Baghouse filter 60% H_2: 837.288 < NPV [€] < 4.997.349

[69] Where the system maximizes the savings, in terms of hydrogen share

As anticipated previously, such an analysis allows to determine the curves between which lay the NPV of the project, for any value of the considered variables. This turns useful because on the one hand enables to assess whether a configuration is indeed profitable or not, on the other defines the conditions that should be at least assumed in order to make the project feasible.

To conclude, in on design conditions the system would be able to provide rather interesting performances both from the CH_4/CO_2 and economic viewpoints. Indeed, in case of electrostatic filter, up to 10% of CH_4/CO_2 savings together with a NPV in the range 44.824 and 3.150.312 €. For the case of baghouse filter instead, more ambitious numbers can potentially be pursued such as a 15% cut in CH_4/CO_2 and NPV of 837.288 to 4.997.349 €.

Conclusions

The goal of the Thesis is to address the challenge of decarbonization of the glass industry, which is doubtlessly an energy intensive sector. In doing so, it is fundamental to first analyse the state-of-art of the energy demand and carbon emissions associated with the actual furnaces, for soda-lime and borosilicate glasses. By exploiting the data made available by the Company, it was possible to design a method, based on energy balances, which enables to compute the theoretical specific energy demand $\left[\frac{\mathrm{kWh}}{\mathrm{kg}}\right]$ as a function of the three most important independent variables: pull, cullet and electric input. This, coupled with the *energy efficiency index* which accounts for the ageing of the furnace, allows to have a picture of the overall theoretical specific energy consumption (and emissions) of the given furnace along its lifetime. This turns out to be quite useful when assessing the implementation of a new and alternative technology, as this method represents the reference for the Company.

At first glance, numerical results and plots in chapter 2 show that the specific energy demand can be potentially reduced for all furnaces when operating at higher cullet and pull. Moreover, for combustion-based furnaces, the natural gas demand can be significantly decreased when higher share of cullet is employed, together with a greater electric input. This would also lead to lower direct carbon emission. It is also important to recall that furnace ageing brings to definitely not negligible increase in energy consumption and, therefore, carbon emission which is expressed by means of the energy efficiency index. Typical values of increase are +40/50% for electric, + 50/60% for Cyclope and + 30/35% for end port and unit melter furnaces. Note that these are theoretical values, that would be registered if the furnace was operated at fixed conditions: the actual energy demand and direct CO_2 emissions depend on the combination of the three variables: cullet, pull and electric input.
When assessing the direct carbon emissions, the role played by the raw materials is something that should be addressed. However, this actually depends on the type of glass: borosilicate has indeed a lower carbon content (one order of magnitude in the loss factor) which, combined with the fact that way smaller furnaces are employed for its production, brings to an almost negligible amount of process emissions. This cannot be said for the soda-lime, whose raw materials contribution cannot be ignored.
For what regards the comparison carried out in chapter 3 between the furnaces for borosilicate and soda-lime glasses in terms of heat demand, here are the main outcomes. For the case of soda-lime, **Figure 37** shows that end-port is less energy demanding than unit melter, at same conditions. This is expected, considering that end port is basically the development of the unit melter thanks to its enhanced heat recovery capability. For what concerns the borosilicate instead, **Figure 36** suggests that electric furnaces have a much better thermal efficiency than Cyclope thus leading to a lower energy demand, considering that the mechanism of heat transfer is more effective and that no exhaust gases are present. However, chapter 3 also wants to discuss the reasons why fired-based furnaces are still preferred: from the point of view of the operating costs (electricity, fuel, CO_2) the analysis highlights the fact that up until the recent past the economic conditions in terms of electricity/natural gas/carbon allowances were not fit yet for an overcome of the full electric over the hybrid.
Even though full electric furnaces require a way lower energy input for the same output, it is not granted that these would be the best choice for the glass industry decarbonisation. Indeed, first of all, from the industrial perspective it is believed that they are not really suited for production volumes exceeding the 100 ton/d. Moreover, some glass products such as white soda-lime are typically obtained with a very limited electric input. On the other hand, the life cycle assessment should be considered when discussing whether full electric would really be the solution to the carbon emission problem: how is that electricity being generated? This point, which is absolutely fundamental, has been considered in order to provide evidence of the fact

that neither electric furnaces are that clean. The results obtained, still available in chapter 3, do demonstrate that electric furnaces are less carbon intense than hybrid, but the difference is not outstanding.
This might change in the future, as long as renewables manage to achieve a satisfactory level of extension.

Chapter 4 signs the start of the discussion regarding the decarbonization options. The three main area of concern are waste heat recovery, fuel substitution and process intensification in combustion.
The first approach wants to pose the attention on the possible enhancement of the energy efficiency of the overall furnace system. Huge thermal power is stored in the flue gases, which are already well exploited in the end port regenerative chambers. However, there is still room for heat recovery. The proposed solutions cover the employment of systems able to convert such thermal power into mechanical or electrical power (heat-to-power) and a novel approach consisting in exploiting the flue gases to perform the steam methane reforming thus producing an energy vector (syngas) which can be directly burnt into the furnace, thus achieving a saving in natural gas consumption.
With fuel substitution is meant the introduction of alternative fuels with lower environmental impact. The most promising would be biogas and blue/green hydrogen. The main limitations are their availability, competitive prices and distribution infrastructure. For what regards their combustion characteristics, tests have been conducted with positive feedbacks in terms of product quality. Most likely, in case these would actually be employed, a co-firing (blend of natural gas + biogas/hydrogen) combustion would be pursued, at least while the demand as well as the network are still under development.
Eventually, the process optimization in combustion is addressed. This consists in considering expedients to better perform the combustion. In this regards, the air-fuel ratio is important and it is suggested to find the trade-off between energetic demand and emissions: at low ratios indeed lower NO_x are accompanied with higher CO but lower energy consumption, whereas at higher ratios higher NO_x are expected together with lower CO and greater energy expenditure. Also the choice of the oxidizer is relevant: oxygen allows to save a large amount of fuel, even though no recovery is typically performed, but it comes with higher supply costs. Lastly, the submerged combustion approach is proposed which has a better heat transfer and therefore efficiency. However, it poses serious issues of product quality because of a limited refining capabilities. This is why it is not really likely to see this technology adopted for high-quality products such as pharmaceutical field.

Chapter 5 deals with the waste heat recovery – heat to power approach introduced in chapter 4. It is based on an existing paper [23] that analyses the implementation of four different thermodynamic cycles for the heat recovery from waste gases downstream an end port furnace operating at 150 ton/d, which is a close case to the actual operating conditions of interest. This is a rather suitable case study for Bormioli Pharma too because it analyses the feasibility in terms of potential power output from these systems as well as their economic performances. The goal of the authors is to determine whether alternative cycles to the well-established and market-ready ORC are actually more competitive. Even though the *Closed loop, sCO_2 JB cycle with combustion air preheating* can potentially achieve the best net power output of 473,3 kW, authors claim that *ORC* is still ahead in terms of economic performances: ROI between 6 and 7,5 years and net power output of 359 kW.

The last section of the Thesis, chapter 6, provides the thermodynamic and economic model of the steam methane reforming unit applied to an end port glass furnace. The purpose is to evaluate the technical feasibility in on design operations in terms of fuel and carbon emission savings with respect to the system without SMR unit. The project is then completed with a sizing of the main equipment, their quotation as well as an economic evaluation of the project performances in terms of Net Present Value. Moreover, a sensitivity analysis is operated on the most relevant design and operating variables among which there are hydrogen

energetic input, pull, electric input, overall heat transfer coefficient for the methane preheater sizing and CH_4/CO_2 prices.
The model shows very promising results, both from fuel/emissions savings and economic feasibility: in case of electrostatic filter, up to 10% of CH_4/CO_2 savings together with a NPV in the range 44.824 and 3.150.312 €. For the case of baghouse filter instead, more ambitious numbers can potentially be pursued such as a 15% cut in CH_4/CO_2 and NPV of 837.288 to 4.997.349 €.
Hence, the project is not only judged as technically feasible, but also economically convenient with respect to the standard end port furnace.
It is important to understand that such a system, which belongs to those technologies aimed at the energy efficiency enhancement, is not enough for a complete achievement of the decarbonization targets set by the European Union. As a matter of fact, steam reforming generates itself CO_2, which partly compromises the overall emission reduction potential of the system. If carbon capture technologies were implemented, even stronger achievements could be scored. Moreover, it is also important to notice that end port furnaces are already very efficient from the point of view of thermal recovery, and therefore any attempt to enhance it is to be considered as a plus. It would be interesting to assess the beneficial impact of the SMR unit on other furnaces where no significant recovery is pursued, such as oxy-fuel.
Lastly, it is believed that such an approach of heat recovery, based on the exploitation of thermal energy finalised at the direct production of heat, would be the most performing way. Going through the conversion of flue gases thermal content into mechanical first and electrical then is indeed associated with an outstanding loss of energy. Unfortunately, steam reforming applied to glass furnaces is not yet developed and therefore not ready for a market deployment. Tests and pilot projects are under development: hopefully, this technology will succeed in making its entry in the glass sector giving its contribution towards a more sustainable glass production.

List of figures

Figure 1 - furnace section and flow profile 7
Figure 2 - Steps in glass melting 8
Figure 3 - end port 9
Figure 4 - side port 9
Figure 5 - recuperative tower 10
Figure 6 - regenerative towers 11
Figure 7 - Cyclope regenerative chambers 13
Figure 8 - Cyclope furnace 13
Figure 9 - full electric furnace 13
Figure 10 - oxy-fuel furnace 14
Figure 11 - end-port furnace 15
Figure 12 - unit melter furnace 15
Figure 13 - Control volume heat balance 17
Figure 14 - EEI full electric furnace 21
Figure 15 - total heat input for electric furnace as a function of cullet and pull 22
Figure 16 - specific $CO2$ emissions for electric furnace 23
Figure 17 – total $CO2$ for electric furnace as a function of cullet and pull 24
Figure 18 - EEI Cyclope furnace 24
Figure 19 - $Qs, l, h + Qr, p$ for Cyclope furnace as a function of pull and cullet 26
Figure 20 - Natural gas demand for a Cyclope furnace as a function of cullet and electric input at design pull 27
Figure 21 - specific $CO2$ emissions for a cyclope furnace 27
Figure 22 - $CO2$ emissions for a Cyclope furnace as a function of cullet and electric input at design pull 28
Figure 23 - EEI end port furnace 29
Figure 24 - $Qs, l, h + Qr, p$ for end port furnace as a function of pull and cullet 31
Figure 25 - Natural gas demand for an end port furnace as a function of cullet and electric input at design pull 32
Figure 26 - specific $CO2$ emissions for an end port furnace 32
Figure 27 - $CO2$ emissions for an end port furnace as a function of cullet and electric input at design pull 33
Figure 28 - EEI unit melter furnace 34
Figure 29 - $Qs, l, h + Qr, p$ for a unit melter furnace as a function of pull and cullet 35
Figure 30 - Natural gas demand for a unit melter furnace as a function of cullet and electric input at design pull 36
Figure 31 - specific $CO2$ emissions for a unit melter furnace 37
Figure 32 - $CO2$ emissions for a unit melter furnace as a function of cullet and electric input at design pull 38
Figure 33 - Expected EEI for different furnaces 39
Figure 34 - Actual EEI for different furnaces 40
Figure 35 - specific $CO2$ emissions for a unit melter furnace 40
Figure 36 - total heat input for electric and Cyclope furnace as a function of cullet and electric input, at design pull 42
Figure 37 - total heat input for end port and unit melter furnace as a function of cullet and electric input, at design pull 42
Figure 38 - specific cost for energy and emissions of electric and hybrid furnaces in last years 45
Figure 39 - Open loop, air JB cycle 53
Figure 40 - T-s diagram open loop air JB cycle 53
Figure 41 - Closed loop, $sCO2$ JB cycle 54
Figure 42 - T-s diagram closed loop, $sCO2$ JB cycle 54
Figure 43 - Closed loop, $sCO2$ JB cycle with combustion air preheating 55
Figure 44 - T-s diagram closed loop, $sCO2$ JB cycle with combustion air preheating 55
Figure 45 - ORC 56
Figure 46 - T-s diagram ORC 56
Figure 47 - Cost allocation 63
Figure 48 - Furnace base-model domain 66

Figure 49 - Process flow diagram furnace + SMR unit 72
Figure 50 - $\Delta GRj°(Tout)$ for steam reforming and water gas shift 78
Figure 51 - Schematic of reformer reactor 79
Figure 52 - SMR unit 82
Figure 53 - TQ diagram HRSG 85
Figure 54 - Procedure block flow diagram 87
Figure 55 - TQ diagram methane preheater 89
Figure 56 - Savings in carbon emission against pull [ton/y] 91
Figure 57 - Savings in carbon emission against pull [%] 91
Figure 58 - Savings in methane demand against pull [sm3/y] 92
Figure 59 – Savings in methane demand against pull [%] 92
Figure 60 - Savings in carbon emissions against ee [ton/y] 93
Figure 61 - Savings in carbon emissions against ee [%] 93
Figure 62 - Savings in methane demand against ee [sm3/y] 94
Figure 63 - Savings in methane demand against ee [%] 94
Figure 64 - Methane preheater surface against U, pull at fixed ee 97
Figure 65 - Methane preheater surface against U, ee at fixed pull 97
Figure 66 - Reformer reactor quotation against pull and ee 99
Figure 67 - Linearization of the six-tenth rule for a U-tube shell and tube heat exchanger [24] 100
Figure 68 - Methane preheater quotation against U, ee at fixed pull 101
Figure 69 - Sensitivity structure for economic analysis 104
Figure 70 - NPV sensitivity at fixed electric input 105
Figure 71 - NPV sensitivity at fixed pull 105

List of tables

Table 1 - Loss factor for borosilicate and soda-lime glass 19
Table 2 - total heat input as a function of pull and cullet 22
Table 3 – total $CO2$ for electric furnace as a function of cullet and pull 23
Table 4 - $Qs, l, h + Qr, p$ for cyclope furnace as a function of pull and cullet 25
Table 5 - Natural gas demand for a Cyclope furnace as a function of cullet and electric input at design pull 26
Table 6 - $CO2$ emissions for a Cyclope furnace as a function of cullet and electric input at design pull 28
Table 7 - $Qs, l, h + Qr, p$ for end port furnace as a function of pull and cullet 30
Table 8 - Natural gas demand for an end port furnace as a function of cullet and electric input at design pull 31
Table 9 - $CO2$ emissions for an end port furnace as a function of cullet and electric input at design pull 33
Table 10 - $Qs, l, h + Qr, p$ for a unit melter furnace as a function of pull and cullet 35
Table 11 - Natural gas demand for a unit melter furnace as a function of cullet and electric input at design pull 36
Table 12 - $CO2$ emissions for a unit melter furnace as a function of cullet and electric input at design pull 37
Table 13 - natural gas, electricity and $CO2$ prices between 2014-2020 for industrial customers 43
Table 14 - specific cost for energy and emissions of electric and hybrid furnaces in last years 44
Table 15 - Emissive factor for electricity production 46
Table 16 - Overall carbon footprint of electric and Cyclope furnaces 46
Table 17 - Hydrogen transportation 50
Table 18 - Design performances of each HRS 59
Table 19 - components of each HRS 61
Table 20 - MCT coefficients 62
Table 21 - HRS economic performances 63
Table 22 - Inputs and variables for base-model 67
Table 23 - $\Delta Hfi0(298\ K)$ 68
Table 24 - Heat capacity equation constants 69
Table 25 - Model outputs and validation 72
Table 26 - Inputs and variables for furnace + SMR unit model 74
Table 27 - LHV species within syngas 76
Table 28 - example of species mass balance 78
Table 29 – Reaction enthalpies for steam reforming & water gas shift 82
Table 30 - Water properties 83
Table 31 - relative percentual error on results for the case of electrostatic filter 96
Table 32 - relative percentual error on results for the case of baghouse filter 96
Table 33 - relative percentual error on methane preheater surface for the case of electrostatic filter 98
Table 34 - relative percentual error on methane preheater surface for the case of baghouse filter 98
Table 35 - relative percentual error on reactor quotation 100
Table 36 - Methane preheater quotation against U, pull at fixed ee 101
Table 37 - relative percentual error on methane preheater quotation for the case of electrostatic filter 102
Table 38 - relative percentual error on methane preheater quotation for the case of baghouse filter 102

Bibliography

[1] L. Baronchelli, "Lumi4innovation," 28 august 2020. [Online]. Available: https://www.lumi4innovation.it/imprese-energivore-italia-obblighi-incentivi/.

[2] M. Zier, P. Stenzel, L. Kotzur and D. Stolten, "A review of decarbonization options for the glass industry," *Energy Conversion and management: X,* 2021.

[3] A. Schmitz, J. Kaminski, B. M. Scalet and A. Soria, "Energy consumption and CO2 emissions of the European glass industry," *Energy Policy,* 2010.

[4] Ministero della Transizione Ecologica, [Online]. Available: https://www.mite.gov.it/pagina/emission-trading.

[5] European Commission, [Online]. Available: https://ec.europa.eu/info/strategy/priorities-2019-2024/european-green-deal_en.

[6] European Commissions, [Online]. Available: https://ec.europa.eu/clima/eu-action/international-action-climate-change/climate-negotiations/paris-agreement_en.

[7] European Commission, [Online]. Available: https://ec.europa.eu/clima/eu-action/european-green-deal/2030-climate-target-plan_en.

[8] European Commissions, [Online]. Available: https://ec.europa.eu/clima/eu-action/european-green-deal/2030-climate-target-plan_en.

[9] P. S. Satkar, "A review on pharmaceutical packaging materials," *International Journal of Pharmaceutical Science and Research,* vol. 5, no. 3, pp. 10-13, 2020.

[10] Ministero della Transizione Ecologica, 28 January 2021. [Online]. Available: https://www.ets.minambiente.it/News#201-pubblicazione-parametri-standard-nazionali-anno-2020.

[11] ARERA, [Online]. Available: https://www.arera.it/it/dati/gpcfr2.htm.

[12] ARERA, [Online]. Available: https://www.arera.it/it/dati/eepcfr2.htm.

[13] SANDECO2, [Online]. Available: https://www.sendeco2.com/it/prezzi-co2.

[14] M. Ji and J. Wang, "Review and comparison of various hydrogen production methods based on costs and life cycle impact assessment indicators," *international journal of hydrogen energy,* 2021.

[15] Air Liquide , [Online]. Available: https://www.engineering-airliquide.com/pressure-swing-adsorption-psa-hydrogen-purification.

[16] HyNet North West, [Online]. Available: https://hynet.co.uk/.

[17] Life Sugar Project, [Online]. Available: https://www.lifesugarproject.com/.

[18] M. Fiehl, J. Leicher, A. Giese, K. Gorner, B. Fleischmann and S. Spielmann, "Biogas as a co-firing fuel in thermal processing industries: implementation in a glass melting furnace," 2017.

[19] "Global Market Insight," [Online]. Available: https://www.gminsights.com/industry-analysis/biogas-market.

[20] B. C. Tashie-Lewis and S. G. Nnabuife , "Hydrogen Production, Distribution, Storage and Power Conversion in a Hydrogen Economy - A Technology Review," *Chemical Engineering Journal Advances,* 2021.

[21] NSG Group, [Online]. Available: https://www.nsg.com/en/media/ir-updates/announcements-2021/ag-production-powered-by-hydrogen.

[22] D. Rue and J. T. Brown, “Submerged Combustion Melting of Glass,” *International Journal of Applied Glass Science,* 2011.

[23] P. Danieli, S. Rech and A. Lazzaretto, “Supercritical CO2 and air Brayton-Joule versus ORC systems for heat recovery from glass furnaces: Performance and economic evaluation,” 2018.

[24] O. J. Symister, “An Analysis of Capital Cost Estimation Techniques for Chemical Processing,” 2016.

[25] H. C. van Ness, J. M. Smith and M. M. Abbott, Introduction to Chemical Engineering Thermodynamics, New York: McGraw-Hill, 1996.

[26] J. Yun, Y. Kim and S. Yu, “Interactive heat transfer characteristics of 5 kW class shell-and-tube methane steam reformer with intermediate temperature heat source,” *international journal of hydrogen energy,* 2020.

[27] Y. A. çengel, Termodinamica e trasmissione del calore, McGraw - Hill Companies srl, 2009.

[28] “The Engineering Toolbox,” [Online]. Available: https://www.engineeringtoolbox.com/heat-transfer-coefficients-exchangers-d_450.html.

[29] National Renewable Energy Laboratory, “Equipment Design and Cost Estimation for Small Modular Biomass Systems, Synthesis Gas Cleanup, and Oxygen Separation Equipment; Task 1: Cost Estimates of Small Modular Systems,” 2006.

[30] European Commission, 12 October 2021. [Online]. Available: https://ec.europa.eu/clima/system/files/2021-10/policy_ets_allowances_bm_curve_factsheets_en.pdf.

Nomenclature

CCS – carbon capture and storage

EE – electric energy

EEI – energy efficiency index

ETS – emission trading system

HRS – heat recovery system

HRSG – heat recovery steam generator

JB – Joule Brayton

LHV – lower heating value

MCT – module costing technique

NPV – net present value

ORC – organic Rankine cycle

PBP – payback period

PSA – pressure swing adsorption

ROI – return on the investment

sCO_2 – supercritical carbon dioxide

SMR – steam methane reforming

Symbols

ΔT_{ml}[K] – logarithmic mean temperature difference

p_{cr} [bar] – critical pressure

Q_{ee} [W] – electric heat input

Q_{ex} [W] – exhaust gasses heat flux

Q_{ng} [W] – natural gas heat input

$Q_{r,p}$ [W] – heat flow due to reactions and glass leaving the furnace

$Q_{s,l,h}$ [W] – heat leakage due to structure, leakage, holes

T_{cr} [K] – critical temperature

$\varepsilon_j \left[\frac{mol}{s}\right]$ – extent of reaction j

η_{reg} – regenerator heat transfer efficiency

$\eta_{th,furn}$ – Glass furnace + HRS thermal efficiency

η_{th} – HRS thermal efficiency (P_{mech}/Q_{in})

η_{tot} – HRS total efficiency (P_{mech}/Q_{av})

U – overall heat transfer coefficient

Φ – heat transfer coefficient (Q_{in}/Q_{av})

$v_{i,j}$ – stoichiometric coefficient of species i in reaction j

$\Delta G^{\circ}_{R_j}(T)$ - Standard Gibbs free energy of reaction j evaluated at temperature T

$C_{p_i} \left[\frac{J}{mol \cdot K}\right]$ - Specific heat at constant pressure

$\Delta H^{\circ}_{r_j}(T) \left[\frac{J}{mol}\right]$ - Standard heat of reaction j at temperature T

$K_{eq,j}$ - Equilibrium constant for reaction j

$\Delta CH_4 \left[\frac{sm^3}{y}\right]$ – Methane savings

$\Delta CO_2 \left[\frac{tonCO_2}{y}\right]$ – Carbon emission savings